



Available online at www.sciencedirect.com



International Journal of Fatigue 00 (2016) 1–??

Journal
Logo

www.elsevier.com/locate/procedia

International Conference on Fatigue Damage of Structural Materials XI

A new strategy for fatigue analysis in presence of general multiaxial time varying loadings

Ma Zepeng^{a,*}, Patrick Le Tallec^b, Habibou Maitournam^c

^a*Laboratory of Solid Mechanics, Ecole Polytechnique, 91128 Palaiseau Cedex, France*

^b*Laboratory of Solid Mechanics, Ecole Polytechnique, 91128 Palaiseau Cedex, France*

^c*IMSA, ENSTA ParisTech, CNRS, CEA, EDF, Universit Paris-Saclay, 828 bd des Marchaux, 91762 Palaiseau cedex France*

Abstract

The object of this paper is to propose an energy based fatigue approach which takes into account impurities and hardness in the material which affect the fatigue life while handling multidimensional time varying loading histories.

Our fundamental thought is to assume that the local dissipated energy at small scale governs fatigue at failure. The proposal of our model is to consider a plastic behavior at the mesoscopic scale with a dependence of the yield function not only on the deviatoric part of the stress but also on the hydro static part. A kinematic hardening under the assumptions of associative plasticity is also considered. We follow the Dang Van paradigm. The structure is elastic at the macroscopic scale. At each material points, there is a stochastic distribution of weak points which will undergo strong plastic yielding, which contribute to energy dissipation without affecting the overall macroscopic stress.

Instead of using the number of cycles, we use the concept of loading time. To elaborate real life loading history more accurately, mean stress effect is taken into account in mesoscopic yield function and non-linear damage accumulation law are also considered in our model. Fatigue will then be determined from the plastic shakedown cycle and from a phenomenological fatigue law linking lifetime and accumulated mesoscopic plastic dissipation.

Keywords: Fatigue; Energy; High cycle; Plasticity; Mean stress

^{*}Corresponding author. Tel.: +33-634435338
Email address: zepeng.ma@polytechnique.edu

Nomenclature

Σ_{max}	maximum stress during the loading cycles
σ_m	mean stress
σ_H	hydrostatic stress
σ_{-1}	fatigue limit for fully reversed condition
b	back stress
σ_y	macroscopic yield stress
N	current number of cycles
N_F	number of cycles to failure
\dot{p}	accumulated plastic strain rate given as $\sqrt{\frac{2}{3}}\ \dot{\varepsilon}_p\ $
D	damage variable
$M(), \alpha()$	functions in the nonlinear continuous damage model
M_0, a, b, γ	coefficients of the nonlinear continuous damage model
σ_{σ_m}	fatigue limit for a non-zero mean stress
σ_a	stress amplitude
σ_u	ultimate tensile stress
$\langle \rangle$	Macaulay bracket symbol. $\langle \rangle$ is defined as $\langle m \rangle = 0$ if $m \leq 0$, $\langle m \rangle = m$ if $m > 0$
S_{max}	maximum deviatoric stress during the loading cycles
\dot{w}	energy dissipation rate at a certain scale
\dot{W}	energy dissipation rate at all scales
W	dissipated energy
W_{cyc}	dissipated energy per cycle
$\dot{\varepsilon}_p$	rate of effective plastic strain
\dot{p}	accumulated plastic strain rate given as $\sqrt{\frac{2}{3}}\ \dot{\varepsilon}_p\ $
W_F	dissipated energy to failure per unit volume
E	Young's modulus
$k = 500 \sim 800 MPa$	hardening parameter
$\beta = 1 \sim 50$	weakening scales distribution exponent
$\gamma = 0 \sim 50$	material parameter from Chaboche law(Wohler curve exponent)
$\alpha = 1 - a \left(\frac{\max_t \sqrt{J_{2,a}(t)} + a_c P_{max}(t) - b_c}{\sigma_u - 2 \max \sqrt{J_{2,a}}} \right)$	characterizes non-linearity of damage accumulation
a	material parameter from Chaboche law
σ_y	macroscopic yield stress(normal or shear)
$\lambda = 0 \sim 5$	hydrostatic pressure sensitivity
$dev\underline{\Sigma}$	deviatoric part of the stress tensor
$\sigma_H = P$	macroscopic hydrostatic pressure
$A_{II} = \tau_{oct,a} = \sqrt{\frac{1}{3} J_{2,a}}$	the amplitude of octahedral shear stress
s_{-1}	tensile fatigue limit for $R = -1$

1 Introduction of basic fatigue criteria

1.1. Crossland Criterion

In several industries, the required design lifetime of many components often exceeds 10^8 cycles. This requirement is applicable to aircraft (gas turbine disks 10^{10} cycles), automobiles (car engine 10^8 cycles), and railways (high speed train 10^9 cycles). Although a large amount of fatigue data has been published in the form of S-N (where S is stress and N cycles numbers) curves, the data in the literature has been usually limited to fatigue lives up to 10^7 cycles. Using traditional fatigue criteria, a near hyperbolic relationship between stress and fatigue life is assumed, with an asymptotic limit defined as the endurance stress. To predict this asymptotic limit, the Crossland Criterion is probably the most widely known. Crossland proposed that the second invariant of the deviatoric stress tensor and the hydrostatic pressure are the variables governing the endurance limit.

Many fatigue limit criteria can be written as:

$$f(\tau) + g(\sigma) \leq 0 \quad (1)$$

where f and g are given functions of the shear stress and of the normal stress respectively, as applied to different interfaces within the material.

The classical Crossland criterion defines the fatigue limit of metallic specimens subjected to multi-axial in-phase cyclic stress[1] :

$$f(\sqrt{J_{2,a}}, P_{max}) = \tau_{eq} + aP_{max} - b \leq 0 \quad (2)$$

where $\tau_{eq} = \sqrt{J_{2,a}}$ measures the amplitude of variation of the second invariant of the deviatoric stress and P_{max} is the maximum hydrostatic stress observed during a loading cycle. If $f(\sqrt{J_{2,a}}, P_{max})$ is negative or null, there is no damage. If $f(\sqrt{J_{2,a}}, P_{max})$ is positive, there is likely to be damage. The physical constants a and b are material's constants that needs to be determined experimentally. The amplitude of the square root of the second invariant of the stress deviator can be defined, in general case, as the half-length of the longest chord of the deviatoric stress path[2]

$$\sqrt{J_{2,a}} = \frac{1}{2\sqrt{2}} \min_{\underline{\underline{\sigma}}} \left\{ \max_t \sqrt{(\underline{\underline{S}}(t) - \underline{\underline{S}}_1) : (\underline{\underline{S}}(t) - \underline{\underline{S}}_1)} \right\} \quad (3)$$

Recall that the deviatoric stress $\underline{\underline{S}}$ associated to a stress tensor $\underline{\underline{\sigma}}$ is defined by

$$\underline{\underline{S}} = \underline{\underline{\sigma}} - \frac{1}{3} \text{tr} \underline{\underline{\sigma}} \quad (4)$$

The maximum value that the hydrostatic stress reaches during the loading cycle is on the other hand:

$$P_{max} = \max_t \left\{ \frac{1}{3} \text{tr} (\underline{\underline{\sigma}}(t)) \right\}. \quad (5)$$

For a proportional cyclic loading, if one introduces the two extreme stress tensors $\underline{\underline{\sigma}}^A$ and $\underline{\underline{\sigma}}^B$ observed during the loading path, together with the stress amplitude

$$\underline{\underline{\Delta\sigma}} = \underline{\underline{\sigma}}^B - \underline{\underline{\sigma}}^A \quad (6)$$

and its deviatoric part $\underline{\underline{\Delta S}}$, the variation of the second invariant of the stress deviator reduces to

$$\sqrt{J_{2,a}} = \frac{1}{2} \max_t \sqrt{\frac{1}{3} \underline{\underline{\Delta S}} : \underline{\underline{\Delta S}}} = \frac{1}{2} \max_t \sqrt{\frac{1}{3} (\Delta s_{11}^2 + \Delta s_{22}^2 + \Delta s_{33}^2 + 2\Delta s_{12}^2 + 2\Delta s_{13}^2 + 2\Delta s_{23}^2)}. \quad (7)$$

The physical constants a and b can be related to the limit t_{-1} of endurance in alternate pure shears and to the limit f_{-1} of endurance in alternate pure traction and compression by

$$a = \frac{(t_{-1} - \frac{f_{-1}}{\sqrt{3}})}{\frac{f_{-1}}{3}}, \quad b = t_{-1}. \quad (8)$$

Thus the classical Crossland criterion can be written as:

$$\sqrt{J_{2,a}} + aP_{max} - b \leq 0 \quad (9)$$

1.2. Dang Van Criterion

A stress gradient dependent version of Dang Van criterion is proposed here in the same spirit as that of Crossland. The Dang Van criterion presented in [3] is expressed as:

$$\max_t \{\tau(t) + a_D P(t)\} \leq b_D. \quad (10)$$

$\tau(t)$ denotes the mesoscopic shear stress amplitude and is obtained from a mesoscopic stress tensor $\hat{\sigma}$ defined by:

$$\hat{\sigma}(t) = (\sigma(t) - s^*).$$

s^* is the center of the smallest hypersphere circumscribed to the loading path in deviatoric stress space. It is obtained by solving a “min-max” problem as follows:

$$s^* = \arg \min_{s_1} \left\{ \max_t \|s(t) - s_1\| \right\}.$$

In the case of fully reversed loading, the values $s^* = 0$ can be directly deduced without solving the “min-max problem” as in general case.

The principal stress values of stress tensor $\tilde{\sigma}$ denoting by $\hat{\sigma}_{III}(t) \leq \hat{\sigma}_{II}(t) \leq \hat{\sigma}_I(t)$, one gets the amplitude of shear stress by:

$$\tau(t) = \frac{1}{2}(\hat{\sigma}_I(t) - \hat{\sigma}_{III}(t)).$$

$P(t)$ is the hydrostatic stress as a function of the time, given by:

$$P(t) = \frac{\sigma_{kk}(t)}{3}.$$

The material characteristic parameters a_D and b_D of the Dang Van criterion, can be related to the fully reversed bending (or tension compression because of the same stress state between them) fatigue limit, denoted by f_{ref} (or S_{ref}), and to the torsion fatigue limit, denoted by t_{ref} ,

$$a_D = \frac{3t_{ref}}{s_{ref}} - \frac{3}{2};$$

$$b_D = t_{ref}.$$

1.3. Papadopoulos Criterion

At any point O of a body, a material plane Δ can be defined by its unit normal vector \mathbf{n} . This vector \mathbf{n} makes an angle θ with the z-axis of a $Oxyz$ frame attached to the body, and its projection on the xy plane makes an angle φ with axis x , Fig. 1. For each plane Δ a new quantity is introduced called *generalised shear stress* amplitude and denoted as T_a . This shear stress quantity was first introduced in Papadopoulos [6] and was subsequently used by other researchers. The critical plane according to our proposal is that onto which $T_a(\varphi, \theta)$ achieves its maximum value. The fatigue limit criterion is written as:

$$\max T_a + \alpha_\infty \sigma_{H,max} \leq \gamma_\infty \quad (11)$$

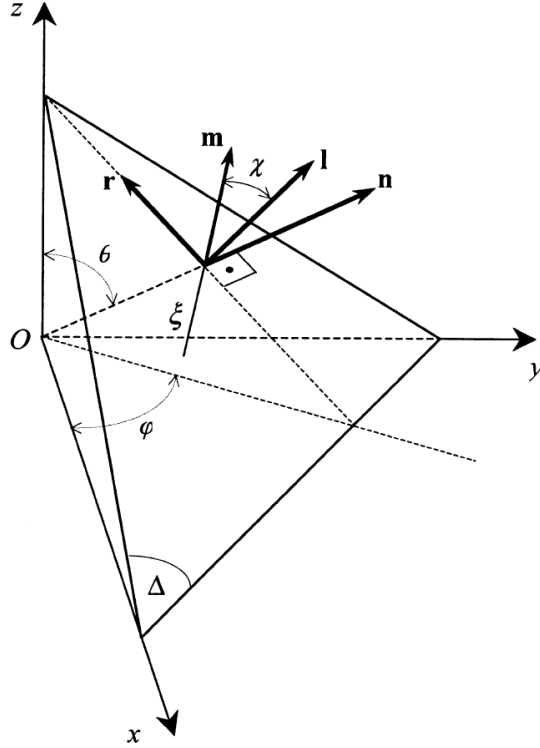


Fig. 1: Material plane Δ passing through point O of a body and its associated (n, l, r) frame.

where α_∞ and γ_∞ are material parameters to be determined[4].

$$\sigma_{H,max} = P_{max} = \max_t \left\{ \frac{1}{3} \text{tr}(\underline{\underline{\sigma}}(t)) \right\}$$

He introduced the resolved shear stress τ :

$$\begin{aligned} \tau = & [\sin\theta \cos\varphi \sigma_{xx} + \sin\theta \sin\varphi \sigma_{xy} + \cos\theta \sigma_{xz}](-\sin\varphi \cos\chi - \cos\theta \cos\varphi \sin\chi) + \\ & [\sin\theta \cos\varphi \sigma_{xy} + \sin\theta \sin\varphi \sigma_{yy} + \cos\theta \sigma_{yz}](\cos\varphi \cos\chi - \cos\theta \sin\varphi \sin\chi) + \\ & [\sin\theta \cos\varphi \sigma_{xz} + \sin\theta \sin\varphi \sigma_{yz} + \cos\theta \sigma_{zz}] \sin\theta \sin\chi \end{aligned} \quad (12)$$

It is clear that the resolved shear stress is a function of φ , θ , χ and of time t in the case of variable loading, i.e. $\tau = \tau(\varphi, \theta, \chi, t)$. Upon fixing a couple (φ, θ) (i.e. a plane Δ) and an angle χ (i.e. a line ξ on Δ), one can define the amplitude of the resolved shear stress τ_a , acting on Δ along ξ by the formula:

$$\tau_a(\varphi, \theta, \chi) = \frac{1}{2} \left[\max_{t \in P} \tau_a(\varphi, \theta, \chi, t) - \min_{t \in P} \tau_a(\varphi, \theta, \chi, t) \right] \quad (13)$$

Finally, for a given plane Δ , i.e. for a fixed couple (φ, θ) , the generalized shear stress amplitude T_a is defined as:

$$T_a(\varphi, \theta) = \sqrt{\frac{1}{\pi} \int_{x=0}^{\frac{\pi}{2}} \tau_a^2(\varphi, \theta, \chi) d\chi} \quad (14)$$

We note the fatigue limit in fully reversed torsion t_{-1} and the fatigue limit in fully reversed bending f_{-1} . From these two tests we get the parameters:

$$\gamma_\infty = t_{-1},$$

$$\alpha_\infty = 3\left(\frac{t_{-1}}{f_{-1}} - \frac{1}{2}\right).$$

The Papadopoulos fatigue limit criterion achieves the form:

$$\max T_a + 3(t_{-1}/f_{-1} - 1/2)\sigma_{H,max} \leq t_{-1}. \quad (15)$$

2 Space gradient effects

The objective of the work is first to extend some classic high cycle fatigue (HCF) criteria (as Crossland, Dang Van, Papadopoulos, ...) to take into account a sensitivity of the criteria to stress spatial variations occurring at length scale l_g , and second to compare the performances of the extensions through numerical simulations of experimental fatigue tests. After an introduction of the basic criteria and their gradient based extensions proposed by Luu et al., we focus on the Crossland criterion to propose a more practical and simple expression taking into account the gradient of the stress amplitude and the maximum hydrostatic stress. The proposition is then tested and applied to different simple situations: 4-point bending and cantilever rotative bending. The relative errors between the exact solutions and the numerical simulations are estimated. Biaxial bending-torsion tests are also simulated to demonstrate the capabilities of the approach. The generalization of the approach to other multiaxial fatigue criteria is briefly shown through the case of Papadopoulos 2001 proposal. Finally, the present study develops a simple formulation of gradient multiaxial fatigue criteria extending the classical HCF criteria. In this work only stress gradient with a beneficial effect on fatigue have been considered.

2.1. Introduction

In several industries, the required design lifetime of many components often exceeds 10^8 cycles. This requirement is applicable to aircraft (gas turbine disks 10^{10} cycles), automobiles (car engine 10^8 cycles), and railways (high speed train 10^9 cycles). Although a large amount of fatigue data has been published in the form of S-N (where S is stress and N the number of cycles to fatigue) curves, the data in the literature have been usually limited to fatigue lives up to 10^7 cycles. Using traditional fatigue criteria, a near hyperbolic relationship between stress and fatigue life is assumed, with an asymptotic limit defined as the fatigue limit (or endurance stress). A large number of multiaxial fatigue criteria, generalizing this notion of fatigue limit, are available in the literature [2][3][5]. They are practically used to design industrial components against failure. Nevertheless, most of these criteria present some drawbacks, for instance when dealing with out-of-phase loading or with metals of different kinds from those used to develop the criteria. In fact, quite all of them are not designed to cope with high stress gradient introducing by surface treatments or notches, and also with scale effect especially present in nano or micro components.

More precisely, as mentioned by Luu et al. [6], in problems related to small electronic components and electro-mechanical devices, at sufficiently small sizes, factors as size, gradient and loading effects affecting fatigue limits are not captured by classical fatigue criteria. The general statement "the smaller the size, the higher the gradient, then the higher fatigue resistance" sums up the following observations.

Loading effects: the three types of tests with different volumes of the most loaded zones are examined in [6]. In descending volume order, they are tension-compression, rotative bending and plane bending, leading to increasing order of fatigue limits.

Size: for the same in-state stress distribution as well as nominal maximum stress and material, the smaller the sample size is, the smaller the surface or the volume of the most stressed zone is, the higher the fatigue limit is.

Stress gradient: the nominal fatigue limit increases in the presence of stress gradient corresponding to a decreasing stress from the surface. Experimental example illustrates and makes clearer "beneficial gradient effect" [7]. The results of the constant moment tests on specimens of the same radius but different lengths shows that the gradient effect is an order of magnitude higher than the pure size effect. In this case, size effect is proved insignificant compared to the gradient effect at the considered scale.

From above it is concluded that the stress gradient factor is the most important contributer to this phenomenon. It has been generalized by several authors to include a gradient dependence [7] in order to

introduce a sensitivity of the endurance limit to space variations occurring at length scale l_g . Uniaxial normal cyclic stress states with non-zero and zero normal stress gradients, respectively, allow drawing some comments about the normal stress gradient effect. The larger the normal stress due to bending, the larger the difference between bending test points and tension-compression ellipse arc (as is shown in Fig. 2).

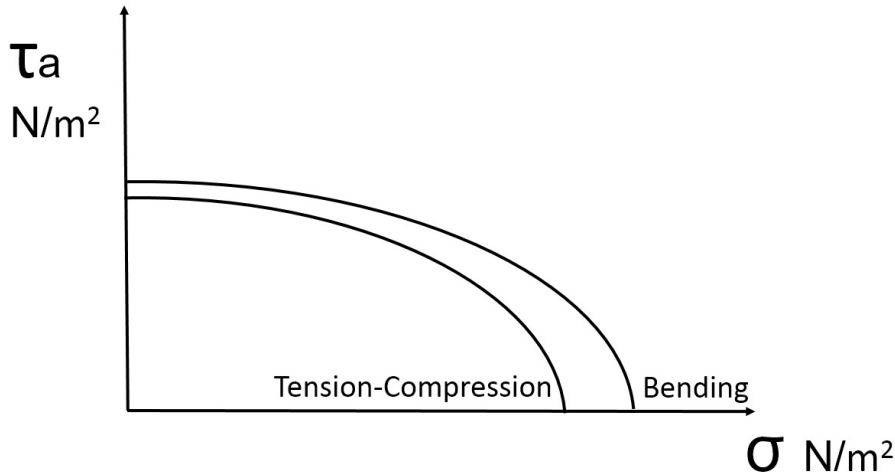


Fig. 2: Schematic representation of the nominal fatigue limit (ellipse arc) for two different tests: the arc is larger in the case of bending-torsion (presence of stress gradient) than in tension-compression.

Apart from gradient approaches[8][7], to take account of these effect, others approaches such critical volume [9], critical distance[10][11], critical layer[12], averaging over a specific volume [13][14] are used. In fact, all the approaches are equivalent to introducing a length scale. In the paper, we consider specifically the gradient approach. We start from the proposition of Luu et al., and propose a simpler way to account for the gradient. The Crossland criterion, one of the most widely known HCF criteria, is used to illustrate the approach. Crossland proposed that the second invariant of the deviatoric stress tensor and the hydrostatic stress are the variables governing the endurance limit. The new proposition adds two gradient terms ; it is then calibrated and its predictions are compared to experimental results to check its relevancy.

2.2. Approach of Luu et al.

2.2.1. General formulation

Luu et al. [6] proposed extensions of classical HCF fatigue criteria using the gradients of the shear and normal stress to account for the gradient effect. In the case of critical plane type criteria, they defined a generalized shear stress amplitude including shear stress gradient and a generalized maximum normal (or hydrostatic) stress. A general form of classical fatigue limit criteria can be written as follows:

$$f(C_a(n^*), N_{max}(n^*)) = C_a(n^*) + aN_{max}(n^*) - b \geq 0, \quad (16)$$

with a, b being two material parameters. f is a function, chosen in many cases as linear, and n^* is the normal vector of the critical plane; $C_a(n^*), N_{max}(n^*)$ are respectively the amplitude of shear stress and the maximum value of the normal stress on the critical plane.

A new class of fatigue criteria extended from classical ones with stress gradient terms introducing not only in the normal stress but also in the shear stress components, was proposed. It concerns only free defect materials and can model both phenomena "smaller is Stronger and Higher Gradient is Stronger".

Besides the stress gradient term appearing in the normal stress part in form of $G = \Delta(\sigma_{11} + \sigma_{22} + \sigma_{33})$, another gradient term, the gradient of the stress tensor amplitude (or alternatively of deviatoric stress tensor amplitude) $\| Y_a \| = \Delta\sigma_a$ is added to the shear stress amplitude part. Basing on all these analyses a new form

of fatigue criteria taking into account gradient effects, is proposed:

$$f(\widetilde{C}_a(n^*), \widetilde{N}_{max}(n^*)) = \widetilde{C}_a(n^*) + a\widetilde{N}_{max}(n^*) - b \geq 0, \quad (17)$$

where $\widetilde{C}_a(n^*)$ and $\widetilde{N}_{max}(n^*)$ are extended definitions of the amplitude of shear stress and of the normal stress taking into account the presence of local gradient.

In the following we just focus on the Crossland criterion and its extension.

2.2.2. Recall of the classical Crossland criterion

The classical Crossland criterion defines the fatigue limit of metallic specimens subjected to multi-axial cyclic stress[1] :

$$f(\sqrt{J_{2,a}}, P_{max}) = \sqrt{J_{2,a}} + aP_{max} - b \leq 0 \quad (18)$$

where $\sqrt{J_{2,a}}$ measures the amplitude of variation of the second invariant of the deviatoric stress and P_{max} is the maximum hydrostatic stress observed during a loading cycle. The parameters a and b are material constants to be calibrated experimentally. The amplitude of the square root of the second invariant of the stress deviator can be defined, in general case, as the half-length of the longest chord of the deviatoric stress path or as the radius of the smallest hypersphere circumscribing the stress deviator loading path [2]

$$\sqrt{J_{2,a}} = \frac{1}{2\sqrt{2}} \min_{\underline{S}_1} \max_t \sqrt{(\underline{S}(t) - \underline{\underline{S}}_1) : (\underline{S}(t) - \underline{\underline{S}}_1)} \quad (19)$$

The deviatoric stress \underline{S} associated with a stress tensor $\underline{\underline{\sigma}}$ is defined by

$$\underline{S} = \underline{\underline{\sigma}} - \frac{1}{3} \text{tr} \underline{\underline{\sigma}} \underline{I} \quad (20)$$

where $\text{tr} \underline{\underline{\sigma}}$ is the trace of the stress tensor $\underline{\underline{\sigma}}$ and \underline{I} the second order unit tensor.

The maximum value that the hydrostatic stress reaches during the loading cycle is on the other hand:

$$P_{max} = \max_t \left\{ \frac{1}{3} \text{tr} (\underline{\underline{\sigma}}(t)) \right\}. \quad (21)$$

For a proportional cyclic loading, if one introduces the two extreme stress tensors $\underline{\underline{\sigma}}^A$ and $\underline{\underline{\sigma}}^B$ observed during the loading path, together with the stress range

$$\Delta \underline{\underline{\sigma}} = \underline{\underline{\sigma}}^B - \underline{\underline{\sigma}}^A \quad (22)$$

and its deviatoric part $\Delta \underline{S}$, the variation of the second invariant of the stress deviator reduces to

$$\sqrt{J_{2,a}} = \frac{1}{2} \max_t \sqrt{\frac{1}{2} \Delta \underline{S} : \Delta \underline{S}} = \frac{1}{2} \max_t \sqrt{\frac{1}{2} (\Delta s_{11}^2 + \Delta s_{22}^2 + \Delta s_{33}^2 + 2\Delta s_{12}^2 + 2\Delta s_{13}^2 + 2\Delta s_{23}^2)}. \quad (23)$$

The material constants a and b can be related to the limit t_{-1} of endurance in alternate torsion and to the limit s_{-1} of endurance in alternate tension-compression by

$$a = \frac{3t_{-1}}{s_{-1}} - \sqrt{3}, \quad b = t_{-1}. \quad (24)$$

2.2.3. Formulation of Crossland criterion with gradient effect

In particular, using as a basis the classical Crossland criterion Eq.(18) and the general framework for the development of a gradient dependent fatigue limit criterion Eq.(17), a new version can be written in the form:

$$\sqrt{J_{2,a}} + a\widetilde{P}_{max} \leq b. \quad (25)$$

This formula takes into account the indicator of the influence of the gradient of the stress deviator which reflects the spatial non-uniform distribution of stress state.

In practice, [6] had proposed:

$$\sqrt{J_{2,a}} \sqrt{1 - \left(l_\tau \frac{\| \underline{Y} \|_a}{\| \underline{\underline{S}} \|_a} \right)^{n_\tau}} + aP_{max} \left(1 - \left(l_\sigma \frac{\| G \|}{P_{max}} \right)^{n_\sigma} \right) - b < 0. \quad (26)$$

Here $\| \underline{Y} \|_a$ is the full stress gradient and $\| G \|$ is used as an indicator of the influence of the normal stresses gradient.

$$\| G \| = \| \nabla P_{max} \| = \sqrt{\left(\frac{\partial P_{max}}{\partial x} \right)^2 + \left(\frac{\partial P_{max}}{\partial y} \right)^2 + \left(\frac{\partial P_{max}}{\partial z} \right)^2}. \quad (27)$$

2.3. Optimized Crossland Criterion formulation

The precedent Luu and al. formula has six materials parameters $a, b, l_\tau, l_\sigma, n_\tau, n_\sigma$ to be identified experimentally. The calibration can be complicated ; it does not lead to a unique set of parameters. Physical considerations, such as the length scales, have to be taken into account for choosing the optimized material constants. For practical application in an industrial context, it is essential to reduce the number of parameters. We therefore wish to investigate a simpler construction, departing from the classical Crossland criterion.

Surfaces with stresses decreasing in depth are, here and after, considered. Failure occurs at the point x_0 when, $(\sqrt{J_{2,a}} + aP_{max} - b)(x_0) \geq 0$. To be more general and avoid singularity, this condition should be satisfied in some x_0 neighboring volume of size l_g , leading to a criterion given by:

$$\inf_{x \in B(x_0, l_g)} (\sqrt{J_{2,a}} + aP_{max} - b)(x) \geq 0. \quad (28)$$

To obtain a suitable expression, an expansion of Eq.(28) is performed in the neighborhood of x_0 . The sought formula should account for the beneficial effect of the stress gradient. Considering that the stress is decreasing in depth, a negative sign is associated with the norm of the gradient of stress tensor in to the proposed formula. In addition, the gradient term should not only affect hydrostatic stress but also shear stress.

An objective formulation based on the lowest possible value of $\sqrt{J_{2,a}}$ and of P_{max} in the neighborhood, is finally:

$$\sqrt{J_{2,a}} + aP_{max} - l_g \| \nabla \sqrt{J_{2,a}} + a \nabla P_{max} \| \leq b, \quad (29)$$

We keep the same material parameters a and b as before. l_g is a characteristic length to be optimized to match the experimental results. The approach has only one supplementary material constant whose calibration is easy.

2.4. Calibration of the criteria

In this section, two different uniaxial fatigue tests with stress gradient effects are used to calibrate the optimized gradient Crossland and Papadopoulos criterion. An application to a biaxial test fatigue test shows the ability of the proposed approach to account the stress gradient in multiaxial cases.

2.4.1. Rotating cantilever bending fatigue tests using Papadopoulos criterion

the stress tensor of cantilever bending is in the following expression:

$$\underline{\underline{\sigma}} = \sigma_{xx} \sin(2\pi t/P) e_x \otimes e_x$$

The resolved shear stress τ acting along a line ξ of a plane Δ is given by Eq.12, which in this case leads to:

$$\tau(\varphi, \theta, \chi, t) = \sigma_{xx} \sin(2\pi t/P) \sin\theta \cos\theta \sin\chi. \quad (30)$$

Clearly, the resolved shear stress amplitude is equal to:

$$\tau_a(\varphi, \theta, \chi) = \sigma_{xx} |\sin\theta \cos\theta \sin\chi|. \quad (31)$$

The generalized shear stress amplitude T_a becomes:

$$T_a(\varphi, \theta) = \sqrt{\frac{1}{\pi} \int_{x=0}^{\frac{\pi}{2}} (\sigma_{xx} |\sin\theta \cos\theta \sin\chi|)^2 d\chi} \quad (32)$$

The maximum value of T_a is obtained at ($\forall \varphi, \theta = \pi/4$) and at ($\forall \varphi, \theta = 3\pi/4$). It is equal to:

$$\max T_a = \sigma_{xx}/2 \quad (33)$$

The hydrostatic stress is given by:

$$\sigma_H(t) = \frac{1}{3} \sigma_{xx} \sin(2\pi t/P) \quad (34)$$

The maximum value of σ_H reached in a loading cycle is:

$$\sigma_{H,max} = \sigma_{xx}/3 \quad (35)$$

Substituting the values of T_a and $\sigma_{H,max}$ to Eq.(15). We obtain the papadopoulos fatigue criterion under cantilever bending case: Papadopoulos criterion with beneficial gradient term as shown in Eq.((??)) is given by:

$$\begin{aligned} \max T_a + \alpha_\infty \sigma_{H,max} - l_g \|\nabla \max T_a + \alpha_\infty \sigma_{H,max}\| = \\ \frac{FLR}{2I} + \frac{\alpha_\infty FLR}{3I} - l_g \left(\frac{FL}{2I} + \frac{\alpha_\infty FL}{3I} \right) = \\ \frac{1}{2} \sigma_{xx} + \frac{a}{3} \sigma_{xx} - l_g \left(\frac{1}{2R} \sigma_{xx} + \frac{a}{3R} \sigma_{xx} \right) \leq \gamma_\infty, \end{aligned} \quad (36)$$

which is to say:

$$\sigma_{xx} \leq \frac{\gamma_\infty}{\frac{1}{2} + \frac{\alpha_\infty}{3} - l_g \left(\frac{1}{2R} + \frac{\alpha_\infty}{3R} \right)}. \quad (37)$$

where

$$\alpha_\infty = \frac{3(s_{-1} - s_0)}{2(2s_0 - s_{-1})},$$

$$\gamma_\infty = \frac{s_0 s_{-1}}{2(2s_0 - s_{-1})}.$$

We do not have sufficient data of the experimental materials of zero-to-tension fatigue limit s_0 to calibrate these two parameters.

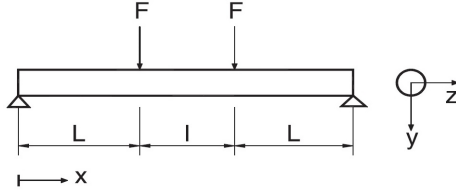


Fig. 3: 4-point bending test [15]

2.4.2. Fully reversed 4-point bending and rotating cantilever bending fatigue tests using Crossland criterion

The model of 4-point bending is first considered. The bar made of steel has both ends fixed. The radius R is a variable ranging from 1mm to 30mm enough to highlight the fact "the smaller, the stronger". The length L of the bar is 100 mm.

The bending moment is the same in the interval $L \leq x \leq L + l$ and equal to $M = FL$ (Fig. 3). The bending stress σ and its gradient \mathbf{Y} for $L \leq x \leq L + l$ and $-R \leq y \leq R$ are then:

$$\underline{\underline{\sigma}} = \sigma_{xx} \sin(wt) \mathbf{e}_x \otimes \mathbf{e}_x = \frac{FLy}{I} \sin(wt) \mathbf{e}_x \otimes \mathbf{e}_x$$

with $I = \frac{\pi R^4}{4}$

The maximum stress during the cyclic loading in the bar is: $\sigma_{max} = \frac{FL}{I}$.

The gradient components of \mathbf{Y} is: $\sigma_{xx,x} = 0, \sigma_{xx,y} = \frac{FL}{I} = \frac{\sigma_{max}}{y}, \sigma_{xx,z} = 0$.

The macroscopic stress range is: $\underline{\underline{\Delta\sigma}}(t) = 2\sigma_{max} \mathbf{e}_x \otimes \mathbf{e}_x$ The hydrostatics stress:

$$P_{max} = \max_t \left\{ \frac{1}{3} \text{tr}(\sigma(t)) \right\} = \frac{1}{3} \sigma_{max} = \frac{FLy}{3I}, \quad (38)$$

Deviator of the macroscopic stresses:

$$\underline{\underline{\Delta S}} = \underline{\underline{\Delta\sigma}} - \frac{1}{3} \text{tr}(\underline{\underline{\Delta\sigma}}) \mathbf{I} = \begin{pmatrix} \frac{4}{3} \sigma_{max} & 0 & 0 \\ 0 & -\frac{2}{3} \sigma_{max} & 0 \\ 0 & 0 & -\frac{2}{3} \sigma_{max} \end{pmatrix}. \quad (39)$$

The second invariant of the stress deviator is then:

$$\sqrt{J_{2,a}} = \frac{1}{2\sqrt{2}} \sqrt{\underline{\underline{\Delta S}} : \underline{\underline{\Delta S}}} = \frac{\sigma_{max}}{\sqrt{3}} = \frac{FLy}{\sqrt{3}I}. \quad (40)$$

Then the gradient part has the value:

$$\nabla \sqrt{J_{2,a}} = \frac{\partial \sqrt{J_{2,a}}}{\partial x} \mathbf{e}_x + \frac{\partial \sqrt{J_{2,a}}}{\partial y} \mathbf{e}_y + \frac{\partial \sqrt{J_{2,a}}}{\partial z} \mathbf{e}_z = (0, \frac{FL}{\sqrt{3}I}, 0), \quad (41)$$

and

$$\nabla P_{max} = (0, \frac{FL}{3I}, 0). \quad (42)$$

The parameters a and b of the standard Crossland criterion, are obtained from fully reversed tension-compression fatigue limit s_{-1} and torsion fatigue limit t_{-1} using Eq.(24).

From Eq.(18), standard Crossland criterion without gradient effect (for radius R) is:

$$\sqrt{J_{2,a}} + aP_{max} = \frac{FLR}{\sqrt{3}I} + \frac{aFLR}{3I} \leq b. \quad (43)$$

The gradient term here is given by:

$$\| \nabla \sqrt{J_{2,a}} + a \nabla P_{max} \| = \frac{FL}{\sqrt{3}I} + \frac{aFL}{3I}. \quad (44)$$

By comparison we can see in 4-point bending test the difference between classical and modified Crossland criterion is related to the product of the characteristic length l_g and the term (44) associated to the decrease of the stress in depth. This value shows how much the modification affects the Crossland criterion. Crossland criterion with beneficial gradient term as shown in Eq.(29) is given by:

$$\begin{aligned} \sqrt{J_{2,a}} + aP_{max} - l_g(\|\nabla\sqrt{J_{2,a}} + a\nabla P_{max}\|) &= \\ \frac{FLR}{\sqrt{3}I} + \frac{aFLR}{3I} - l_g\left(\frac{FL}{\sqrt{3}I} + \frac{aFL}{3I}\right) &= \\ \frac{1}{\sqrt{3}}\sigma_{max} + \frac{a}{3}\sigma_{max} - l_g\left(\frac{1}{\sqrt{3}R}\sigma_{max} + \frac{a}{3R}\sigma_{max}\right) &\leq b, \end{aligned} \quad (45)$$

which is to say:

$$\sigma_{max} \leq \frac{b}{\frac{1}{\sqrt{3}} + \frac{a}{3} - l_g\left(\frac{1}{\sqrt{3}R} + \frac{a}{3R}\right)}. \quad (46)$$

The material parameters a and b are obtained using their classical expressions as Eq.(24) from tests free of stress gradient. The corresponding fatigue limit are denoted s_{ref} for the alternate tension-compression test, and t_{ref} for the alternate torsion test. For a specimen of radius R the alternate bending fatigue limit is denoted $f(R)$. We can observe that:

$$f(R) = \frac{b}{\frac{1}{\sqrt{3}} + \frac{a}{3} - l_g\left(\frac{1}{\sqrt{3}R} + \frac{a}{3R}\right)} \geq s_{ref} \quad (47)$$

$f(R)$ tends to s_{ref} for large radii.

Table 1: Length scales of different materials

	1220 steel	Carbon steel	1035 steel	40Kh steel
S_{ref} [MPa]	191	222	234	297
t_{ref} [MPa]	143	151	172	180
l_g [mm]	0.3755	0.3297	0.2861	0.1424

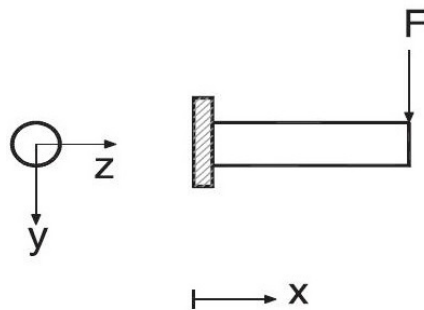


Fig. 4: Cantilever bending test [15]

In the case of cantilever fully reversed bending. Let us denote the corresponding fatigue limit by σ_{max} . The second invariant of the stress deviator is then:

$$\sqrt{J_{2,a}} = \frac{1}{2\sqrt{2}} \sqrt{\underline{\Delta S} : \underline{\Delta S}} = \frac{\sigma_{max}}{\sqrt{3}}. \quad (48)$$

The hydrostatics stress:

$$P_{max} = \max_t \left\{ \frac{1}{3} \text{tr}(\sigma(t)) \right\} = \frac{1}{3} \sigma_{max}. \quad (49)$$

Which results in the same gradient terms as in 4-point bending.

Eq.(47) with a et b calibrated from given S_{ref} and t_{ref} is used to estimate the characteristic length l_g in order to give the best correlation between simulated and experimental fatigue limit obtained in rotating cantilever bending tests for different materials and radii. The results are sketched in Fig.(5).

The fatigue limit of carbon steel is in alternate torsion is $t_{ref} = 151\text{MPa}$ and the fatigue limit in alternate tension-compression is $s_{ref} = 222\text{MPa}$. After fitting, we get $l_g = 0.3297$.

The fatigue limit of SAE 1220 steel is in alternate torsion is $t_{ref} = 143\text{MPa}$ and the fatigue limit in alternate tension-compression is $s_{ref} = 191\text{MPa}$. After fitting, we get $l_g = 0.3755$.

The fatigue limit of SAE 1035 steel is in alternate torsion is $t_{ref} = 172\text{MPa}$ and the fatigue limit in alternate tension-compression is $s_{ref} = 234\text{MPa}$. After fitting, we get $l_g = 0.2861$.

The fatigue limit of 40Kh steel is in alternate torsion is $t_{ref} = 180\text{MPa}$ and the fatigue limit in alternate tension-compression is $s_{ref} = 297\text{MPa}$. After fitting, we get $l_g = 0.1424$.

We can observe a very interesting phenomenon that the smaller fatigue limit is, the larger influence of gradient effect is.

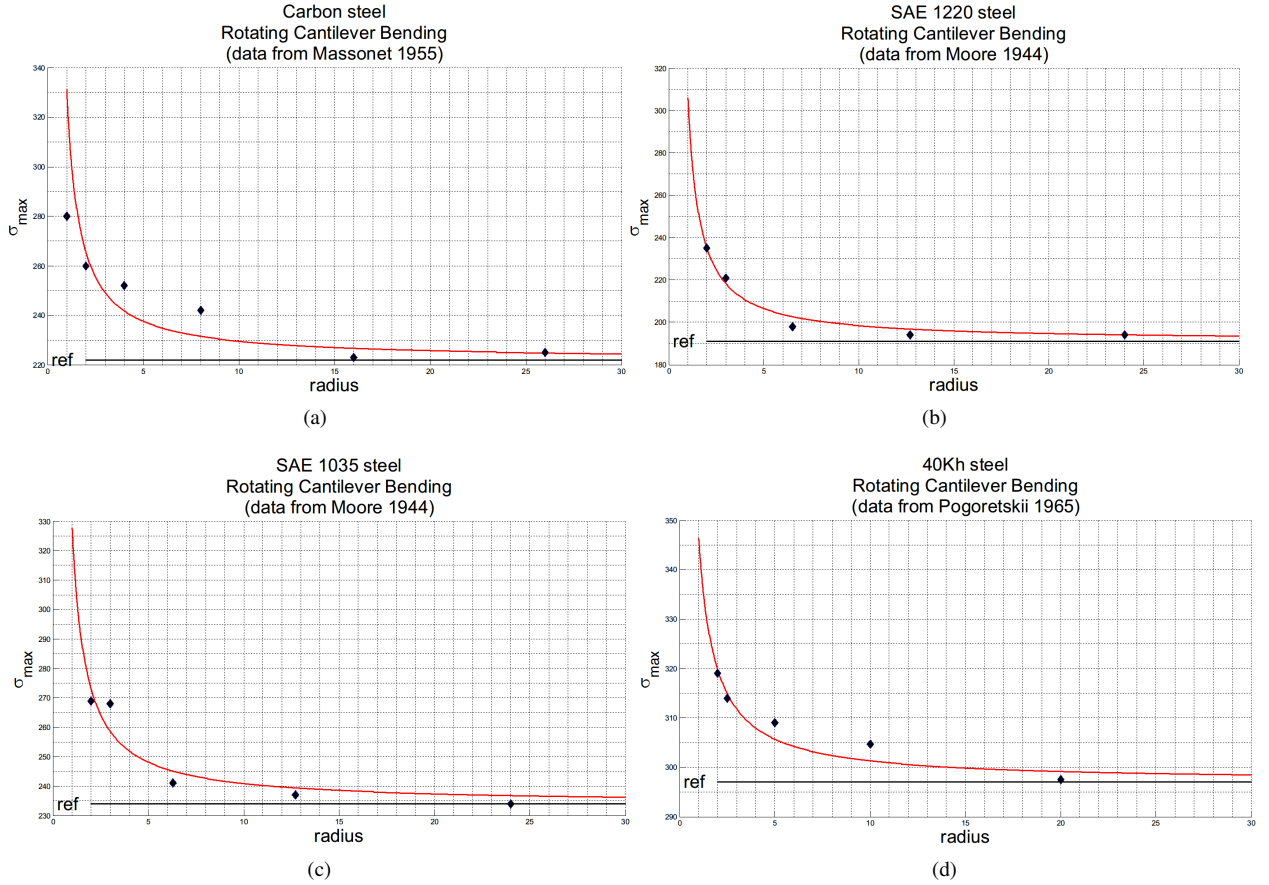


Fig. 5: Fatigue limits with gradient effect for different radii.

2.4.3. Bending-torsion fatigue tests

With Crossland criterion The bending moment is a linear function of x , $M_b = -F(L - x)$. The twisting moment is denoted M_t . The stress σ_{xx} now varies along the depth (i.e. y-axis) and the length (i.e. x-axis) of the specimen. Consequently, the gradient of σ_{xx} has two non-zero components, the derivatives with respect to x and y . Considering the critical points (located at $y = \pm R$) The bending stress and its gradient for $0 \leq x \leq L$ are given by the formulas:

$$\sigma_a = \frac{-F(L - x)}{I} R = \frac{M_b}{I} y \quad (50)$$

with $I = \frac{\pi R^4}{4}$, $\tau_a = \frac{M_t}{J} y$ and $J = \frac{1}{2}\pi R^4$. The stress tensor $\underline{\underline{\sigma}}$ is then:

$$\underline{\underline{\sigma}}(t) = \begin{pmatrix} \sigma_a \sin(\omega t) & \tau_a \sin(\omega t) & 0 \\ \tau_a \sin(\omega t) & 0 & 0 \\ 0 & 0 & 0 \end{pmatrix}. \quad (51)$$

The stress range tensor is:

$$\underline{\underline{\Delta\sigma}} = \begin{pmatrix} 2\sigma_a & 2\tau_a & 0 \\ 2\tau_a & 0 & 0 \\ 0 & 0 & 0 \end{pmatrix}. \quad (52)$$

Deviator of the macroscopic stresses:

$$\underline{\Delta S} = \underline{\Delta \sigma} - \frac{1}{3} \text{tr} \underline{\Delta \sigma} = \begin{pmatrix} \frac{4}{3} \sigma_a & 2\tau_a & 0 \\ 2\tau_a & -\frac{2}{3} \sigma_a & 0 \\ 0 & 0 & -\frac{2}{3} \sigma_a \end{pmatrix}. \quad (53)$$

The second invariant of the stress deviator is then:

$$\sqrt{J_{2,a}} = \frac{1}{2\sqrt{2}} \sqrt{\underline{\Delta S} : \underline{\Delta S}} = \sqrt{\frac{1}{3} \sigma_a^2 + \tau_a^2} = \sqrt{\frac{M_b^2}{3I^2} + \frac{M_t^2}{4J^2}} y. \quad (54)$$

The hydrostatics stress:

$$P_{max} = \max_t \left\{ \frac{1}{3} \text{tr}(\sigma(t)) \right\} = \frac{\sigma_a}{3} = \frac{M_b}{3I} y, \quad (55)$$

Then the gradient part has the value:

$$\begin{aligned} \nabla \sqrt{J_{2,a}} &= \frac{\partial \sqrt{J_{2,a}}}{\partial x} \underline{e}_x + \frac{\partial \sqrt{J_{2,a}}}{\partial y} \underline{e}_y + \frac{\partial \sqrt{J_{2,a}}}{\partial z} \underline{e}_z = (0, \sqrt{\frac{M_b^2}{3I^2} + \frac{M_t^2}{4J^2}}, 0) \\ &= (0, \frac{\sqrt{\frac{1}{3} \sigma_a^2 + \tau_a^2}}{y}, 0), \end{aligned} \quad (56)$$

and

$$\nabla P_{max} = (0, \frac{M_b}{3I}, 0) = (0, \frac{\sigma_a}{3y}, 0). \quad (57)$$

The parameters a and b of the standard Crossland criterion, are obtained from fully reversed tension-compression fatigue limit s_{ref} and torsion fatigue limit t_{ref} using Eq.(24).

From Eq.(18), standard Crossland criterion without gradient effect writes:

$$\sqrt{J_{2,a}} + aP_{max} = \sqrt{\frac{\sigma_a^2}{3} + \tau_a^2} + \frac{\sigma_a}{3} \leq b. \quad (58)$$

The gradient term here is given by:

$$\| \nabla \sqrt{J_{2,a}} + a \nabla P_{max} \| = \frac{\sqrt{\frac{\sigma_a^2}{3} + \tau_a^2}}{y} + \frac{a \sigma_a}{3y}. \quad (59)$$

Crossland criterion with beneficial gradient term as shown in Eq.(29):

$$\begin{aligned} \sqrt{J_{2,a}} + aP_{max} - l_g \| \nabla \sqrt{J_{2,a}} + a \nabla P_{max} \| &= \\ \sqrt{\frac{\sigma_a^2}{3} + \tau_a^2} + \frac{a \sigma_a}{3} - l_g \left(\frac{\sqrt{\frac{\sigma_a^2}{3} + \tau_a^2}}{y} + \frac{a \sigma_a}{3y} \right) &\leq b \end{aligned} \quad (60)$$

With Papadopoulos criterion We can find the resolved shear stress $\tau_a(\varphi, \theta, \chi, t)$ with Eq.(12):

$$\begin{aligned} \tau_a(\varphi, \theta, \chi, t) &= [\sin(\theta) \cos(\phi) \sigma_a \sin(\omega t) + \sin(\theta) \sin(\phi) \tau_a \sin(\omega t)] [-\sin(\phi) \cos(\chi) - \\ &\quad \cos(\theta) \cos(\phi) \sin(\chi)] + [\sin(\theta) \cos(\phi) \tau_a \sin(\omega t)] \\ &\quad [\cos(\phi) \cos(\chi) - \cos(\theta) \sin(\phi) \sin(\chi)], \end{aligned} \quad (61)$$

We use 1stOpt to calculate $\max_{t \in P} \tau_a(\varphi, \theta, \chi, t) = 0.05\sigma_a + 1.0944\tau_a$ and $\min_{t \in P} \tau_a(\varphi, \theta, \chi, t) = -0.2236\sigma_a - 0.8944\tau_a$. Therefore we can get:

$$\tau_a(\varphi, \theta, \chi) = \frac{1}{2} [\max_{t \in P} \tau_a(\varphi, \theta, \chi, t) - \min_{t \in P} \tau_a(\varphi, \theta, \chi, t)] = 0.1368\sigma_a + 0.9944\tau_a,$$

The generalized shear stress amplitude T_a is then:

$$T_a(\varphi, \theta) = \sqrt{\frac{1}{\pi} \int_{x=0}^{\frac{\pi}{2}} \tau_a^2(\varphi, \theta, \chi) d\chi} = \sqrt{\frac{1}{2} \tau_a^2(\varphi, \theta, \chi)} = 0.0967\sigma_a + 0.7031\tau_a.$$

$$\sigma_{H,max} = \frac{1}{3}\sigma_a$$

The modified Papadopoulos criterion from Eq.(??) is:

$$\max T_a + \alpha_\infty \sigma_{H,max} - l_g \|\nabla \max T_a + \alpha_\infty \sigma_{H,max}\| \leq \gamma_\infty,$$

with

$$\alpha_\infty = \frac{3(s_{-1} - s_0)}{2(2s_0 - s_{-1})},$$

$$\gamma_\infty = \frac{s_0 s_{-1}}{2(2s_0 - s_{-1})}.$$

Then the gradient part has the value:

$$\nabla \max T_a = \frac{\partial \max T_a}{\partial x} \underline{e}_x + \frac{\partial \max T_a}{\partial y} \underline{e}_y + \frac{\partial \max T_a}{\partial z} \underline{e}_z = (0, \frac{0.0967\sigma_a + 0.7031\tau_a}{y}, 0), \quad (62)$$

and

$$\nabla P_{max} = (0, \frac{M_b}{3I}, 0) = (0, \frac{\sigma_a}{3y}, 0). \quad (63)$$

$$\max T_a + \alpha_\infty \sigma_{H,max} - l_g \|\nabla \max T_a + \alpha_\infty \sigma_{H,max}\| =$$

$$0.0967\sigma_a + 0.7031\tau_a + \frac{\alpha_\infty \sigma_a}{3} - l_g \left(\frac{0.0967\sigma_a + 0.7031\tau_a}{y} + \frac{\alpha_\infty \sigma_a}{3y} \right) \leq \gamma_\infty. \quad (64)$$

But currently we lack the experimental data of fatigue limits in zero-to-tension s_0 .

2.4.4. Comparison with experimental data

This ellipse arc delimits in the $s_{ref} - t_{ref}$ plane the safe domain against fatigue failure (the blue arc). Clearly, Eq. (58) is the Crossland criterion for combined normal and shear stress. However, if one tries to predict the behavior of the material in combined bending and torsion, which involves the gradients of normal and shear stresses, high discrepancies between predictions and experimental data will be found.

By introducing the values of $\sqrt{J_{2,a}}$ and P_{max} in the the classical Crossland criterion, along with the change of parameter a from $(\frac{3t_{-1}}{s_{-1}} - \sqrt{3})$ to $(\frac{3t_{-1}}{f_{-1}} - \sqrt{3})$ in Eq.(18), we obtain the "Papadopoulos ellipse arc" equation in the plane of amplitudes σ_a and τ_a (the black arc):

$$(\frac{\tau_a}{t_{-1}})^2 + (\frac{2f_{-1}}{\sqrt{3}t_{-1}} - 1)(\frac{\sigma_a}{f_{-1}})^2 + (2 - \frac{2f_{-1}}{\sqrt{3}t_{-1}})\frac{\sigma_a}{f_{-1}} \leq 1 \quad (65)$$

Our proposal takes into account both gradients of hydrostatic stress and shear stress. Choosing the proper l_g allows us to predict the experiments within the acceptable range as shown in Fig. 6 (the red arc). These results illustrate that our proposal is quite satisfactory in biaxial case.

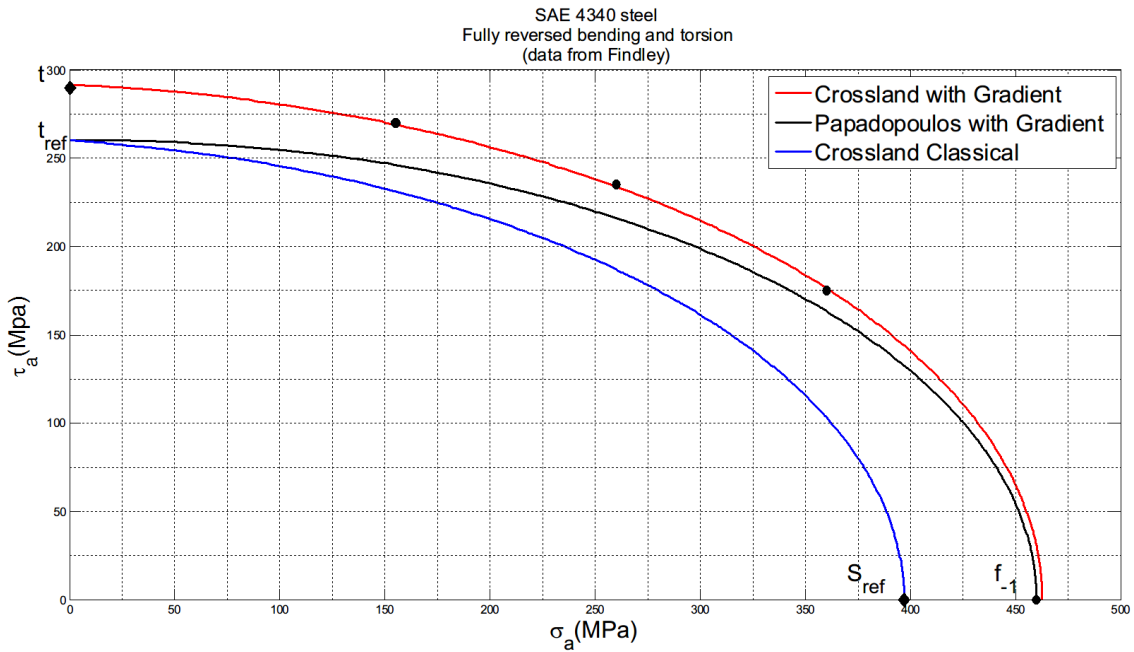


Fig. 6: Fully reversed combined bending-twisting fatigue limit data (Findley et al.[16], Papadopoulos and Panoskaltsis[15]).

2.5. Discussion

Remark 1 (Gradient terms). In this paper, the pure size effect has not been considered and only stress gradient effect is modeled.

Remark 2 (Material characteristic length scale l_g). We study here the fatigue limit of macroscopic specimens and components for which the crack initiation is generally detected by loss of stiffness corresponding to crack length which can reach a millimeter. We choose l_g ranging from 0.1 to 0.5mm. To verify the relevancy of this choice, we need more experimental data.

Remark 3 (Extensions to other criteria). The extension of the proposition to other fatigue criteria is straightforward. For instance, the modified Papadopoulos criterion [4] is written as :

$$\max T_a + a_p P_{max} - l_g \|\nabla \{\max T_a\} + a_p \nabla P_{max}\| \leq b_p. \quad (66)$$

2.6. Conclusion

The present study develops a simple formulation of gradient multi-axial fatigue criteria extending the classical HCF criteria. The objective is to model the surface gradient effects (yielding apparent size and loading effects), which is not included yet in classical mechanics but become important at small scale or in the presence of notches, by taking into account just the gradient effect. Besides, for notched fatigue problems, this approach may be still applicable.

Nevertheless, in this work only simple fatigue tests have been examined. In these tests, the gradient has a beneficial effect on fatigue. However, cases where the effect can be presumably negative, especially under the circumstances of residual stresses, can be encountered. A reexamination and validation for complex loading could be perspective for this research direction.

3 Time varying load : the standard approach

Fatigue failure is a damage accumulation process in which material property deteriorates continuously under fatigue loading and the damage depends on the size of stress and strain. With the accumulation of

fatigue damage, some accidents occur for these components. Research shows that a reliable lifetime prediction method is particularly important in the design, safety assessments, and optimization of engineering components and structures. Thus, it is important to formulate an accurate method to evaluate the fatigue damage accumulation and effectively predict the fatigue life of these components. The objective of this work is to contribute to the development life model that take into account the presence of complex variations of the stress tensor. We focus on Chaboche damage accumulation law in case of multiaxial high cycle fatigue. Heuristic formulations with different multiaxial fatigue criteria have been proposed. An application to an industrial structure is then performed.

3.1. The notion of damage in fatigue

In the case of fatigue, we usually employ the concept of the loading cycle instead of time to evaluate the evolution of damage and to measure the fatigue lifetime. The equations then depend on the load through globally defined quantities over a cycle, such as amplitude, maximum value, mean value. The growth equation of fatigue damage is therefore taken in the form:

$$\delta D = f(\dots)\delta N$$

$$\delta N = f\delta t$$

where δt is a time sampling of the history in a given number of time intervals $\delta t_1, \delta t_2, \dots, \delta t_i, \dots$ and f is the mean frequency of those cycles during the considered time step.

3.1.1. Linear and nonlinear accumulation of damage

Cumulative effects, whether linear or nonlinear, are of great importance in fatigue. The rule of linear accumulation is in fact a property of any linear or nonlinear differential equation with separable variables. One approach to variable load histories uses the concept of fraction of life(also referred to as cycle ratio) used up by an event. These fractions are added together; when their sum reaches 1.0 or 100 percent we expect failure. This is the most common measure of damage, and is the quantifying measure we use here.

The Palmgren-Miner linear rule as explained in [17] is based on the assumption that damage is accumulated additively when it is defined by the associated life ratio N_i/N_{F_i} where N_i is the number of cycles applied under a given load for which the number of cycles to fracture(under periodic conditions) would be N_{F_i} . The fracture criterion is:

$$\sum_i N_i/N_{F_i} = 1.$$

Therefore, in periodic tests, damage evolution is considered to be linear in that:

$$D = N/N_F.$$

For a test at two stress levels, the evolution is as shown schematically in Fig. 8. In fact, the linear accumulation rule can be applied even to a damage which evolves nonlinearly. For this it is sufficient that a one-to-one relationship between D and N/N_F exists, or even that the damage evolution curve be a unique function(independent of the applied cycle) of the life ratio N/N_F .

There are, therefore, two ways of defining a damage incremental law incorporating the linear accumulation rule. It can be linear of the form and shown in Fig. 7:

$$\delta D = \delta N/N_F(\dots),$$

where N_F is the number of cycles to failure defined by the chosen parametric data. The damage evolution can be nonlinear such as:

$$\delta D = \frac{(1 - D)^{-k}}{k + 1} \frac{\delta N}{N_F(\dots)}.$$

Here in any case, the damage evolution curve as function of life ratio $\delta N/N_F$ is supposed to be independent of the local state of stress (Fig. 8).

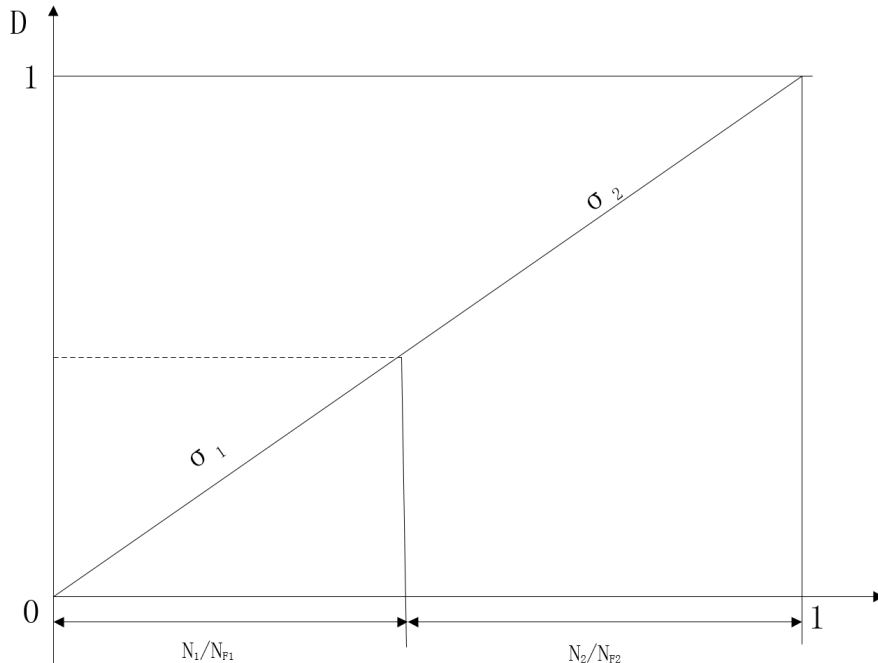


Fig. 7: Linear accumulation of damage with linear evolution

In contrast, if the damage evolution curve, as a function of the life ratio N/N_F , depends on the applied loading we have the effect of nonlinear accumulation as shown in Fig. 9. There, D_1 represents the state of internal damage at the end of the first level σ_1 . Evolution at the second level σ_2 continues from the same state, and it is clear that the sum of the life ratio is less than 1. From the point of view of the damage law, this nonlinearity always corresponds to the case where the variables which represent the load σ and the damage variable D have coupled evolution.

The Palmgren-Miner linear accumulation law gives good results only for loads for which there is little variation in the amplitude and mean value of stress. The assumption of linear damage is open to many objections. For example, sequence and interaction of events may have major influences on life, the rate of damage accumulation may depend on the load amplitude, experimental evidence often indicates that $\sum_i N_i/N_{F_i} \neq 1$ for a low-to-high or a high-to-low loading sequence.

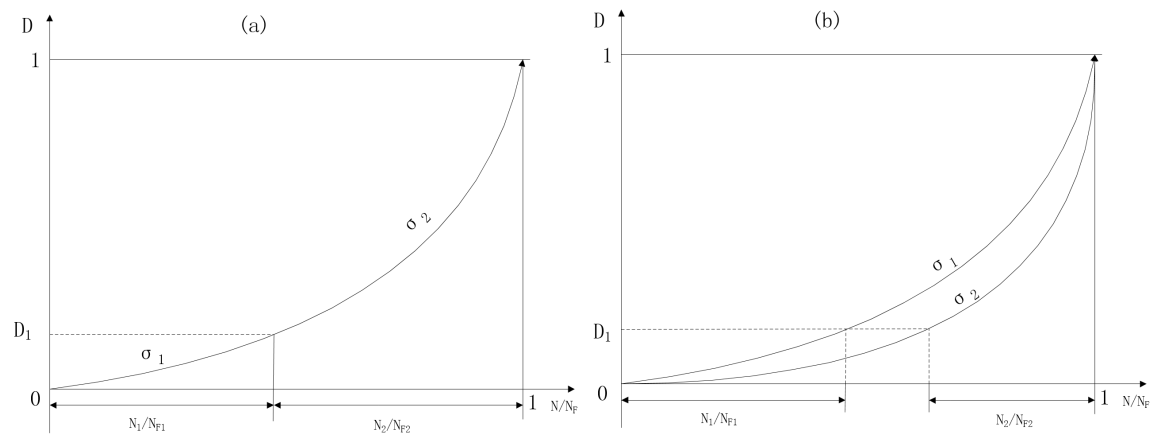


Fig. 8: Damage with nonlinear evolution and linear accumulation Fig. 9: Damage with nonlinear evolution and nonlinear accumulation

3.1.2. Classic Chaboche damage law

In periodic cyclic loadings, one way of writing a damage law which expresses the experimental results is to assume that the damage per cycle is a function of the maximum and the mean values of the stress:

$$\delta D/\delta N = f(\sigma_{Max}, \sigma_m).$$

In order to recover, after integration, one of the many forms proposed to represent the Wohler curves, we let:

$$\delta D/\delta N = \frac{\sigma_{Max} - \sigma_l(\sigma_m)}{\sigma_u - \sigma_{Max}} \left(\frac{\sigma_{Max} - \sigma_m}{B(\sigma_m)} \right)^\gamma. \quad (67)$$

with:

$$\sigma_l(\sigma_m) = \sigma_m + s_{-1}(1 - b\sigma_m) : \text{mean stress component in the fatigue limit.}$$

$$B(\sigma_m) = B_0(1 - b\sigma_m) : \text{the mean stress component in the fatigue limit.}$$

The number of cycles to failure is obtained by an obvious integration, with the condition:

$$N = 0 \rightarrow D = 0 \text{ (initial undamaged state)}$$

$$N = N_F \rightarrow D = 1 \text{ (macro-crack initiation)}$$

so that by integration Eq.(67) from $D = 0$ to $D = 1$ we get:

$$N_F = \frac{\sigma_u - \sigma_{Max}}{\sigma_{Max} - \sigma_l(\sigma_m)} \left(\frac{\sigma_{Max} - \sigma_m}{B(\sigma_m)} \right)^{-\gamma}. \quad (68)$$

Eq.(67) then writes:

$$\delta D = \delta N/N_F.$$

The constants are determined from conventional data: σ_u is usually known, s_{-1}, b fit the results on the fatigue limits with relation $\sigma_l(\sigma_m) = \sigma_m + s_{-1}(1 - b\sigma_m)$. Exponent γ is collaborated from the S-N curve for reversed conditions, by plotting σ_{Max} as function of $N_F(\sigma_{Max} - \sigma_l(\sigma_m))/(\sigma_u - \sigma_{Max})$, as deduced from Eq.(68). Coefficient $B(\sigma_m)$ is obtained from one point of the S-N curve.

Uniaxial case

The equation studied below allows us to describe the effects of nonlinear accumulation in the case of non-periodic cyclic loads[18]. A simple way to introduce such effects in the damage growth equation consists in rendering the load and damage variables non-separable. For example, we may take:

$$\delta D = D^{\alpha(\sigma_{Max}, \sigma_m)} \left(\frac{\sigma_{Max} - \sigma_m}{C(\sigma_m)} \right)^\gamma \delta N$$

The exponent α depends on the loading (σ_{Max}, σ_m) , which results in non-separability.

$$\alpha(\sigma_{Max}, \sigma_m) = 1 - a \left\langle \frac{\sigma_{Max} - \sigma_l(\sigma_m)}{\sigma_u - \sigma_{Max}} \right\rangle$$

$$M(\sigma_m) = M_0(1 - b\sigma_m)$$

The exponent α represents the internal variables(for example the hardening state of the material), which depends on the loading (σ_{Max}, σ_m) , resulting in non-separability. α allows a non-linear damage cumulative rule as it is experimentally observed. a and γ are material parameters. M_0 represent the fatigue limit and the static fracture. The coefficients γ and M_0 are determined from these experimental Woehler's curves by plotting Eq.(71) and take one point from it.

The concept of effective stress applied to fatigue provides an indirect measure. The measured evolutions are extremely nonlinear. With this concept, damage can really be measured only in the last part of the life-time, when microscopic initiations have already occurred(this is the phase of micro-propagation of defects).

And these damage evolutions are extremely nonlinear. To reproduce this phenomenological aspect it is sufficient to make a change of variable by replacing D in the previous equation by:

$$1 - (1 - D)^{\gamma+1}.$$

The differential law can be written as:

$$\delta D = [1 - (1 - D)^{\gamma+1}]^{\alpha(\sigma_{Max}, \sigma_m)} \left[\frac{\sigma_{Max} - \sigma_m}{M(\sigma_m)} \right]^\gamma \delta N \quad (69)$$

This form is more complex, but its properties are identical to the properties of the previous equation, except for the current value of damage. Now we integrate it to see how damage D evolves with cycle numbers N and the influence of different parameters. By differential calculus, we get from Eq.(69):

$$\delta[1 - (1 - D)^{\gamma+1}]^{1-\alpha} = (1 - \alpha)(\gamma + 1) \left[\frac{\sigma_{Max} - \sigma_m}{M(\sigma_m)} \right]^\gamma \delta N \quad (70)$$

The number of cycles to failure, obtained by integrating D from 0 to 1 is:

$$N_F = \frac{1}{(\gamma + 1)(1 - \alpha)} \left(\frac{\sigma_{Max} - \sigma_m}{M(\sigma_m)} \right)^{-\gamma} \quad (71)$$

and we find that $M(\sigma_m) = C(\sigma_m)(\gamma + 1)^{1/\gamma}$. In differential form, the relation (72) writes from Eq.(70) and Eq.(71):

$$\delta[1 - (1 - D)^{\gamma+1}]^{1-\alpha} = \frac{\delta N}{N_F} \quad (72)$$

When we integrate Eq.(70) from 0 to D at constant loading conditions. The damage, expressed as a function of N/N_F is:

$$D = 1 - \left[1 - \left(\frac{N}{N_F} \right)^{\frac{1}{1-\alpha}} \right]^{\frac{1}{\gamma+1}}. \quad (73)$$

This expression is in good agreement with experimental results[17].

Multiaxial case

The applied stress and strain tensors are often multiaxial and present a complex path during a loading cycle. In the case of multiaxial loading fatigue, the Chaboche model is represented by the following equation:

$$\delta D = \left(1 - (1 - D)^{\gamma+1} \right)^\alpha \left(\frac{\tilde{A}_{II}}{M(\sigma_H)} \right)^\gamma \delta N \quad (74)$$

Where the amplitude $\sigma_{Max} - \sigma_l(\sigma_m)$ is replaced by the deviatoric norm A_{II} and the average stress is replaced by the hydrostatic pressure. We should note that for an isotropic damage theory:

$$\tilde{A}_{II} = A_{II}/(1 - D)$$

$$\alpha = 1 - a \left\langle \frac{A_{II} - A_{II}^*(\sigma_H)}{\sigma_u - \sigma_{eqMax}} \right\rangle. \quad (75)$$

α represents the internal variables, characterizes the non-linearity of the damage evolution, defines the non-linear cumulation, and allows to take into account the mean stress effect and describes the damage occurrence of the material: as long as $\alpha < 1$, there is damage creation. The coefficient a gives the amount of fragility which is suggested by a given occurrence of fatigue limit violation.

A_{II} is the amplitude of octahedral shear stress given by:

$$A_{II} = \frac{1}{2} \max_i \sqrt{\frac{1}{2} \underline{\Delta s} : \underline{\Delta s}} = \sqrt{J_{2a}} = \frac{1}{2} \Delta \sigma_{eqmax}, \quad (76)$$

The quantity $A_{II}^*(\sigma_H)$ represents the infinite life fatigue limit. For example, the Sines fatigue limit criterion is formulated by the following equation:

$$A_{II}^*(\sigma_H) = s_{-1}(1 - 3b\sigma_H). \quad (77)$$

Above, s_{-1} and σ_u are respectively the fatigue limit at zero mean stress and the ultimate tensile stress. For steel, normally $s_{-1} \approx 0.48\sigma_u$.

The function $M(\sigma_H)$ in Eq.(110) quantifies the mean stress effect through Low Cycle Fatigue(LCF) loading range:

$$M(\sigma_H) = s_{-1} \left(1 - 3 \frac{\sigma_H}{\sigma_u} \right).$$

We can get the $D - N$ curve in Fig. 10 by integrating Eq.(110). This is in the case of constant loading conditions because we regard α and γ as invariable parameters.

$$N = \frac{(1 - (1 - D)^{\gamma+1})^{1-\alpha}}{(1 + \gamma)(1 - \alpha)} \left[\frac{A_{II}}{M(\sigma_H)} \right]^{-\gamma} \quad (78)$$

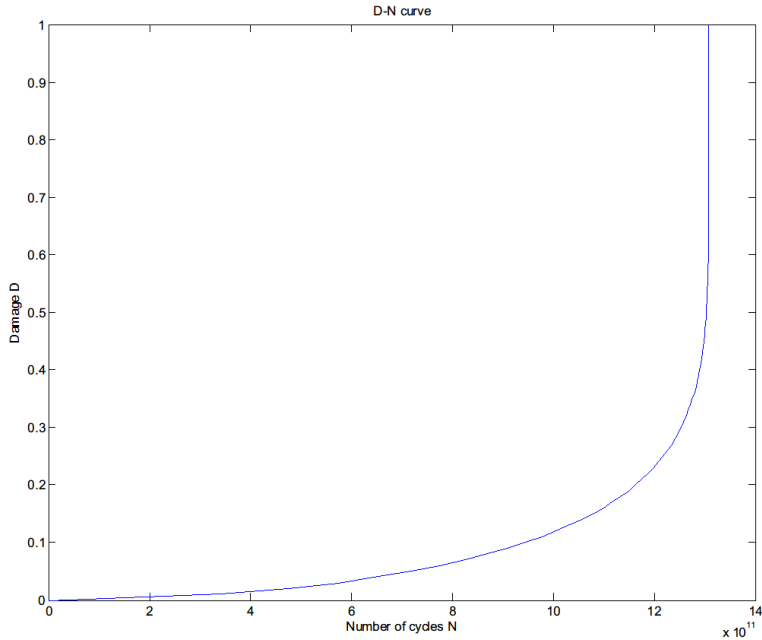


Fig. 10: Damage accumulation in terms of N in constant loading condition, with D and N are related by the evolution equation (78)

The number of cycles to failure, obtained at $D = 1$, is:

$$N_F = \frac{1}{(\gamma + 1)(1 - \alpha)} \left[\frac{\tilde{A}_{II}}{M(\sigma_H)} \right]^{-\gamma} \quad (79)$$

It should be noted that in multiaxial case the effective stress amplitude is written as:

$$\tilde{A}_{II} = \frac{\tilde{A}_{II}}{(1 - D)}$$

In Eq.(79), γ , b and a are material parameters determined from fatigue tests.

In the case of multiaxial fatigue loading, an infinite life is obtained if the stress amplitude A_{II} respects:

$$A_{II} \leq A_{II}^*(\sigma_H) = s_{-1}(1 - 3b\sigma_H). \quad (80)$$

In terms of Sines criterion which Chaboche uses, it writes:

$$\sqrt{J_{2a}} + 3bs_{-1}\sigma_H - s_{-1} \leq 0. \quad (81)$$

σ_H is the mean hydrostatic stress defined by:

$$\sigma_H = \frac{1}{6}[\max \operatorname{tr}(\underline{\underline{\sigma}}(n)) + \min \operatorname{tr}(\underline{\underline{\sigma}}(n))], \quad (82)$$

The damage is expressed the same as in uniaxial case:

$$D = 1 - \left[1 - \left(\frac{N}{N_F} \right)^{\frac{1}{1-\alpha}} \right]^{\frac{1}{\gamma+1}}. \quad (83)$$

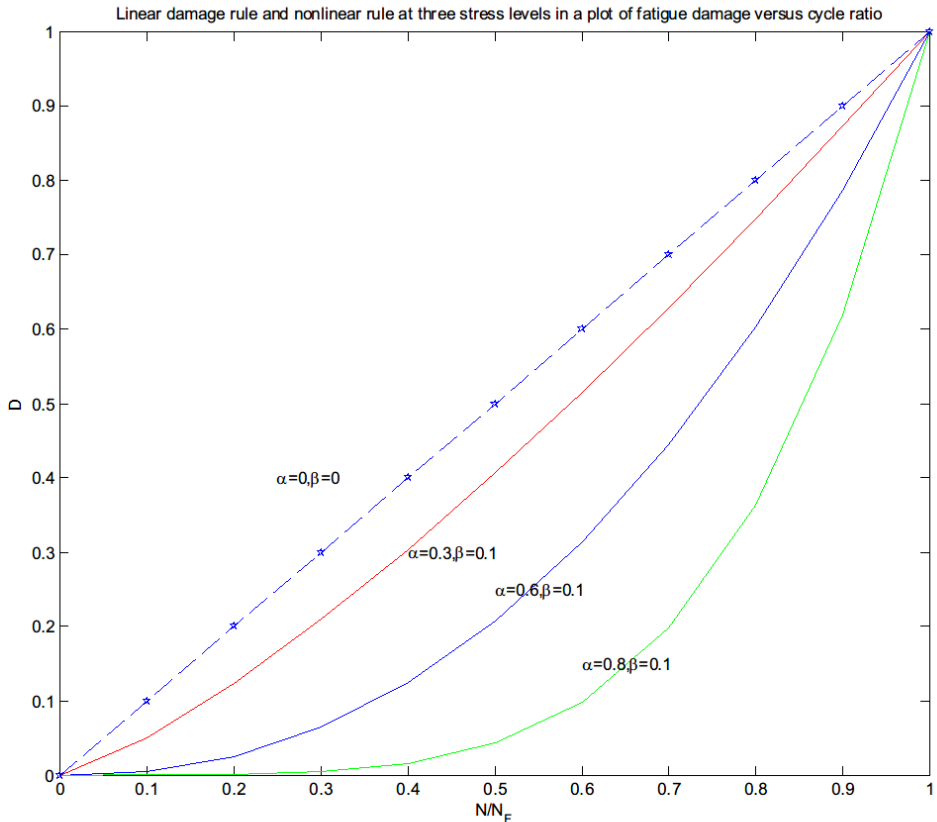
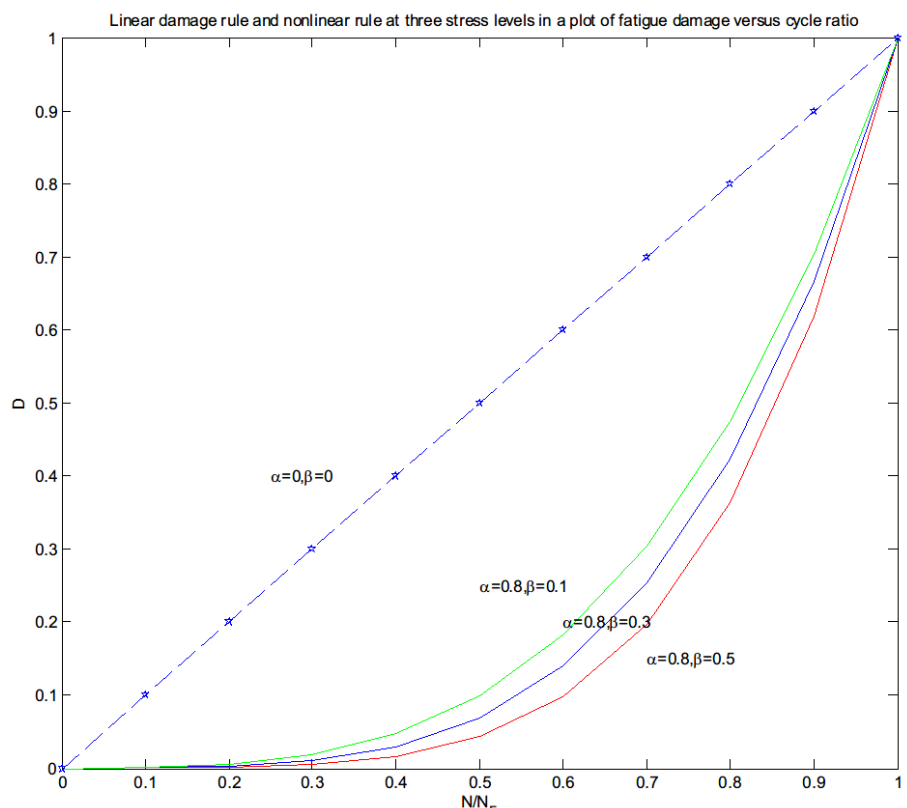


Fig. 11: Influence of function α in a plot of fatigue damage versus cycle ratio

These theories account for the nonlinear nature of fatigue damage accumulation by using nonlinear relations such as Eq.(117) where the power α depends on the load level(see Fig. 11).



3.2. Verification method of Chaboche law

Many fatigue damage accumulation models are based on the two level loading experiments which is one of the basic random loading analysis. To facilitate our verification of the law we use two-stress level loading, the specimen is firstly loaded at stress σ_1 for N_1 cycles and then at stress σ_2 for N_2 cycles until failure. We can then observe if the experimental results are satisfactory.

After N_1 cycles, we have from Eq.(117), a damage D_1 given by:

$$[1 - (1 - D_1)^{\gamma+1}]^{1-\alpha_1} = \frac{N_1}{N_{F1}} \quad (84)$$

By integrating Eq.(72) from $D = D_1$ to $D = 1$, we get:

$$1 - [1 - (1 - D_1)^{\gamma+1}]^{1-\alpha_2} = \frac{N_2}{N_{F2}} \quad (85)$$

Which yields:

$$1 - \frac{N_2}{N_{F2}} = 1 - [1 - (1 - D_1)^{\gamma+1}]^{1-\alpha_2} \quad (86)$$

From Eq.(84) and Eq.(86), after elimination of $[1 - (1 - D_1)^{\gamma+1}]$ we get:

$$\frac{N_2}{N_{F2}} = 1 - \left(\frac{N_1}{N_{F1}}\right)^{\frac{1-\alpha_2}{1-\alpha_1}} = 1 - \left(\frac{N_1}{N_{F1}}\right)^\eta \quad (87)$$

with

$$\eta = \frac{1 - \alpha_2}{1 - \alpha_1} = \frac{A_{II2} - A_{II}^*(P_{m2})}{A_{III} - A_{II}^*(P_{m1})} \frac{\sigma_u - \sigma_{eqMax1}}{\sigma_u - \sigma_{eqMax2}} = \frac{\sqrt{J_{2,a2}} - s_{-1}(1 - 3bP_{m2})}{\sqrt{J_{2,a1}} - s_{-1}(1 - 3bP_{m1})} \frac{\sigma_u - \max(2\sqrt{J_{2,a1}})}{\sigma_u - \max(2\sqrt{J_{2,a2}})} \quad (88)$$

In the case of high-low loading sequence($\sigma_1 > \sigma_2$):

$$\eta = \frac{1 - \alpha_2}{1 - \alpha_1} < 1; \frac{N_2}{N_{F2}} = 1 - \left(\frac{N_1}{N_{F1}}\right)^\eta < 1 - \frac{N_1}{N_{F1}}; \frac{N_1}{N_{F1}} + \frac{N_2}{N_{F2}} < 1$$

The cumulative damage under high-low loading sequence, as we deduced, has the addition of partial lives less than unit.

Similarly, the cumulative damage under low-high loading sequence has addition of partial lives more than 1.

$$\frac{N_1}{N_{F1}} + \frac{N_2}{N_{F2}} > 1$$

For constant two-level stress loading, $\alpha_1 = \alpha_2$, the Chaboche law returns to the Miner rule where:

$$\frac{N_1}{N_{F1}} + \frac{N_2}{N_{F2}} = 1$$

3.3. Chaboche law containing different criteria

3.3.1. Chaboche law with Crossland criterion

In the previous model we used Sines fatigue criterion constructing the damage criterion exponent α . Now we want to see Chaboche law with different criteria and compare the numerical results. Firstly, α represents the internal variables and contains the fatigue criterion, so we first change α to satisfy Crossland Criterion:

$$\alpha = 1 - a \left(\frac{\max_n \sqrt{J_{2a}}(n) + a_c P_{max}(n) - b_c}{\sigma_u - 2 \max_n \sqrt{J_{2a}}} \right). \quad (89)$$

with

$$a_c = \frac{(t_{-1} - \frac{f_{-1}}{\sqrt{3}})}{\frac{f_{-1}}{3}}, \quad b_c = t_{-1}. \quad (90)$$

$$\eta_c = \frac{1 - \alpha_2}{1 - \alpha_1} = \frac{\sqrt{J_{2,a_2}} + a_c P_{M_2} - b_c}{\sqrt{J_{2,a_1}} + a_c P_{M_1} - b_c} \frac{\sigma_u - \max(2\sqrt{J_{2,a_1}})}{\sigma_u - \max(2\sqrt{J_{2,a_2}})} \quad (91)$$

In Eq.(78), the amplitude of octahedral shear stress A_{II} remain unchanged.

3.3.2. Chaboche law with Dang Van criterion

We change α to express it through Dang Van Criterion:

$$\alpha = 1 - a \left\langle \frac{\max_n \{\tau(n) + a_D P(n)\} - b_D}{\sigma_u - 2 \max \sqrt{J_{2a}}} \right\rangle. \quad (92)$$

with

$$\tau(n) = \frac{1}{2}(\hat{\sigma}_I(n) - \hat{\sigma}_{III}(n)) \quad (93)$$

$$a_D = \frac{3t_{-1}}{f_{-1}} - \frac{3}{2}, \quad b_D = t_{-1}.$$

$$\eta_D = \frac{1 - \alpha_2}{1 - \alpha_1} = \frac{\max_t \{\tau_2(n) + a_D P_2(n)\} - b_D}{\max_t \{\tau_1(n) + a_D P_1(n)\} - b_D} \frac{\sigma_u - \max(2\sqrt{J_{2a_1}})}{\sigma_u - \max(2\sqrt{J_{2a_2}})} \quad (94)$$

In Eq.(78), we proposed to change A_{II} to $\max\tau(n)$:

$$N_F = \frac{1}{(\gamma + 1)(1 - \alpha)} \left[\frac{\max\tau(n)}{M(\sigma_H)} \right]^{-\gamma} \quad (95)$$

3.4. Numerical testing on different loading patterns

The fatigue limit with different criteria are distinctive. We compare different criteria in a $A_{II} - N_F$ figure as predicted in Eq.(79). Here γ , b and a are material parameters determined from fatigue tests.

In this case we have

$$N_F = \frac{1}{(\gamma + 1)(1 - \alpha)} \left[\frac{A_{II}}{M(\sigma_H)} \right]^{-\gamma},$$

$$M(\sigma_H) = s_{-1} (1 - 3\sigma_H/\sigma_u).$$

For Sines and Crossland criteria:

$$A_{II} = \sqrt{J_{2a}} = \frac{1}{2} \max_t \sqrt{\frac{1}{2}(\Delta s_{11}^2 + \Delta s_{22}^2 + \Delta s_{33}^2 + 2\Delta s_{12}^2 + 2\Delta s_{13}^2 + 2\Delta s_{23}^2)}.$$

For Dang Van criterion:

$$A_{II} = \max\tau(n).$$

3.4.1. Test on pure rotation

From the fatigue zone we select $r = 0.1$ as the radius to study. We select here:

$$s_{-1} = f_{-1} = 0.8 \text{ MPa},$$

$$\sigma_u = 1.67 \text{ MPa}$$

$$\gamma = 6$$

$A_{II} - N_F$ figure is shown in Fig. 13.

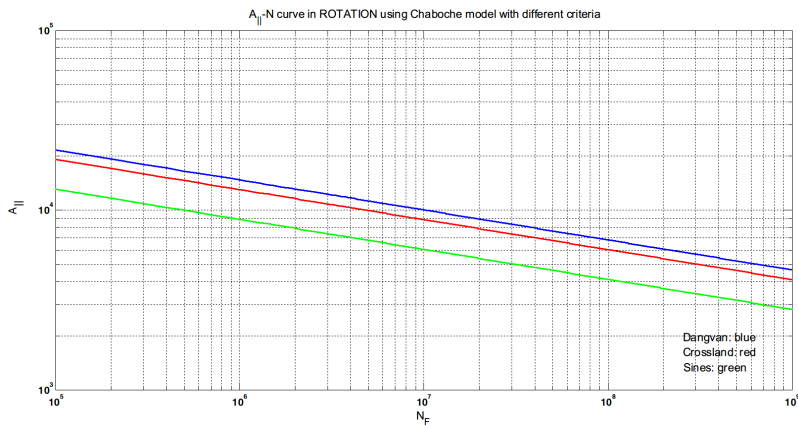


Fig. 13: $A_{II} - N_F$ curve in rotation at $r=0.1$

In pure rotation, we assume the first and second rotating speed are respectively $w_1 = 20 \text{ rpm}$ and $w_2 = 15 \text{ rpm}$.

$$A_{II1} = \sqrt{J_{2,a_1}} = 7.7606E5 \text{ Pa}$$

$$A_{II2} = \sqrt{J_{2,a_2}} = 4.3653E5 \text{ Pa}$$

$$P_{m_1} = 8.8342E5 \text{ Pa}$$

$$P_{m_2} = 4.9693E5 \text{ Pa}$$

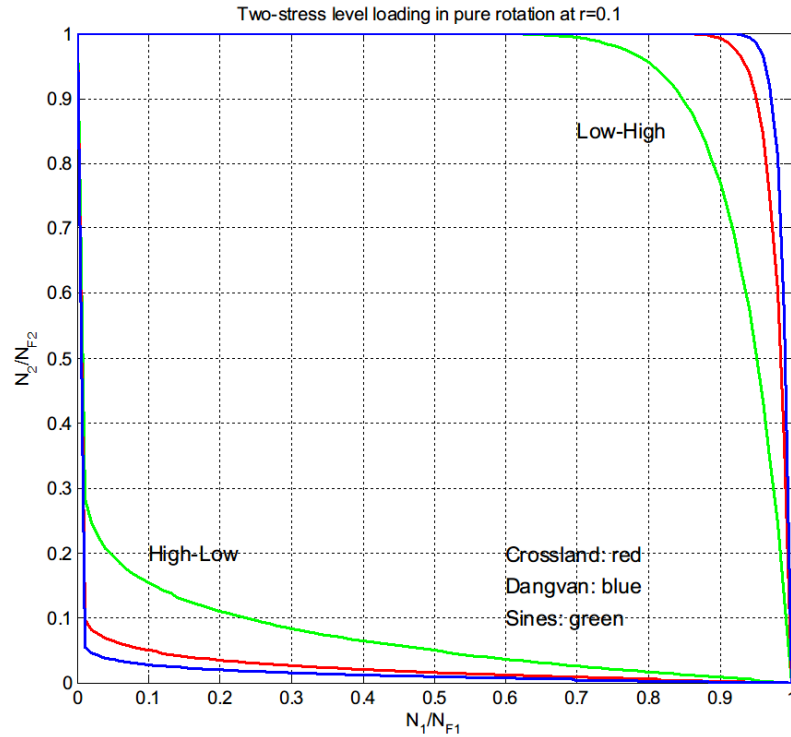
Substituting the above to Eq.(127) we can get η in High-Low sequence:

$$\eta_1 = 0.0721,$$

in Low-High sequence:

$$\eta_2 = 13.8654.$$

The predicted results are shown in Fig. 14.

Fig. 14: Two-stress level loading in pure rotation at $r=0.1$

3.4.2. Test on 4-point bending

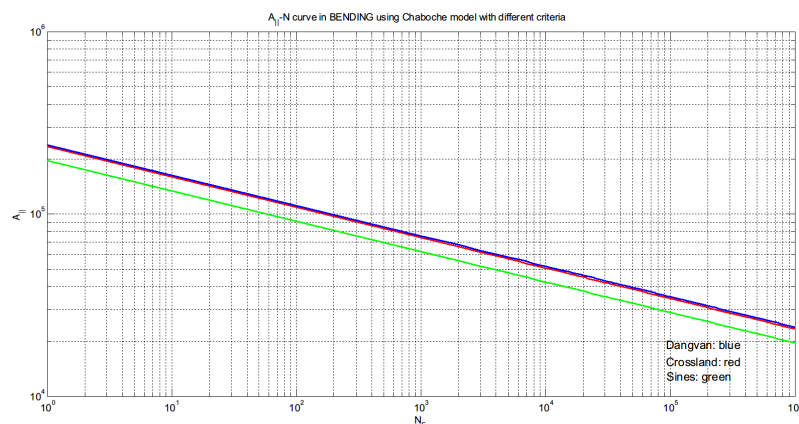
From the fatigue zone we select $y = 3$ to study. We select here:

$$s_{-1} = f_{-1} = 0.8 \text{ MPa},$$

$$\sigma_u = 1.67 \text{ MPa}$$

$$\gamma = 6$$

The $A_{II} - N_F$ figure is shown in Fig. 15.

Fig. 15: $A_{II} - N_F$ curve in 4-point bending at $y=3$

In 4-point bending, we assume the first and second loading are respectively $F_1 = 1E6N$ and $F_2 = 0.8E6N$.

$$\sqrt{J_{2a_1}} = 7.2194E5Pa$$

$$\sqrt{J_{2a_2}} = 5.7755E5Pa$$

$$P_{m_1} = 3.9298E5Pa$$

$$P_{m_2} = 3.1438E5Pa$$

Substituting the above to Eq.(127) we can get η in High-Low sequence:

$$\eta_1 = 0.3174,$$

in Low-High sequence:

$$\eta_2 = 3.1510.$$

The predicted results are shown in Fig. 16.

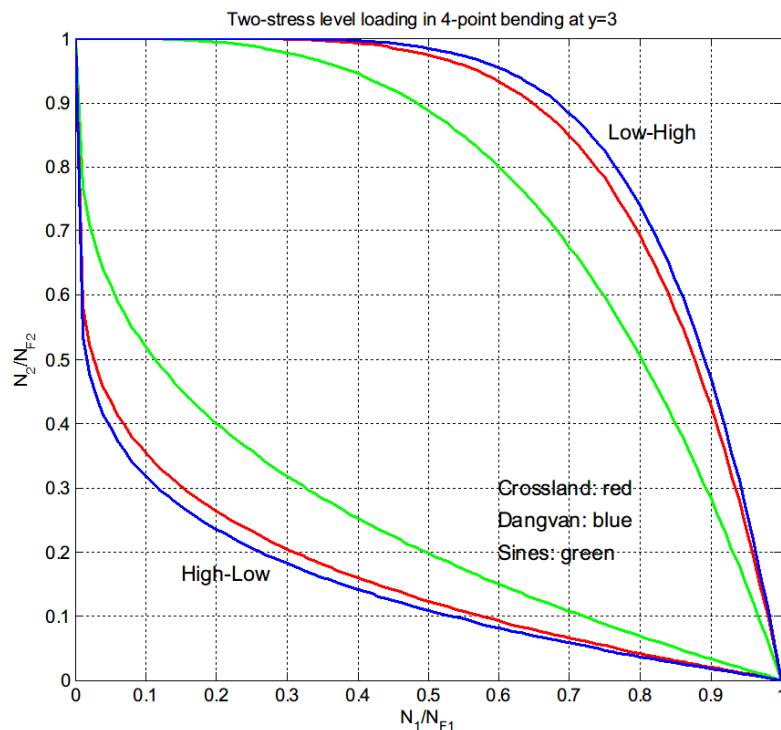


Fig. 16: Two-stress level loading in 4-point bending at $y=3$

3.4.3. Test on rotative bending

From the fatigue zone we select $r = 0.5$ as the radius to study. The $A_{II} - N_F$ figure is shown in Fig. 17.

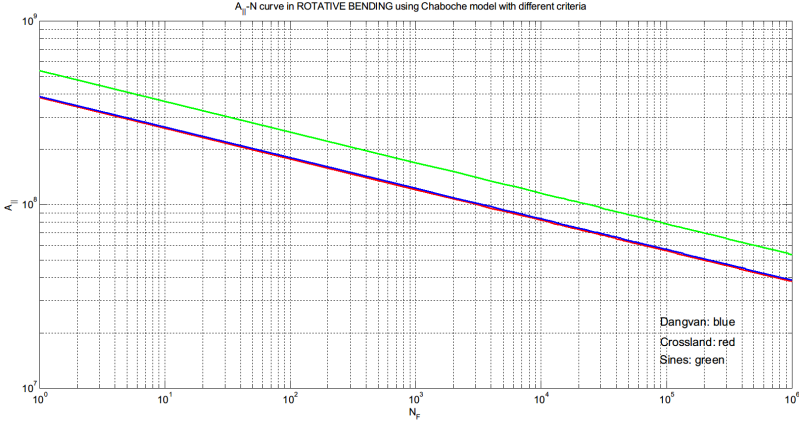


Fig. 17: $A_{II} - N_F$ curve in rotative bending at $r=3$

In rotative bending, we assume the rotating speed are $w = 5\text{ rpm}$. The applied force are respectively $F = 9E5\text{N}$ and $F = 3E5\text{N}$. We select:

$$s_{-1} = f_{-1} = 400\text{MPa}, \sigma_u = 1000\text{MPa}$$

$$\sqrt{J_{2a_1}} = 7.0226E8\text{Pa}$$

$$\sqrt{J_{2a_2}} = 6.6454E8\text{Pa}$$

$$P_{m_1} = 6.8921E8\text{Pa}$$

$$P_{m_2} = 7.1700E8\text{Pa}$$

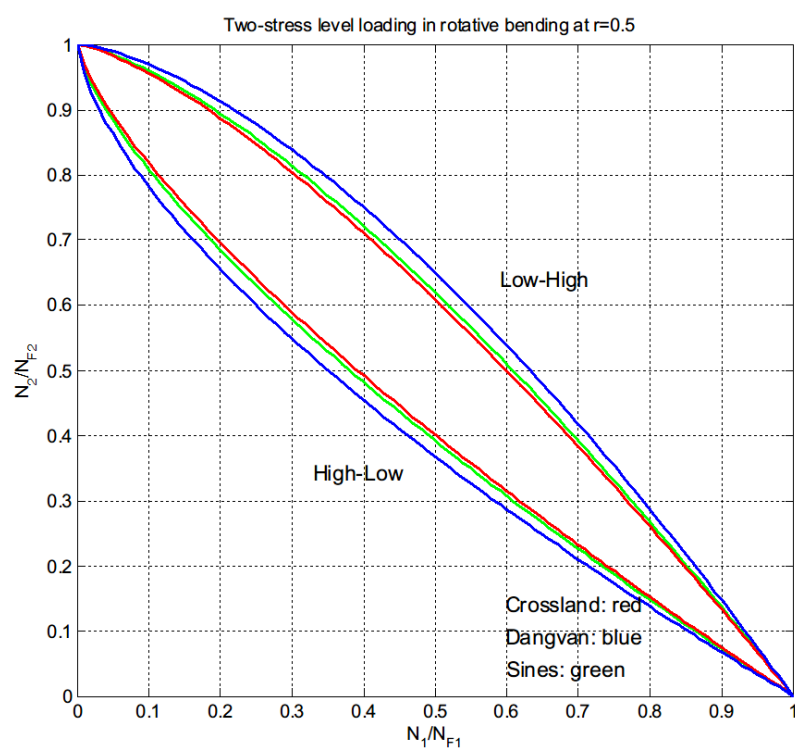
Substituting the above to Eq.(127) we can get η in High-Low sequence:

$$\eta_1 = 0.7170,$$

in Low-High sequence:

$$\eta_2 = 1.3947.$$

The predicted results are shown in Fig. 18.

Fig. 18: Two-stress level loading in rotative bending at $r=0.5$

3.5. Experimental verification of the proposed model

What makes automobile fatigue so difficult to predict is that, unlike standard tests done in a laboratory, an automobile's structure has to endure a complex, mostly random, set of static as well as cyclical stresses when in service, such as in Fig. 19 which could represent load data from testing or measurement, extracting the cyclic information can be challenging.

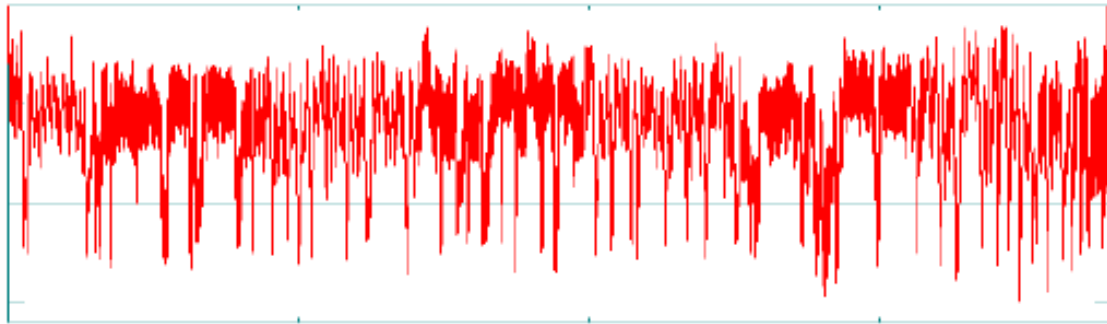


Fig. 19: Complex Cyclic Loading

3.5.1. Cycle Counting Method

The object of all cycle counting methods is to compare the effect of variable amplitude load histories to fatigue data and curves obtained with simple constant amplitude load cycles. Rainflow counting is a process to obtain cyclic data of complex loading. Its name comes from the original description from the Japanese researchers Matsuishi and Endo where they describe the process in terms of rain falling off a pagoda style roof. A more insightful description based on cyclic plasticity is usually used to explain the method.

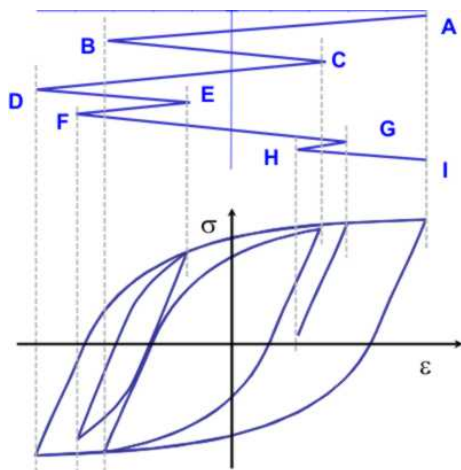


Fig. 20: Complex Cyclic Loading

In Fig. 20 a simple loading history (points A - I) is plotted vertically so that it resembles a Japanese pagoda. The resulting deformation, stresses and strains, is plotted directly below the loading history. In the lower part of the figure, four cycles are easily identified. One large overall cycle, one intermediate cycle in the center of the plot, and two smaller cycles. Each cycle has its own strain range and mean stress. From a deformation viewpoint the process proceeds as follows. Start at A, the maximum strain, and unload the material to B. Then reload to point C and unload to D. When the material reaches the strain at point B during the unloading from C to D the material remembers its prior deformation and deforms along a path from A

to D as if the event C-D never happened. This is better illustrated in the next part of the loading. Load from D to E and unload to F. Now load from F to G. When the material reaches the strain at point E during the loading from F to G the material remembers its prior deformation and deforms along a path from D to G as if the event E-F never happened. The same process occurs for G-H.

Rainflow counting will identify four cycles, A-D-I, B-C-B, E-F-E and G-H-G. Rainflow counting identifies the major load excursions, for example D to I, and treats subcycles like E-F and G-H as interruptions to the overall loading event D-I.

The five-step procedure to extract the cyclic data is summarized as follows:

1. Determine the peaks and valleys of the stress/strain during cycling, and reorder to start from the absolute maximum (Fig. 21).
2. Visualize as draining water starting at the deepest valley (Fig. 22).
3. Measure total depth drained (stress range) and mean depth (mean stress), (Fig. 22), and the number of these cycles in the load history.
4. Continue by draining the next lowest (Fig. 23) and repeat until all valleys are drained. A Rainflow cycle is counted if the second segment is vertically shorter than the first and the third segments(i.e. 6-7 is smaller than 5-6 and 7-8).
5. Use the damage rule to obtain the life from all cycles.

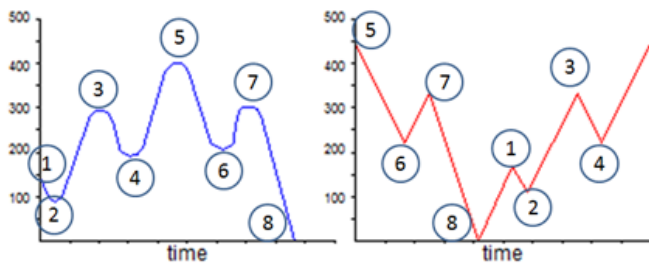


Fig. 21: Reorder to Start from Absolute Maximum

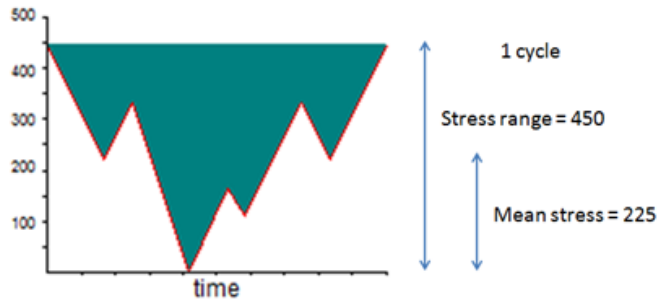


Fig. 22: Imagine Filling with Water and Extract Stress Range and Mean Stress

Once all the cycles have been categorized, the Palmgren-Miner Rule is applied. Even though the linear damage rule ignores sequence effects, it is most widely used because of its simplicity and the fact that though many nonlinear damage models have been developed, unfortunately none can encompass many of the complicating factors encountered during complex variable amplitude loading. As an example, for this case assuming mean stress is ignored:

$$\sum_i \frac{N_i}{N_{F_i}} = \frac{1}{N_{F_{450}}} + \frac{1}{N_{F_{200}}} + \frac{1}{N_{F_{50}}} + \dots = 1.$$

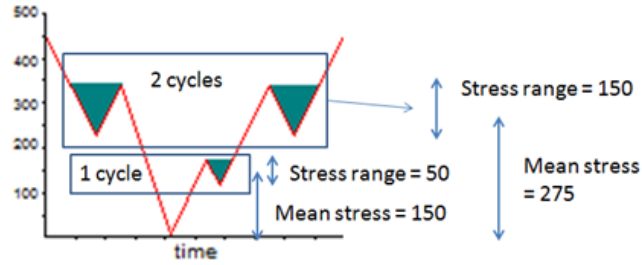


Fig. 23: Drain Water Starting at Lowest Valley and Repeat Cycle Extraction

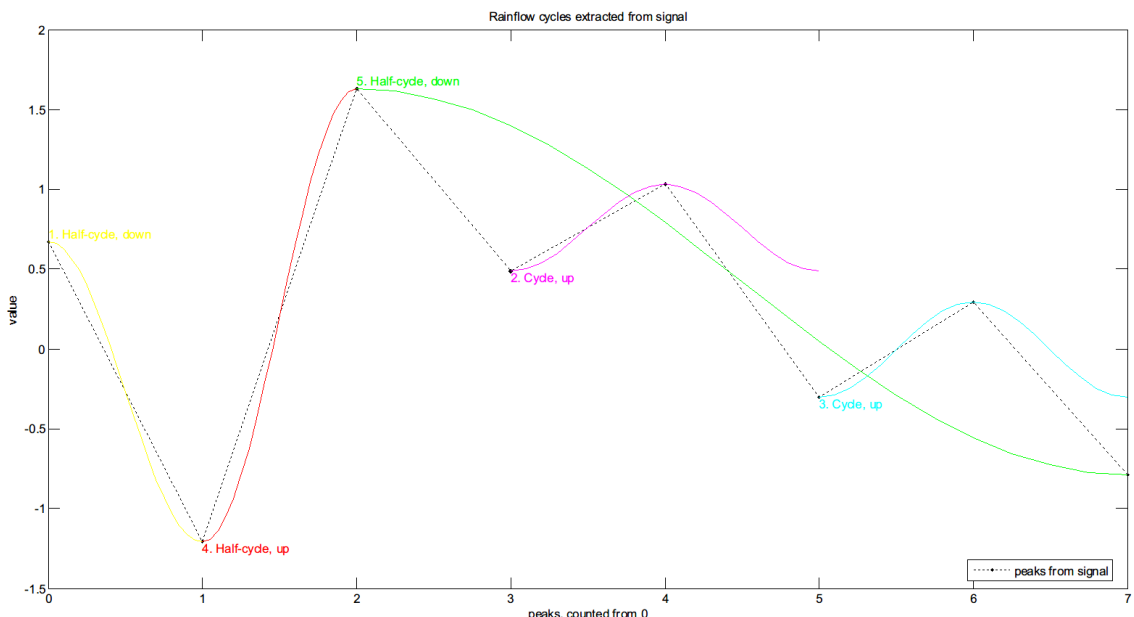


Fig. 24: Rainflow counting method demonstration

where n is replaced with the number of actual cycles of its corresponding type in the load history, for instance $N_{F_{450}}$ represents the life obtained from the $S - N$ data for a stress range of 450 MPa . From this equation, the number of total cycles through the entire load history can be found.

The rainflow procedure can be automated so that cyclic content of complex loading can be extracted efficiently. For example, fatigue computer codes such as *nCodeDesignLife* will accept files of test data, or the input of multiple load steps from a static or transient finite element analysis, and use the rainflow approach to automatically extract the cyclic data. In addition, *DesignLife* automates the Palmgrem-Miner Damage Rule calculation to determine number of cycles to failure, with the term cycle here defined as one pass through the entire time history. A computer program that accomplishes rainflow cycle counting applied to a complex history such as that in Fig. 25 results in a table of ranges and means shown in Fig. 26.

3.5.2. Using the method of plasticity accumulation

In HCF, the material undergoes elastic deformation at the macroscopic level; plastic deformation occurs only near a stress concentration area, if there is.

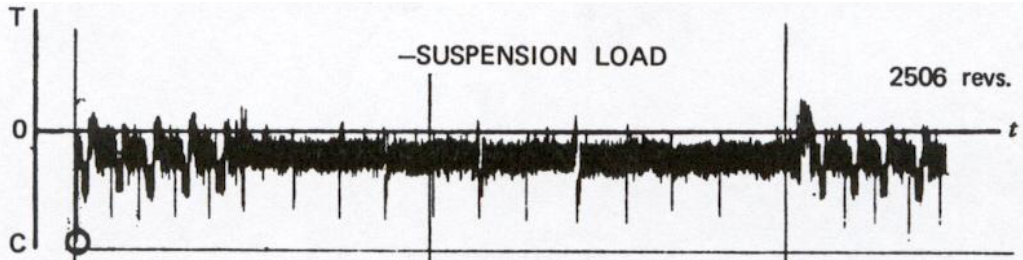


Fig. 25: Suspension load

Stress Range (MPa)	Mean Stress (MPa)														
	-500	-450	-400	-350	-300	-250	-200	-150	-100	-50	0	50	100	150	
200	8	16	24	8	6	66	358	104	6	10	6	6	4	2	
250	2	16	46	10	4	72	564	118	20	10	10	2	2	6	
300	2	8	22	6		36	312	90	14	8	4				
350		4	6			14	148	36	20	6	2				
400		2	10	6		4	64	12	10	6					
450			4			2	20	10	4				2		
500			2	2			8	12					4		
550				4	2		8	2				2			
600				2				2							
650				2	4	4	2								
700				4	2										
750			2												
800				2											
850				4	2										
900				4	4										
950				2	4	2									
1000			2			2									
1050						2									
1100															
1150															
1200															
1250															
1300															
1350					2										

Fig. 26: Example of the Number of cycles at Various Stress Ranges and Mean Stress Combinations from the Suspension Load History in Fig. 25

3.6. Discussion

The Chaboche law is based on this assumption: fatigue damage occurs and accumulates only when the loading stress is higher than its fatigue limit. However, Eq.(110) neglects the damage contribution of the loading stress which is lower than the fatigue limit. According to some experimental results such as: Lu and Zheng [19] [20] [21], Sinclair [22], and Makajima et al. [23], it has shown that the damage of low amplitude loads is one of the main reasons for prediction errors.

Impurities in the material affect the fatigue life. So does the material's hardness, and especially its surface condition. How the components were heat-treated in the factory is another factor. The operating temperature makes a difference, too. Worse still is the structural component's shape: notches and sharp corners create concentrations of stress that can initiate cracks. Thus further studies should be carried out concerning these factors.

4 Multiscale energy dissipation approach

The object of this work is to propose an energy based fatigue approach which takes into account impurities and hardness in the material which affect the fatigue life while handling multidimensional time varying

loading histories.

Our fundamental thought is to assume that the local dissipated energy at small scale governs fatigue at failure. The proposal of our model is to consider a plastic behavior at the mesoscopic scale with a dependence of the yield function not only on the deviatoric part of the stress but also on the hydro static part. A kinematic hardening under the assumptions of associative plasticity is also considered. We follow the Dang Van paradigm. The structure is elastic at the macroscopic scale. At each material points, there is a stochastic distribution of weak points which will undergo strong plastic yielding, which contribute to energy dissipation without affecting the overall macroscopic stress.

Instead of using the number of cycles, we use the concept of loading time. To elaborate real life loading history more accurately, mean stress effect is taken into account in mesoscopic yield function and non-linear damage accumulation law are also considered in our model. Fatigue will then be determined from the plastic shakedown cycle and from a phenomenological fatigue law linking lifetime and accumulated mesoscopic plastic dissipation.

4.1. Kinematic Hardening Models

4.1.1. Linear Kinematic Hardening

A hardening rule is needed to describe the behavior of the material once it is plastically deformed or yielded. One possible hardening rule is the isotropic rule, which assumes that strain hardening corresponds to an enlargement of the yield surface (i.e. an increase in yield stress) without change of shape or position in the stress space. Another is the kinematic rule, which assumes that strain hardening shifts the yield surface without changing its size or shape.

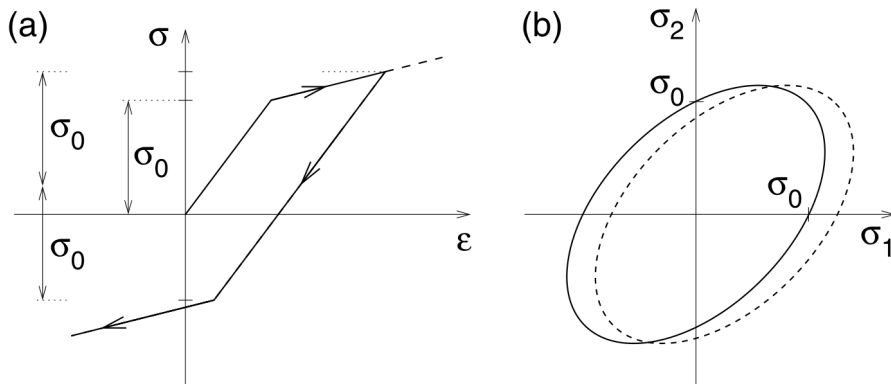


Fig. 27: Kinematic hardening: a) uniaxial stress-strain diagram, b) evolution of the yield surface in the biaxial stress plane

Kinematic hardening rules are necessary, especially for the case of unloading and cyclic loading. In Kinematic Hardening the current loading surface is assumed not to expand but to move as a rigid body within the stress space (Fig. 27(b)). The use of kinematic hardening is, for example, necessary to model the so-called Bauschinger effect (Bauschinger, 1881). This effect is often observed in metals subjected to cyclic loading. Even if the magnitudes of the yield stress in tension and in compression are initially the same, this is no longer the case when the material is preloaded into the plastic range and then unloaded. For example, after previous yielding in tension, yielding in compression may start at a stress level lower than the initial yield stress (Fig. 27(a)).

Kinematic hardening leads to a translation of the loading surface, i.e. to a shift of the origin of the initial yield surface. If the initial yield surface is described by a yield function of the form

$$f(\sigma) = F(\sigma) - \sigma_0$$

the shifted surface is obviously described by

$$f(\sigma, \sigma_b) = F(\sigma - \sigma_b) - \sigma_0$$

where σ_b is the so-called backstress that represents the center of the shifted elastic domain and plays the role of a tensorial hardening variable. Now we need a kinematic hardening law that governs the evolution of the back stress. Melan (1938b) proposed a law of the form

$$\sigma_b = \bar{H}_K \dot{\varepsilon}_p \quad (96)$$

where $\dot{\varepsilon}_p$ is the rate of effective plastic strain. According to which the rate of the back stress is proportional to the plastic strain rate. It is a macroscopic variable representing the dislocation sub-structure resistance to deformation. The proportionality factor \bar{H}_K is directly related to the plastic modulus and is derived from a simple monotonic uniaxial curve. The linear hardening law Eq.(96) is often credited to Prager (1955, 1956); we will call it the MelanPrager hardening rule.

4.1.2. Non-linear Kinematic Hardening

To describe cyclic plasticity, one of the famous model is the non-linear kinematic hardening model formulated by Armstrong and Frederick. It is based on a physical mechanism of strain hardening and dynamic recovery and is capable of simulating the multiaxial Bauschinger effect (movement of the yield surface in the stress space). Therefore, the model has been examined and implemented in commercial software and finite element analysis.

The Armstrong-Frederick model (AF) is a modification of the MelanPrager linear kinematic hardening model. The only modification of this simple model is the "recal" term which changes the evolution law for the symmetric backstress tensor σ_b from a classical linear kinematic hardening law (MelanPrager) to a nonlinear kinematic hardening law. The term is proportional to the current back stress multiplied by the norm of the plastic strain rate. According to the Armstrong-Frederick rule, the evolution of the back stress is governed by the differential equation:

$$\dot{\sigma}_b = \underbrace{\bar{H}_K \dot{\varepsilon}_p}_{\text{lin.kin.hardening}} - \underbrace{\gamma \dot{p} \sigma_b}_{\text{recall-term,nonlinearhardening}} \quad (97)$$

where \dot{p} is the accumulated plastic strain rate given as $\sqrt{\frac{2}{3} \|\dot{\varepsilon}_p\|}$. The constants \bar{H}_K and γ are determined from uniaxial tests. At the onset of yielding, the back stress is still zero and Eq.(97) gives the same response as the linear hardening law Eq.(96). As the back stress develops, the additional term becomes activated and slows down the rate at which the back stress grows (i.e. reduces the tangent plastic modulus).

4.2. Existing Energy Based Fatigue Models

4.2.1. Energy dissipation based on law of thermodynamics

In case of shell model. We assume the temperature in the thickness direction does not change. Based on the first and second law of thermodynamics, for any point M, we define $T(M, t)$ is the temperature field of M at time t . Its 2D heat transfer function is [24]:

$$\rho C \frac{\partial T(M, t)}{\partial t} - k \Delta_2 T(M, t) + \frac{2\sigma_e \varepsilon_m T(M, t)^4}{e} + \frac{2h}{e} [T(M, t) - T(M, t)^{air}] = d_1(M, t) + S_{th}(M, t) + r(M, t)$$

ρ is the density of the steel, C is specific heat capacity, k is heat transfer coefficient, σ_e is the bolzmann constant, ε_m is the surface thermal emissivity, h is heat convection factor, $T(M, t)^{air}$ is the environment temperature at point M, Δ_2 is two dimensional Laplace operator. $d_1(M, t)$ is the dissipative source of fatigue relevant irreversible strain ε_{ir} , strain hysteresis ε_{ve} and micro structure deformation; $S_{th}(M, t)$ is the thermoelastic source composing of elastic strain ε_e ; $r(M, t)$ is thermal radiation term.

In a single cycle the dissipated energy is only a function of dissipative source $d_1(M, t)$:

$$E_{d_1}(t) = \int_{t-\frac{t_f}{2}}^{t+\frac{t_f}{2}} d_1(t) dt$$

Experiments with different stress amplitude loadings shows that the correlation coefficient between dissipated energy in one cycle and fatigue life is more than S-N curve.

$$\lg E_{d_1}^m = -0.77 \lg N_F + 8.33 \text{ correlation coefficient: 0.94}$$

$$\lg \sigma_a = -0.13 \lg N_F + 2.85 \text{ correlation coefficient: 0.89}$$

4.2.2. Energy dissipation based on strain energy density

In their fatigue criterion, Froustey et al. (1992) have considered a complete cycle of stresses. They use the mean value on one cycle of the volumic density of the elastic strain energy, W_a , whatever the point M in the mechanical part.

$$W_a(M) = \frac{1}{T} \int_0^T \frac{1}{2} \sigma_{ij}(M, t) \varepsilon_{ij}^e(M, t) dt$$

where $\sigma_{ij}(M, t)$ and $\varepsilon_{ij}^e(M, t)$ are respectively the tensor of stresses and the tensor of elastic strains at the considered point M function of time T . Usually the endurance limit is low enough to consider that the material remains elastic at the macroscopic scale (Lemaitre and Chaboche, 1988). Thus, W_a can be considered as the mean value on one cycle of the total strain energy density at the considered point.

In 1998 Thierry PALIN-LUC and Serge LASSEUR proposed the failure criterion of W_a :

Their studies show that another limit, called σ^* , can be defined below the usual endurance limit of the material, σ_D . At a considered point a stress amplitude below this new limit does not initiate observable damage at the microscopic scale (no micro-cracks).

From σ^* and by analogy with a sinusoidal traction load the corresponding mean value of the strain energy volumetric density, W_{a^*} , can be calculated, where E is the Young modulus of the material.

$$W_{a^*} = \frac{\sigma^{*2}}{4E}$$

Around each point it is always possible to define the volume $V^*(C_i)$ by the set of points M where $W_a(M)$ is higher than $W_{a^*}(C_i)$. They postulate that the part of $W_a(M)$ exceeding $W_{a^*}(C_i)$ is the damaging part of the strain energy volumetric density. $\bar{\omega}_a(C_i)$ is the volumetric mean value of the strain energy around the critical point C_i

$$V^*(C_i) = \{ \text{points } M(x, y, z) \text{ around } C_i \text{ such that } W_a(M) \geq W_{a^*}(C_i) \}$$

$$\bar{\omega}_a(C_i) = \frac{1}{V^*(C_i)} \int \int \int_{V^*(C_i)} [W_a(x, y, z) - W_{a^*}(C_i)] d\nu$$

This stress limit σ^* can be estimated from fatigue test results in fully reversed tension and in rotating bending

$$\sigma^* = \sqrt{2(\sigma_{Ten,-1}^D)^2 - (\sigma_{RotBend,-1}^D)^2}$$

4.2.3. A critical plane approach based on energy concepts

$$W(t) = \frac{1}{2} \sigma(t) \varepsilon(t) \operatorname{sgn}[\sigma(t), \varepsilon(t)]$$

$$\operatorname{sgn}(x, y) = \frac{\operatorname{sgn}(x) + \operatorname{sgn}(y)}{2}$$

$\operatorname{sgn}(x), \operatorname{sgn}(y) = 0, 1, -1$ for distinguishing positive and negative works in a fatigue cycle[26].

If the stress and strain reach their maximum values, σ_a and ε_a , then the maximum energy density value is

$$W_a = \frac{1}{2} \sigma_a \varepsilon_a$$

In the case of high-cycle fatigue, when the characteristic $(\sigma_a - N_F)$ is used, the axis σ_a should be replaced by W_a , where

$$W_a = \frac{\sigma_a^2}{2E}$$

In the case of low and high-cycle fatigue, when the characteristic $(\varepsilon_a - N_F)$ is used, we can do similar rescaling. We assume

$$\sigma_a = \sigma'_f (2N_F)^b$$

From Manson-Coffin-Basquin equation we obtain

$$\begin{aligned} \varepsilon_a &= \varepsilon_a^e + \varepsilon_a^p = \frac{\sigma'_f}{E} (2N_F)^b + \varepsilon'_f (2N_F)^c \\ W_a &= \frac{1}{2} \sigma_a \varepsilon_a = \frac{\sigma_a}{2} \left[\frac{\sigma'_f}{E} (2N_F)^b + \varepsilon'_f (2N_F)^c \right] = \frac{(\sigma'_f)^2}{2E} (2N_F)^{2b} + 0.5 \varepsilon'_f \sigma'_f (2N_F)^{b+c} \end{aligned}$$

Fatigue characteristic for high-cycle fatigue takes the form

$$W_a = \frac{(\sigma'_f)^2}{2E} (2N_F)^{2b}$$

For the stress model we have:

$$\lg N_F = A - m \lg \sigma_a$$

For the energy model we have:

$$\lg N_F = A' - m' \lg W_a$$

m' is slope of fatigue curve expressed by energy.

4.3. Weakening scales and yield function

4.3.1. The concept of weakening scales

We follow the Dan Van paradigm. The structure is elastic at the macroscopic scale. At each material points, there is a stochastic distribution of weak points which will undergo strong plastic yielding, without contributing to the overall macroscopic stress. From a microscopic point of view, there is a distribution of weakening scales, namely $s \in [1, \infty)$. Let S_{max} be the macroscopic stress intensity at present time. Let σ_y be the yield limit before weakening. Then we imagine that for a given scale s :

- either $1 \leq s \leq \sigma_y/S_{max}$, then $S_{max} \leq \sigma_y/s$, the material stays in the elastic regime and there is no energy dissipation at this scale.
- or $\sigma_y/S_{max} \leq s \leq \infty$, then $S_{max} \geq \sigma_y/s$, the material is in the plastic regime and there is dissipated energy at scale s , contributing to the fatigue limit, which evolve through kinematic hardening.

In more details, at each scale s of a plastic evolution process there is a weakened yield limit σ_y/s , zero initial plastic strain $\underline{\varepsilon}_p$ and zero initial backstress \underline{b} at initial time t_0 .

4.3.2. Distribution of weakening scales

We assume the weakening scales have a probability distribution of power law:

$$P(s) = Cs^{-\beta},$$

where β is a material constant and C is hardening constant. The choice of a power law has two reasons: on one hand, this type of distribution corresponds to a scale invariant process, on the other hand it leads

in cyclic loading to a prediction of a number of cycles to life limit as a power law function of the stress intensity. More general laws can also be proposed.

The integrated probability ranging from macroscopic to microscopic stress is unity. From this we can conclude:

$$\int_1^\infty P(s)ds = \left[\frac{Cs^{1-\beta}}{1-\beta} \right]_1^\infty = 0 - \frac{C}{1-\beta} = 1.$$

Then we know $C = \beta - 1$, so the distribution is given by:

$$P(s) = Cs^{-\beta} = (\beta - 1)s^{-\beta}$$

and it is shown in Fig. 28.

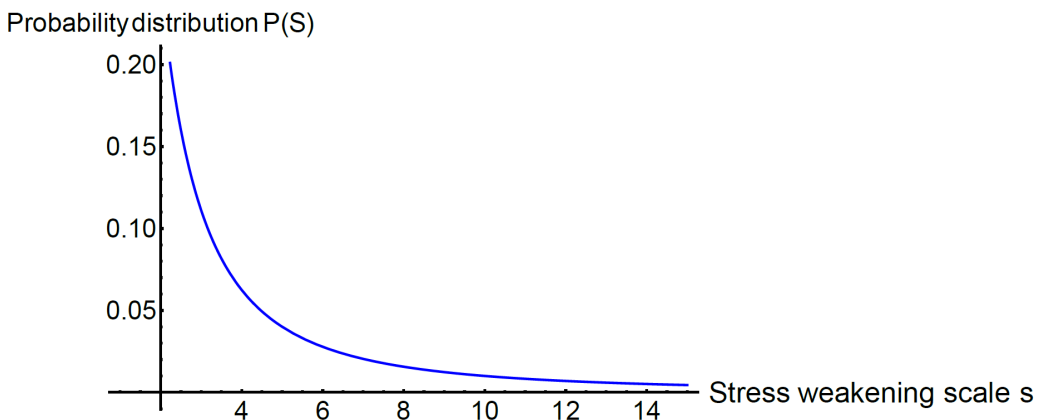


Fig. 28: Weakening scales s probability distribution curve

4.3.3. Yield function with mean stress effect

Positive mean stress clearly reduces the fatigue life of the material. In design evaluation of multiaxial fatigue with mean stress, a simplified, conservative relation between mean stress and equivalent alternating stress is necessary. We can improve the model by modifying the yield function σ_y and the localization tensor.

Christensen approach We can improve the model by modifying the yield function σ_y and the localization tensor. There are several different models of yield function (Johnson Cook model if there is strain hardening, Christensen for mean stress effect), or we could integrate yield function with damage. Moreover, Sylvain Calloc at ENSTA Bretagne may have physical evidence and interpretation on the thermal dissipation in fatigue loading.

The yield function that was given by Christensen[27] integrates measures of damage, as well as intrinsic yield strength and concept of transitions. The derived yield function formalism resulted in the form as:

$$\frac{\alpha K}{\sqrt{3}}\sigma_{kk} + \frac{(1+\alpha)^2}{2}s_{ij}s_{ij} \leq \frac{K^2}{(1+\alpha)}, \quad (98)$$

where α changes the shape of the yield function, thus it is called the shape parameter.

$$\alpha = \frac{|\sigma_{11}^C|}{\sigma_{11}^T} - 1,$$

the new parameter K is called the ideal or intrinsic strength which uniformly expands or contrasts the yield function, thus is called the scale parameter:

$$K = \frac{(\sigma_{11}^C)^2}{\sqrt{3}\sigma_{11}^T}.$$

The intrinsic strength would occur if there were no damage or microstructure disturbance. σ_{11}^C and σ_{11}^T are respectively compressive and tensile yield stress in uniaxial states ($|\sigma_{11}^C| \geq \sigma_{11}^T$, for ductile materials, $\frac{1}{2} \leq \frac{|\sigma_{11}^C|}{\sigma_{11}^T} \leq 1$). The yield stress in uniaxial and shear states are give by:

$$\begin{aligned}\sigma_{11}^C &= \frac{-\sqrt{3}K}{(1+\alpha)} \\ \sigma_{12}^Y &= \frac{K}{(1+\alpha)^{3/2}} \\ \sigma_{11}^T &= \frac{\sqrt{3}K}{(1+\alpha)^2}.\end{aligned}\quad (99)$$

At $\alpha = 0$, relations Eq.(98) and Eq.(99) show the behavior to be that of purely Mises type. This is taken to be the ideal condition where the intrinsic strength K solely determines the yield strength. As the shape parameter increases beyond the value $\alpha = 1$, the yield function behaves in accordance with a state of increasing crack density or any other physical weakening. The term fracture, as used here for behavior at or near $\alpha = 1$, actually corresponds to fracture mechanics for non-interacting cracks. Beyond this range near $\alpha = 1$ or $\alpha \rightarrow \infty$ has simply been called yield or failure. Parameter α could be easily viewed as a damage measure or microstructure parameter since it represents microstructure changes on any scale that causes deviation from the ideal state.

It is concluded a decrease in mean stress σ_{kk} reduces the effective value of α . That is, moving the behavior toward ductile case. Alternatively, increasing the mean stress moves α toward larger values, which is taken to be that of brittle behavior.

The fully expanded form of the yield function Eq.(98) is:

$$\begin{aligned}&\frac{\alpha K}{\sqrt{3}}(\sigma_{11} + \sigma_{22} + \sigma_{33}) \\ &+ (1+\alpha)^2 \left[\frac{(\sigma_{11} - \sigma_{22})^2 + (\sigma_{22} - \sigma_{33})^2 + (\sigma_{33} - \sigma_{11})^2}{6} + (\sigma_{12}^2 + \sigma_{23}^2 + \sigma_{31}^2) \right] \\ &\leq \frac{K^2}{(1+\alpha)}.\end{aligned}\quad (100)$$

The most compact form of Eq.(98) is:

$$\frac{1}{2} s_{ij} s_{ij} \leq \eta K^2, \quad (101)$$

where η is a nondimensional scaling factor on K^2 , determined by mean normal stress.

$$\eta = \frac{1 - \frac{\alpha(1+\alpha)}{\sqrt{3}K} \sigma_{kk}}{(1+\alpha)^3} < 1$$

The mean stress σ_{kk} has a positive relationship with the shape parameter α . We suppose the material endures transition from ductile to brittle when α reaches 1. That means α has a very similar physical meaning with the damage parameter D .

The Gerber parabola Several models are available addressing the influence of tensile mean stress on fatigue life. Among these are the Gerber (Germany, 1874), Goodman (England, 1899), and Soderberg (USA, 1930) models. The modified Goodman criterion is often used as a design criterion because it is more conservative than the Gerber criterion. The use of the Gerber criterion in the determination of member size is generally more computationally intensive and so rather unattractive for many designers.

The effect of mean stress on the fatigue strength is commonly presented in Haigh diagrams as shown in Fig. 29, where S_a/S_f is plotted against S_m/S_u . So is the fatigue strength at a given life under fully reversed

$(S_m = 0, R = -1)$ conditions. S_u is the ultimate tensile strength. S_f is the reversed fatigue strength. The data points thus represent combinations of S_a and S_m giving that life. The results were obtained for small unnotched specimens, tested at various tensile mean stresses. The straight lines are the modified Goodman and the Soderberg lines, and the curved line is the Gerber parabola. These are empirical relationships that are represented by the following equations:

$$\text{Modified Goodman: } S_a/S_f + S_m/S_u = 1$$

$$\text{Gerber: } S_a/S_f + (S_m/S_u)^2 = 1$$

$$\text{Soderberg: } S_a/S_f + S_m/S_y = 1$$

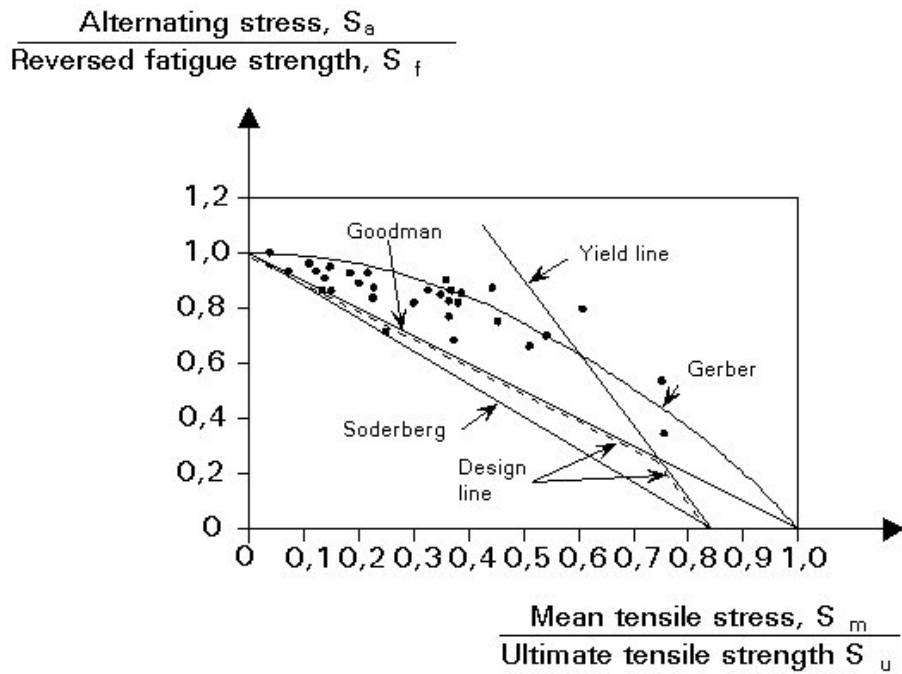


Fig. 29: Haigh diagram showing test data points for the effect of mean stress, and the Gerber, modified Goodman and Soderberg relations.

The idea is to consider as in Maitournam and Krebs[28] that the yield limit σ_y can be reduced in presence of positive mean stress. The mesoscopic yield function can therefore be written as:

$$f(s) = \|\underline{\underline{S}}(s) - \underline{\underline{b}}(s)\| + (\lambda \Sigma_H - \sigma_y)/s \leq 0 \quad (102)$$

with $\underline{\underline{S}}$ denoting the deviatoric part of the stress tensor at microscale, and $\underline{\underline{b}}(s)$ the corresponding backstress at the same scale. The material remain in elastic regime when $f < 0$ and in plastic regime when $f = 0$.

4.3.4. Local plastic model

First we should describe the mesoscopic stress state. The model considers a plastic behavior at the mesoscopic scale. The mesoscopic evolution equations are thus:

$$\dot{\underline{\underline{S}}}(s, M, t) = \text{dev}\dot{\underline{\underline{\Sigma}}}(M, t) - \frac{E}{1 + \nu} \dot{\epsilon}^p(s, M, t), \quad (103)$$

which defines a Taylor-Lin scale transition model with unit localization tensor[29].

$$\dot{\underline{\underline{b}}}(s, M, t) = \frac{kE}{E - k} \dot{\epsilon}^p(s, M, t), \quad (104)$$

which is our isotropic kinematic hardening model.

$$\underline{\dot{\varepsilon}}^p(s, M, t) = \gamma \frac{\partial f(s, M, t)}{\partial \underline{S}}, \quad (105)$$

which is the associated plastic flow rule assuming $\gamma = 0$ when $f < 0$ and $\gamma \geq 0$ when $f = 0$.

Here E denotes the Young's modulus and k the hardening parameter. The local dissipated energy rate per volume at weakening scales s is given by the local entropy dissipation:

$$\dot{w}(s, M, t) = (\underline{S} - \underline{b})(s, M, t) : \underline{\dot{\varepsilon}}^p(s, M, t). \quad (106)$$

4.3.5. Energy dissipation in shear cycle with mean stress

Calibration on 39NiCrMo3 steel Monotonic properties of the 39NiCrMo3 steel:

Young modulus $E = 206000 \text{ MPa}$

Tensile strength $\sigma_u = 856 \text{ MPa}$

Tensile yield strength $\sigma_y = 625 \text{ MPa}$

Table 2: Torsion test results on the 39NiCrMo3 steel

$\tau_m = 0$		$\tau_m = 45 \text{ MPa}$		$\tau_m = 90 \text{ MPa}$	
τ_a	N_f	τ_a	N_f	τ_a	N_f
255	5,00E+06	240	5,00E+06	240	5,00E+06
255	5,00E+06	255	5,00E+06	240	5,00E+06
255	5,00E+06	255	5,00E+06	240	5,00E+06
255	5,00E+06	255	3,54E+06	240	5,00E+06
255	5,00E+06	255	5,00E+06	255	2,29E+06
270	2410000	255	5,00E+06	255	5,00E+06
270	1076000	255	5,00E+06	255	2,53E+06
270	1720000	255	5,00E+06	255	2,95E+06
270	1263000	270	2516000	255	5,00E+06
270	5,00E+06	270	1397000	255	3,85E+06
270	1,58E+06	270	7,24E+05	255	3,21E+06
285	697000	270	2,55E+06	270	6,55E+05
285	2,89E+05	270	2,05E+06	270	1,06E+06

The results are plotted in Fig. 30. Collaborated parameters are shown in Table. 3.

4.4. Construction of an energy based fatigue approach

In a preliminary step, we will consider a simple macroscopic loading history $\underline{\Sigma}(M, t)$ which is uniaxial and time periodic of deviatoric amplitude S_{max} , and a Von Mises flow rule to see if we get a prediction of local failure for a number of cycles N_F varying as $\Sigma^{-\beta}$.

In uniaxial cyclic loading, there will be 3 kinds of loading patterns, as is shown in Fig. 31:

1. Elastic regime, in phase 2 and 4, where $\underline{\dot{\varepsilon}}^p(s, M, t) = 0$, and $|\underline{S} - \underline{b}| < (\sigma_y - \lambda \Sigma_H) / s$.

Table 3: Parameter comparison of SM45C

	Yield stress(MPa)	W_F	β	k	λ
$\tau_m = 0 \text{ MPa}$	625	1.336E10	13.92	0.3404	0
$\tau_m = 45 \text{ MPa}$	625	5.102E11	6.671	0.506	1.734
$\tau_m = 90 \text{ MPa}$	625	4.907E12	7.221	0.9293	3.003

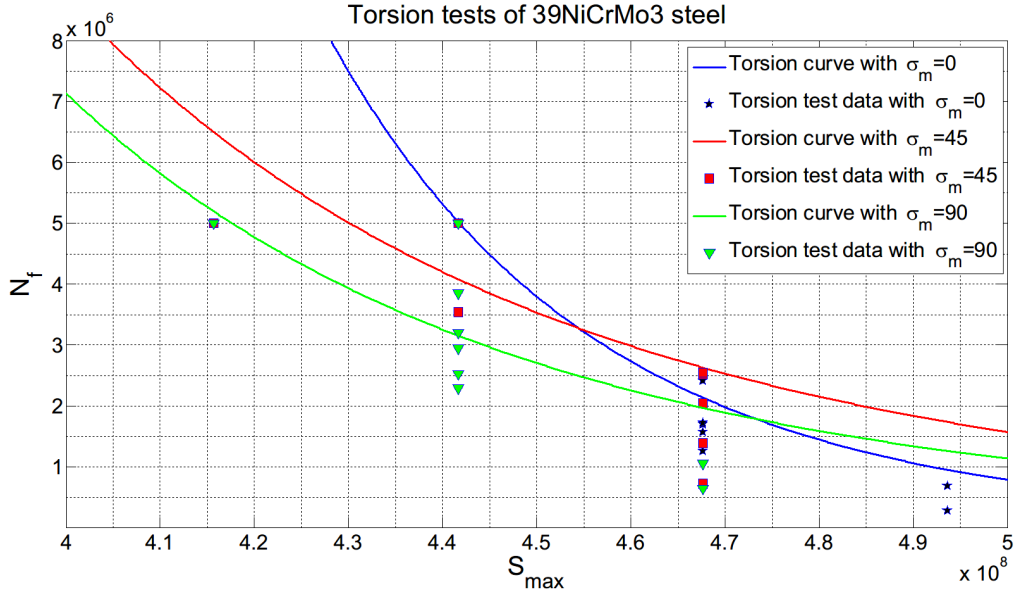


Fig. 30: Torsion test with mean stress

2. Plastic regime according to plastic flow rule, with increasing plastic deformation, in phase 5 and 1, where $\underline{\dot{\varepsilon}}^p(s, M, t) = \gamma \frac{\underline{S}(s) - \underline{b}(s)}{\|\underline{S}(s) - \underline{b}(s)\|} > 0$ with $\gamma = (dev \dot{\Sigma}) \left(\frac{kE}{E-k} + \frac{E}{1+\nu} \right)^{-1}$, with $\underline{S} - \underline{b} = (\sigma_y - \lambda \Sigma_H) / s$ and $\dot{\underline{S}} - \dot{\underline{b}} = 0$.
3. Plastic regime in the other direction, in phase 3, there is $\underline{\dot{\varepsilon}}^p(s, M, t) < 0$, then $\underline{S} - \underline{b} = -(\sigma_y - \lambda \Sigma_H) / s$ and $\dot{\underline{S}} - \dot{\underline{b}} = 0$

Phase 1: The deviatoric stress amplitude increases from σ_y / s to S_{max} .

The material is in local plastic regime, then $\dot{\varepsilon}^p > 0$ and $\dot{\sigma} - \dot{b} = 0 \Rightarrow \dot{\Sigma} - \frac{E}{1+\nu} \dot{\varepsilon}^p = \frac{kE}{E-k} \dot{\varepsilon}^p \Rightarrow$

$$\dot{\varepsilon}^p = \frac{(E-k)(1+\nu)}{E(E+k\nu)} \dot{\Sigma}.$$

$$\Rightarrow \dot{\varepsilon}^p \text{ varies from 0 to } \frac{(E-k)(1+\nu)(S_{max} - \sigma_y / s)}{E(E+k\nu)}.$$

From Taylor-Lin scale transition model:

$$\dot{\sigma} = \dot{\Sigma} - \frac{E}{1+\nu} \dot{\varepsilon}_p = \dot{\Sigma} - \frac{E-k}{E-\nu k} \dot{\Sigma} = \frac{k(1-\nu)}{E-k\nu} \dot{\Sigma}.$$

$$\Rightarrow \sigma \text{ varies from } \sigma_y / s \text{ to } \sigma_y / s + \frac{k(1-\nu)(S_{max} - \sigma_y / s)}{E-k\nu}.$$

$$\dot{b} = \dot{\Sigma} - \frac{E}{1+\nu} \dot{\varepsilon}_p = \dot{\Sigma} - \frac{E-k}{E-\nu k} \dot{\Sigma} = \frac{k(1-\nu)}{E-k\nu} \dot{\Sigma}.$$

$$\Rightarrow b \text{ varies from 0 to } \frac{k(1-\nu)(S_{max} - \sigma_y / s)}{E-k\nu}.$$

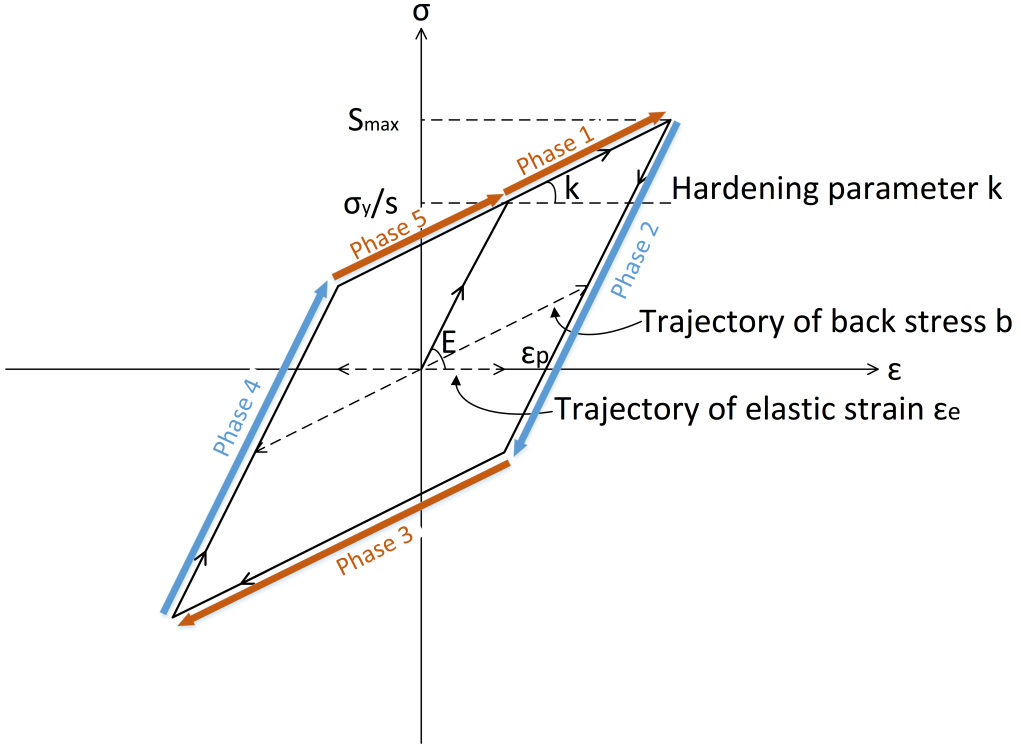


Fig. 31: Uniaxial load with plastic dissipation

So the energy dissipation rate is:

$$(\sigma - b)\dot{\varepsilon}^p = \frac{\sigma_y}{s}\dot{\varepsilon}^p = \frac{\sigma_y}{s} \frac{(E - k)(1 + \nu)}{E(E + k\nu)} \dot{\Sigma}.$$

The energy dissipation is:

$$(\sigma - b)\Delta\varepsilon^p = \frac{\sigma_y}{s} \frac{(E - k)(1 + \nu)(S_{max} - \sigma_y/s)}{E(E + k\nu)}.$$

Phase 2: The deviatoric stress amplitude decreases from S_{max} to $S_{max} - 2\sigma_y/s$.
The material is in local elastic regime, then $\dot{\varepsilon}^p = 0$ and $\dot{\sigma} - \dot{b} = 0 \Rightarrow$

$$\dot{b} = 0, \dot{\sigma} = \dot{\Sigma} - \frac{E}{1 + \nu} \dot{\varepsilon}_p = \dot{\Sigma}.$$

$$\sigma \text{ varies from } \sigma_y/s + \frac{k(1 - \nu)(S_{max} - \sigma_y/s)}{E - k\nu} \text{ to } -\sigma_y/s + \frac{k(1 - \nu)(S_{max} - \sigma_y/s)}{E - k\nu}.$$

$\sigma - b$ varies from σ_y/s to $-\sigma_y/s$.

The energy dissipation rate is:

$$(\sigma - b)\dot{\varepsilon}^p = 0.$$

Phase 3: The deviatoric stress amplitude decreases from $S_{max} - 2\sigma_y/s$ to $-S_{max}$.
The material is in local plastic regime, then $\dot{\varepsilon}^p > 0$ and $\dot{\sigma} - \dot{b} = 0 \Rightarrow$

$$\dot{\varepsilon}^p = \frac{(E - k)(1 + \nu)}{E(E + k\nu)} \dot{\Sigma}$$

as opposite to phase 1 for $\dot{\Sigma} < 0$.

$$\Rightarrow \dot{\varepsilon}^p \text{ varies from } \frac{(E-k)(1+\nu)(S_{max} - \sigma_y/s)}{E(E+k\nu)} \text{ to } \frac{(E-k)(1+\nu)(S_{max} - \sigma_y/s - S_{max} - (S_{max} - 2\sigma_y/s))}{E(E+k\nu)} = -\frac{(E-k)(1+\nu)(S_{max} - \sigma_y/s)}{E(E+k\nu)}.$$

From Taylor-Lin scale transition model:

$$\begin{aligned} \dot{\sigma} &= \dot{\Sigma} - \frac{E}{1+\nu} \dot{\varepsilon}_p = \dot{\Sigma} - \frac{E-k}{E-\nu k} \dot{\Sigma} = \frac{k(1-\nu)}{E-k\nu} \dot{\Sigma}. \\ \Rightarrow \sigma &\text{ varies from } -\sigma_y/s + \frac{k(1-\nu)(S_{max} - \sigma_y/s)}{E-k\nu} \text{ to } -\sigma_y/s - \frac{k(1-\nu)(S_{max} - \sigma_y/s)}{E-k\nu}. \\ \dot{b} &= \dot{\Sigma} - \frac{E}{1+\nu} \dot{\varepsilon}_p = \dot{\Sigma} - \frac{E-k}{E-\nu k} \dot{\Sigma} = \frac{k(1-\nu)}{E-k\nu} \dot{\Sigma}. \\ \Rightarrow b &\text{ varies from } \frac{k(1-\nu)(S_{max} - \sigma_y/s)}{E-k\nu} \text{ to } -\frac{k(1-\nu)(S_{max} - \sigma_y/s)}{E-k\nu}. \end{aligned}$$

So the energy dissipation rate is:

$$(\sigma - b) \dot{\varepsilon}^p = -\frac{\sigma_y}{s} \dot{\varepsilon}^p = -\frac{\sigma_y}{s} \frac{(E-k)(1+\nu)}{E(E+k\nu)} \dot{\Sigma}.$$

The energy dissipation is:

$$(\sigma - b) \Delta \dot{\varepsilon}^p = -\frac{\sigma_y}{s} \frac{(E-k)(1+\nu)(-2S_{max} + 2\sigma_y/s)}{E(E+k\nu)} = \frac{2\sigma_y}{s} \frac{(E-k)(1+\nu)(S_{max} - \sigma_y/s)}{E(E+k\nu)}.$$

Phase 4: The deviatoric stress amplitude increases from $-S_{max}$ to $-S_{max} + 2\sigma_y/s$.

The material is in local elastic regime, then $\dot{\varepsilon}^p = 0$ and $\dot{\sigma} - \dot{b} = 0 \Rightarrow$

$$\begin{aligned} \dot{b} &= 0, \dot{\sigma} = \dot{\Sigma} - \frac{E}{1+\nu} \dot{\varepsilon}_p = \dot{\Sigma}. \\ \sigma &\text{ varies from } -\sigma_y/s - \frac{k(1-\nu)(S_{max} - \sigma_y/s)}{E-k\nu} \text{ to } \sigma_y/s - \frac{k(1-\nu)(S_{max} - \sigma_y/s)}{E-k\nu}. \\ \sigma - b &\text{ varies from } -\sigma_y/s \text{ to } \sigma_y/s. \end{aligned}$$

So the energy dissipation rate is:

$$(\sigma - b) \dot{\varepsilon}^p = 0.$$

Phase 5: The deviatoric stress amplitude increases from $-S_{max} + 2\sigma_y/s$ to σ_y/s .

The material is in local plastic regime, then $\dot{\varepsilon}^p > 0$ and $\dot{\sigma} - \dot{b} = 0 \Rightarrow$

$$\dot{\varepsilon}^p = \frac{(E-k)(1+\nu)}{E(E+k\nu)} \dot{\Sigma}$$

as in phase 1.

$$\Rightarrow \dot{\varepsilon}^p \text{ varies from } -\frac{(E-k)(1+\nu)(S_{max} - \sigma_y/s)}{E(E+k\nu)} \text{ to } 0.$$

$$\dot{\sigma} = \dot{\Sigma} - \frac{E}{1+\nu} \dot{\varepsilon}_p = \dot{\Sigma} - \frac{E-k}{E-\nu k} \dot{\Sigma} = \frac{k(1-\nu)}{E-k\nu} \dot{\Sigma}.$$

$\Rightarrow \sigma$ varies from $\sigma_y/s - \frac{k(1-\nu)(S_{max} - \sigma_y/s)}{E - k\nu}$ to σ_y/s .

$$\dot{b} = \dot{\Sigma} - \frac{E}{1+\nu} \dot{\varepsilon}_p = \dot{\Sigma} - \frac{E-k}{E-\nu k} \dot{\Sigma} = \frac{k(1-\nu)}{E-k\nu} \dot{\Sigma}.$$

$\Rightarrow b$ varies from $-\frac{k(1-\nu)(S_{max} - \sigma_y/s)}{E - k\nu}$ to 0.

So the energy dissipation rate is:

$$(\sigma - b) \dot{\varepsilon}^p = \frac{\sigma_y}{s} \dot{\varepsilon}^p = \frac{\sigma_y}{s} \frac{(E-k)(1+\nu)}{E(E+k\nu)} \dot{\Sigma}.$$

The energy dissipation is:

$$(\sigma - b) \Delta \varepsilon^p = \frac{\sigma_y}{s} \frac{(E-k)(1+\nu)(S_{max} - \sigma_y/s)}{E(E+k\nu)}.$$

From the three phase analysis in local plastic regime, the dissipated energy is like $dW(\text{phase1}) = \frac{1}{2} dW(\text{phase3}) = dW(\text{phase5})$ and the dissipation rate is like $d\dot{W}(\text{phase1}) = d\dot{W}(\text{phase3}) = d\dot{W}(\text{phase5})$.

$$d\dot{W} = \frac{(E-k)(1+\nu)}{E(E-k\nu)} \left(\frac{\sigma_y}{s} \right) |\dot{\Sigma}| \quad (107)$$

We can then calculate the local dissipated energy W at point M during one cycle by cumulating the input of all sub-scales with their probabilities [30].

$$\begin{aligned} W_{cyc} &= 4 \int_{(\sigma_y - \lambda \Sigma_H)/S_{max}}^{\infty} dW(s, M, t) P(s) ds \\ &= 4 \int_{(\sigma_y - \lambda \Sigma_H)/S_{max}}^{\infty} \frac{(E-k)(1+\nu)}{E(E+k\nu)} \frac{\sigma_y - \lambda \Sigma_H}{s} \left(S_{max} - \frac{\sigma_y - \lambda \Sigma_H}{s} \right) (\beta - 1) s^{-\beta} ds \\ &= \frac{4(E-k)(1+\nu)(\beta-1)}{E(E+k\nu)\beta(\beta+1)} \frac{S_{max}^{\beta+1}}{\left(\sigma_y - \lambda \Sigma_H \right)^{\beta-1}}. \end{aligned} \quad (108)$$

If the dissipated energy accumulates linearly until a failure value W_F , we can get directly the time to failure from Eq.(109):

$$T_{fail} = N_F t_{cyc} = \frac{W_F}{W_{cyc}} t_{cyc} = C(S_{max})^{-\beta-1}. \quad (109)$$

From Eq.(108), we then obtain that the model predicts as expected a power law dependence in function of S_{max} . However, experiments shows that the damage or the energy accumulation of a material evolves non-linearly in time. We should introduce below a method to handle such a nonlinearity.

4.5. Nonlinearity of damage accumulation

4.5.1. Energy approach with Chaboche law

The Chaboche law[17] is essentially a damage incremental law for cyclic loading of stress intensity σ with a deviatoric part A_{II} and hydrostatic part Σ_H , defining the damage increase by:

$$\delta D = \left(1 - (1 - D)^{\gamma+1} \right)^\alpha \left(\frac{A_{II}/(1-D)}{M(\Sigma_H)} \right)^\gamma \delta N \quad (110)$$

which writes equivalently as Eq.(111)

$$\delta [1 - (1 - D)^{\gamma+1}]^{1-\alpha} = (1 - \alpha)(\gamma + 1) \left(\frac{A_{II}}{M(\Sigma_H)} \right)^\gamma \delta N = \frac{\delta N}{N_F(\sigma)}. \quad (111)$$

Here $N_F(\sigma)$ denotes the number of cycles at intensity σ to failure as obtained by integration of Eq.(111) from $D = 0$ to $D = 1$.

In our model, in case of a simple uniaxial cyclic loading, we propose to replace $\frac{1}{N_F(\sigma)}$ which is the relative unit increment of cycles by $\frac{W_{cyc}}{W_F}$, yielding the nonlinear damage incremental law:

$$\delta[1 - (1 - D)^{\gamma+1}]^{1-\alpha} = \frac{W_{cyc}}{W_F} \delta N. \quad (112)$$

This is a nonlinear law but used with a constant α , there will be no sequence effect. In other words, when applying two successive cycles of different intensities, the failure will occur at the same number of cycles whatever the order of the loading (high then low versus low then high).

4.5.2. Generalized damage accumulation

Formula (111) is a general accumulation law which can be applied for any cyclic loading sequence provided that we can identify the multiscale value of the dissipated energy per cycle.

But the notion of cycle itself may be hard to identify for general loadings. The idea is then to replace the relative increment of dissipated energy per cycle by the relative increment of dissipated energy per unit time, yielding:

$$\delta[1 - (1 - D)^{\gamma+1}]^{1-\alpha} = \frac{\dot{W}}{W_F} \delta t. \quad (113)$$

In a general loading case, \dot{W} is to be computed. By integrating Eq.(106) over all microscales, we get:

$$\dot{W}(M, t) = \int_{s=1}^{\infty} \dot{w}(s, M, t) P(s) ds = \int_{s=1}^{\infty} (\underline{S} - \underline{b})(s, M, t) : \underline{\dot{\epsilon}}^p(s, M, t) P(s) ds. \quad (114)$$

The evolution of \underline{S} , \underline{b} and $\underline{\dot{\epsilon}}^p$ are given in section 1.4. Equation (113) and (114) are therefore our proposed damage law.

4.6. Loop on time and scales

4.6.1. Integration rules for \dot{W} and δD

Our first approach takes one cycle as unit time. We compute analytically the energy dissipation at each scale during this cycle. The method is valid for simple loading history and which includes the integration on all weakening scales. The damage D is accumulated after each cycle.

However, there are certain limitations of this method. Firstly we need a load history decomposition in cycles. Secondly in real life the perfect close loop cycle is hardly applicable.

Thus we propose in Eq.(113) a more general method which can be integrated by a step by step strategy. We compute numerically the dissipation at different scales using an implicit Euler time integration of the constitutive laws of section 1.4. After which we make a numerical integration on different scales. Then we can update the damage and go to next time step.

Instead of doing the scale integration directly which can be difficult for complex loading, the Gaussian Quadrature rule with Legendre points is used to give the value of local dissipated energy rate.

To use the Gaussian quadrature rule the limit range of integral must be from -1 to 1 , while the total dissipated energy is expressed by integrating all the weakening scale s ranging from 1 to infinity with their occurrence probabilities:

$$\dot{W} = \int_1^{\infty} \dot{w}(s) (\beta - 1) (s)^{-\beta} ds.$$

To change the limit range of integral from $[1, \infty]$ to $[1, 0]$ we take as new integration variable $u(s) = s^{-p}$ with $p = \beta - 1$, yielding $u(1) = 1$ and $u(\infty) = 0$ with

$$du = -ps^{-p-1} ds$$

that is

$$du = (-\beta + 1)s^{-\beta}ds = (-\beta + 1)s^{-\beta}ds.$$

Therefore the dissipated energy summed on all scales is:

$$\begin{aligned} \dot{W} &= \int_1^\infty \dot{w}(s)(\beta - 1)(s)^{-\beta}ds \\ &= \int_1^0 \dot{w}\left(u^{\frac{1}{1-\beta}}\right)(\beta - 1)\frac{1}{-\beta + 1}du \\ &= \int_0^1 \dot{w}\left(u^{\frac{1}{1-\beta}}\right)(\beta - 1)\frac{1}{\beta - 1}du \\ &= \int_0^1 \dot{w}\left(u^{\frac{1}{1-\beta}}\right)du \\ &= \frac{1}{2} \int_{-1}^1 \dot{w}\left[\left(\frac{x+1}{2}\right)^{\frac{1}{1-\beta}}\right]dx \end{aligned} \quad (115)$$

if we set $u = \frac{x+1}{2}$.

So the dissipated energy rate integrated over all scales takes the form of Eq.(116):

$$\dot{W} = \frac{1}{2} \int_{-1}^1 \dot{w}\left[\left(\frac{x+1}{2}\right)^{\frac{1}{1-\beta}}, t\right]dx \approx \frac{1}{2} \sum_i \omega_i d\dot{w}\left[\left(\frac{x_i+1}{2}\right)^{\frac{1}{1-\beta}}, t\right], \quad (116)$$

where ω_i and x_i are respectively the weights and nodes of the Gauss Legerndre integration rule used for the numerical integration. In this work, we used 25 points[31]. After changing the integration limit, $\left(\frac{x+1}{2}\right)^{\frac{1}{1-\beta}}$ represents the scale s . The values are shown in Table.4.

After changing the integration limit, $\left(\frac{x+1}{2}\right)^{\frac{1}{1-\beta}}$ represents the weakening scale s .

Damage accumulation is deduced from Eq.(113):

$$g_{n+1} = g_n + \frac{\dot{W}dt}{W_F} \quad (117)$$

with $g_n = \left[1 - (1 - D_n)^{\gamma+1}\right]^{1-\alpha}$.

We upgrade the damage step by step following Eq.(117). When D reaches one, the material fails.

4.6.2. Regime determination under multiple scales

The material could be both in elastic and plastic regime under different scales. To be more elaborate, we reuse the fundamental equations in different regimes. At scale s , we have a dissipation rate given by:

$$\dot{w}(s) = \left(\underline{\underline{S}} - \underline{\underline{b}}\right) : \underline{\underline{\dot{\epsilon}}^p},$$

which differs between plastic and elastic regime.

Elastic regime:

There we have $\underline{\underline{\dot{\epsilon}}^p} = 0$, $\underline{\underline{b}} = 0$ and $\dot{\underline{\underline{S}}} = dev \dot{\underline{\underline{\Sigma}}}$, so

$$\dot{\underline{\underline{S}}} - \underline{\underline{b}} = dev \dot{\underline{\underline{\Sigma}}},$$

Table 4: Weighting factors ω_i , function arguments x used in Gauss Quadrature Formulas and equivalent scales s'_i .

Scales x_i	Scales s'_i	Scale weighting factors ω_i
-0.99555697	21.21658	0.011393799
-0.976663921	9.257656	0.026354987
-0.942974571	5.922168	0.040939157
-0.894991998	4.364192	0.054904696
-0.833442629	3.465238	0.068038334
-0.759259263	2.882307	0.0801407
-0.673566368	2.475241	0.091028262
-0.57766293	2.176133	0.100535949
-0.473002731	1.948098	0.108519624
-0.361172306	1.769388	0.114858259
-0.243866884	1.626357	0.119455764
-0.122864693	1.510017	0.122242443
0	1.414214	0.123176054
0.122864693	1.334601	0.122242443
0.243866884	1.268026	0.119455764
0.361172306	1.212156	0.114858259
0.473002731	1.165234	0.108519624
0.57766293	1.125921	0.100535949
0.673566368	1.093185	0.091028262
0.759259263	1.066228	0.0801407
0.833442629	1.044435	0.068038334
0.894991998	1.027333	0.054904696
0.942974571	1.014569	0.040939157
0.976663921	1.005886	0.026354987
0.99555697	1.001113	0.011393799

yielding

$$\left(\underline{\underline{S}} - \underline{\underline{b}}\right)(t + dt) = \left(\underline{\underline{S}} - \underline{\underline{b}}\right)(t) + dev \dot{\underline{\Sigma}} dt := \left(\underline{\underline{S}} - \underline{\underline{b}}\right)_{trial}(s, t + dt). \quad (118)$$

We are in elastic regime at scale s as long as we satisfy

$$\left(\underline{\underline{S}} - \underline{\underline{b}}\right)(t + dt) \leq \left(\sigma_y - \lambda \Sigma_H\right) / s.$$

Plastic regime:

When we leave elastic regime at scale s , we have:

$$\begin{cases} \dot{\underline{\underline{\varepsilon}}}^p = \gamma \frac{\underline{\underline{S}} - \underline{\underline{b}}}{\|\underline{\underline{S}} - \underline{\underline{b}}\|}, \gamma > 0, & \text{plastic flow,} \end{cases} \quad (119)$$

$$\begin{cases} \|\underline{\underline{S}} - \underline{\underline{b}}\| = \left(\sigma_y - \lambda \Sigma_H\right) / s, & \text{yield limit,} \end{cases} \quad (120)$$

$$\begin{cases} \left(\underline{\underline{S}} - \underline{\underline{b}}\right) : \left(\dot{\underline{\underline{S}}} - \dot{\underline{\underline{b}}}\right) = 0, & \text{yield limit time invariance,} \end{cases} \quad (121)$$

$$\begin{cases} \dot{\underline{\underline{b}}} = \frac{kE}{E - k\underline{\underline{\varepsilon}}} \dot{\underline{\underline{\varepsilon}}}^p, & \text{kinematic hardening rule,} \end{cases} \quad (122)$$

$$\begin{cases} \dot{\underline{\Sigma}} = dev \dot{\underline{\Sigma}} - \frac{E}{1 + \nu \underline{\underline{\varepsilon}}} \dot{\underline{\underline{\varepsilon}}}^p, & \text{localisation rule.} \end{cases} \quad (123)$$

In all cases, at a certain scale s_i , after elimination of $\dot{\underline{\varepsilon}}^p$, there are

$$\dot{\underline{\underline{S}}} - \dot{\underline{\underline{b}}} = dev\dot{\underline{\underline{\Sigma}}} - E\gamma \left(\frac{1}{1+\nu} + \frac{k}{E-k} \right) \frac{\underline{\underline{S}} - \underline{\underline{b}}}{\|\underline{\underline{S}} - \underline{\underline{b}}\|}.$$

If we are at yield limit at $(t+dt)$, we get on the other hand:

$$\begin{aligned} \left(\underline{\underline{S}} - \underline{\underline{b}} \right) (t+dt) &= \left(\underline{\underline{S}} - \underline{\underline{b}} \right) (t) + \left(\dot{\underline{\underline{S}}} - \dot{\underline{\underline{b}}} \right) dt, \\ \left\| \left(\underline{\underline{S}} - \underline{\underline{b}} \right) (t+dt) \right\| &= (\sigma_y - \lambda\sigma_m) / s_i. \end{aligned} \quad (124)$$

Replacing $\left(\dot{\underline{\underline{S}}} - \dot{\underline{\underline{b}}} \right)$ in the integration by its expression we get:

$$\left(\underline{\underline{S}} - \underline{\underline{b}} \right) (t+dt) = \left(\underline{\underline{S}} - \underline{\underline{b}} \right) (t) + dev\dot{\underline{\underline{\Sigma}}} dt - E\gamma dt \left(\frac{1}{1+\nu} + \frac{k}{E-k} \right) \frac{\left(\underline{\underline{S}} - \underline{\underline{b}} \right) (t+dt)}{\|\underline{\underline{S}} - \underline{\underline{b}}\| (t+dt)} \quad (125)$$

Putting all terms with $\left(\underline{\underline{S}} - \underline{\underline{b}} \right) (t+dt)$ on the left hand side, we get:

$$\left(\underline{\underline{S}} - \underline{\underline{b}} \right) (t+dt) (1+\eta) = \left(\underline{\underline{S}} - \underline{\underline{b}} \right) (t) + dev\dot{\underline{\underline{\Sigma}}} dt = \left(\underline{\underline{S}} - \underline{\underline{b}} \right)_{trial} (t+dt) \quad (126)$$

with

$$\eta = \frac{E\gamma dt}{\|\underline{\underline{S}} - \underline{\underline{b}}\| (t+dt)} \left(\frac{1}{1+\nu} + \frac{k}{E-k} \right). \quad (127)$$

To see whether the structure is in elastic or plastic regime at each time step, we use $\left(\underline{\underline{S}} - \underline{\underline{b}} \right)_{trial} (t+dt)$ to compare with the yield stress at the same scale s_i , thus to give a value to $\left(\underline{\underline{S}} - \underline{\underline{b}} \right) (t+dt)$.

Since $\left(\underline{\underline{S}} - \underline{\underline{b}} \right) (t+dt)$ is in the same direction as $\left(\underline{\underline{S}} - \underline{\underline{b}} \right)_{trial} (t+dt)$, we have

$$\left(\underline{\underline{S}} - \underline{\underline{b}} \right) (t+dt) = (\sigma_y - \lambda\sigma_m) / s \frac{\left(\underline{\underline{S}} - \underline{\underline{b}} \right)_{trial} (t+dt)}{\|\underline{\underline{S}} - \underline{\underline{b}}\|_{trial} (t+dt)} \quad (128)$$

We now compare Eq.(126) and Eq.(128), the only solution is to have:

$$1 + \eta = \frac{\|\underline{\underline{S}} - \underline{\underline{b}}\|_{trial}}{(\sigma_y - \lambda\sigma_m) / s} \quad (129)$$

that is:

$$\eta = \frac{\|\underline{\underline{S}} - \underline{\underline{b}}\|_{trial}}{(\sigma_y - \lambda\sigma_m) / s} - 1 \quad (130)$$

which is positive in plastic regime.

$$\left(\underline{\underline{S}} - \underline{\underline{b}} \right) (s, t+dt) = \frac{\left(\underline{\underline{S}} - \underline{\underline{b}} \right)_{trial} (s, t+dt)}{1 + \eta}, \quad (131)$$

with

$$\eta = \max \left\{ \underbrace{0}_{\text{elastic regime}}, \underbrace{\frac{\| \underline{S} - \underline{b} \|_{\text{trial}}}{(\sigma_y - \lambda \Sigma_H) / s} - 1}_{\text{plastic regime when this number is positive}} \right\},$$

$$(\underline{S} - \underline{b})_{\text{trial}}(s, t + dt) = (\underline{S} - \underline{b})(s, t) + \text{dev} \dot{\underline{\Sigma}}(t) dt.$$

That is to say, when the structure is in elastic regime at time t and scale s , we have $(\underline{S} - \underline{b})(s, t) = (\underline{S} - \underline{b})_{\text{trial}}(s, t)$. Otherwise, if the norm of $(\underline{S} - \underline{b})_{\text{trial}}(s, t)$ is greater than the local yield limit $(\sigma_y - \lambda \Sigma_H) / s$, $(\underline{S} - \underline{b})(s, t)$ will be projected on the yield limit.

Knowing the distinction between elastic and plastic regime under multiple scales, we compute the general expression of the dissipated energy rate.

$$\dot{w} = (\underline{S} - \underline{b}) : \dot{\underline{\epsilon}}^p = \gamma \frac{\sigma_y - \lambda \Sigma_H}{s}. \quad (132)$$

From Eq.(127) and Eq.(130) in annex, we get:

$$E\gamma dt = \left\langle \left\| \underline{S} - \underline{b} \right\|_{\text{trial}} - \frac{\sigma_y - \lambda \Sigma_H}{s} \right\rangle / \left(\frac{1}{1 + \nu} + \frac{k}{E - k} \right) = \left\langle \left\| \underline{S} - \underline{b} \right\|_{\text{trial}} - \frac{\sigma_y - \lambda \Sigma_H}{s} \right\rangle \frac{(E - k)(1 + \nu)}{(E + k\nu)}, \quad (133)$$

where $\langle \rangle$ is Macaulay bracket symbol defined as $\langle m \rangle = 0$ if $m \leq 0$, otherwise $\langle m \rangle = m$.

We replace γ deduced from Eq.(133) in Eq.(132) to give the expression of local energy dissipation rate at scale s :

$$\dot{w} dt = \frac{(E - k)(1 + \nu)}{E(E + k\nu)} \left\langle \left\| \underline{S} - \underline{b} \right\|_{\text{trial}} - \frac{\sigma_y - \lambda \Sigma_H}{s} \right\rangle \frac{\sigma_y - \lambda \Sigma_H}{s}. \quad (134)$$

With Eq.(116), the final expression of energy dissipation W during time step dt writes:

$$\begin{aligned} W &= \dot{W} dt \\ &= \frac{1}{2} \sum_i \omega_i \dot{w} \left[\left(\frac{x_i + 1}{2} \right)^{\frac{1}{1-\beta}} \right] dt \\ &= \frac{(E - k)(1 + \nu)}{2E(E + k\nu)} \sum_i \omega_i \left\langle \left\| \underline{S} - \underline{b} \right\|_{\text{trial}} - \frac{\sigma_y - \lambda \Sigma_H}{\left(\frac{x_i + 1}{2} \right)^{\frac{1}{1-\beta}}} \right\rangle \frac{\sigma_y - \lambda \Sigma_H}{\left(\frac{x_i + 1}{2} \right)^{\frac{1}{1-\beta}}}. \end{aligned} \quad (135)$$

We have the damage accumulation deduced in Eq.(117):

$$g_{n+1} = g_n + \frac{\dot{W} dt}{W_F} = g_n + \frac{W}{W_F},$$

$$\text{with } D_n = \left[1 - \left(1 - g_n^{\frac{1}{1-\alpha}} \right)^{\frac{1}{\gamma+1}} \right].$$

Now we are able to put these formula into numerical tests.

Parameters	Value
Load	$\Sigma = 5e8 \sin(t)$ Pa
Young's modulus	$E = 2e11$ Pa
Hardening parameter	$k = 6e8$ Pa
Weakening scales distribution exponent	$\beta = 3$
Hydrostatic pressure sensitivity	$\lambda = 0.5$
Macroscopic yield stress	$\sigma_y = 6.38e8$ Pa
Material parameter from Chaboche law(Wohler curve exponent)	$\gamma = 0.5$
Non-linearity of damage accumulation	$\alpha = 0.5$
Initial damage	$D = 0$
Initial time	$t = 0$ s
Dissipated energy to failure per unit volume	$W_F = 3e6$ J
Looping step	1 s

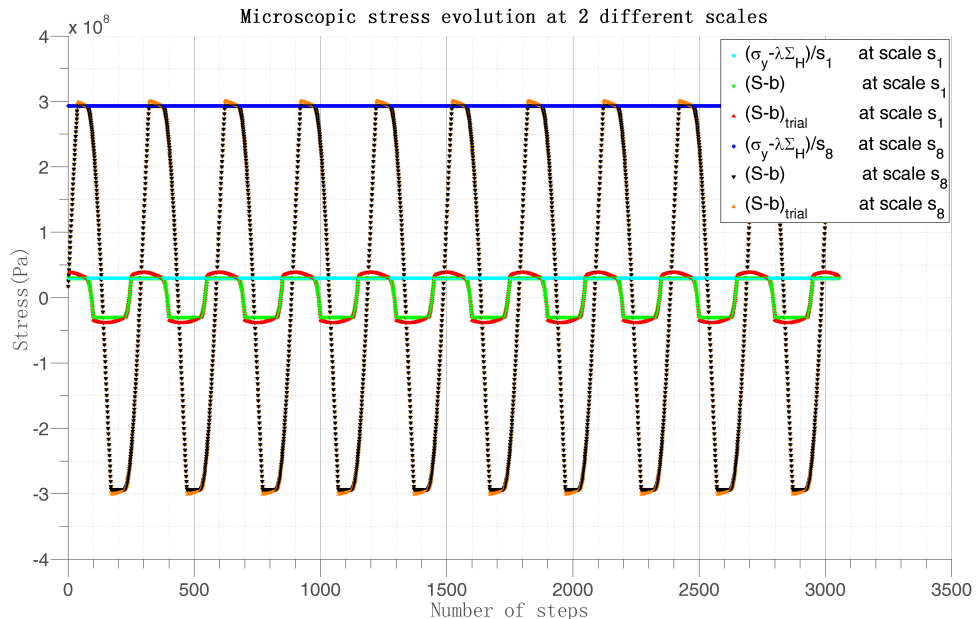
Table 5: Material parameters in a simple cyclic load

4.7. Test on different load histories

4.7.1. One dimensional application to simple cyclic data

The test is first performed on a sinusoidal axial load $\Sigma = C \sin(t)$ with parameters in Table 5, giving a deviatoric amplitude $S_{max} = \sqrt{\frac{2}{3}}C$.

We use matlab to realize our analytical method. We plot $(\underline{\underline{S}} - \underline{\underline{b}})_{trial}$ and $(\underline{\underline{S}} - \underline{\underline{b}})$ for two different scales ($s_1 = 21.21657929229650$ and $s_8 = 2.176132808422946$) in Fig. 32.

Fig. 32: Microscopic $(\underline{\underline{S}} - \underline{\underline{b}})_{trial}$ and $(\underline{\underline{S}} - \underline{\underline{b}})$ evolution with time under different weakening scales in sinusoidal load

The nonlinearity is determined by

$$\alpha = 1 - a \left\langle \frac{\max_t \sqrt{J_{2,a}(t)} + a_c P_{max}(t) - b_c}{\sigma_u - 2 \max \sqrt{J_{2,a}}} \right\rangle,$$

which is predominated by Crossland criterion, for simplicity we take α as a constant. The damage evolves like in Fig. 33, where we compare the damage evolution as predicted by the cycle accumulation Eq.(108) and by the numerical strategy of section 4.

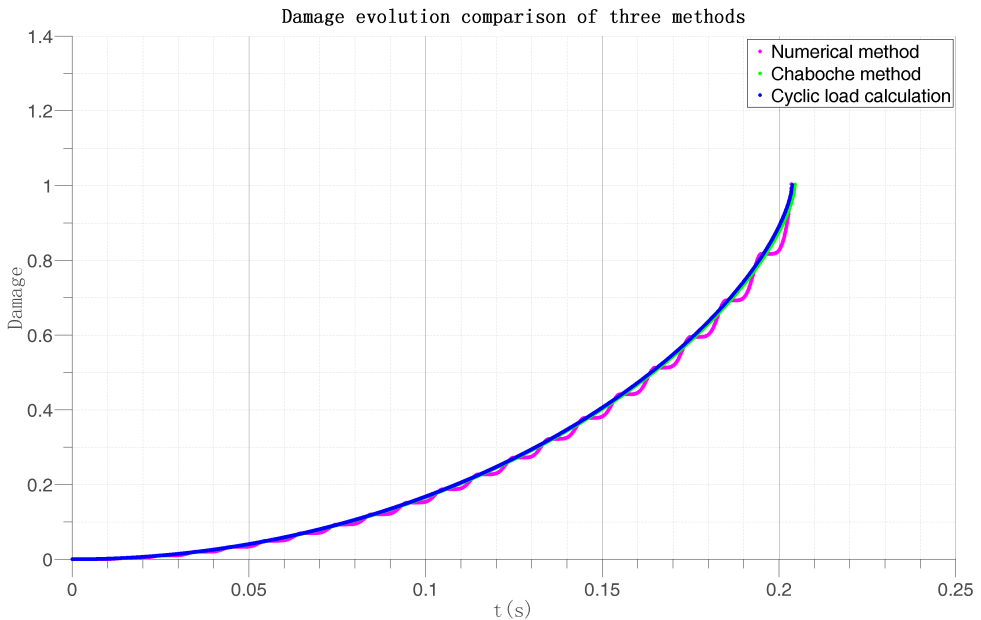


Fig. 33: Damage evolution with time under sinusoidal load with two different methods

Now we compare the result to the one demonstrated in Fig. 31. The first cycle has 3 phases which have the energy loss identical to phase 1. The following cycles each have 4 times energy loss as phase 1. We can see from Fig. 34 and Fig. 35 the difference between cyclic load calculation and numerical method as function of time(time step=1/5000s and 1/15000s separately). Because the step by step damage accumulation grows in a power law, so the amplitude of difference grows with time. However, the difference between the two methods swing around 0 and from Fig. 33 we can see the difference is not symmetrical, we could consider the numerical method converges in cyclic load calculation method.

The cyclic load calculation is only valid for very simple such as proportional loading in fatigue, nevertheless it can still be used as a comparison group to verify the numerical results. The outcome seems satisfactory. Hence, to be more general for any loading history, we adopt the numerical method.

4.7.2. One dimensional application to PSA data

In this test, we reconstruct a unidimensional macroscopic stress history from recorded force data proposed by PSA group.

The sample recording rate is 256 per second. In order to accumulate damage using very small steps, we have created 10 additional points between every 2 recorded points by linear interpolation. So the sample rate is $256 * 10$ per second.

The force on wheel is firstly considered as under uniaxial loading F_x . Here we temporally set $\Sigma_x = F_x/A$ where $A = \frac{1}{1e6} m^2$ is the area of force, and $W_F = 3e6 J$. The other data are as Table.5. The plot of $(\underline{\underline{S}} - \underline{\underline{b}})_{trial}$

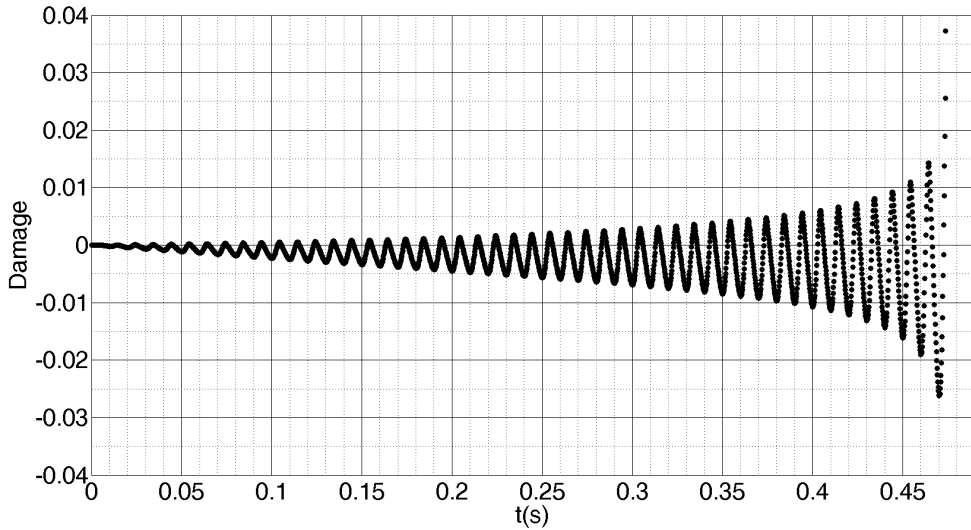


Fig. 34: Difference between cyclic load calculation and numerical method as function of time(time step=1/5000s)

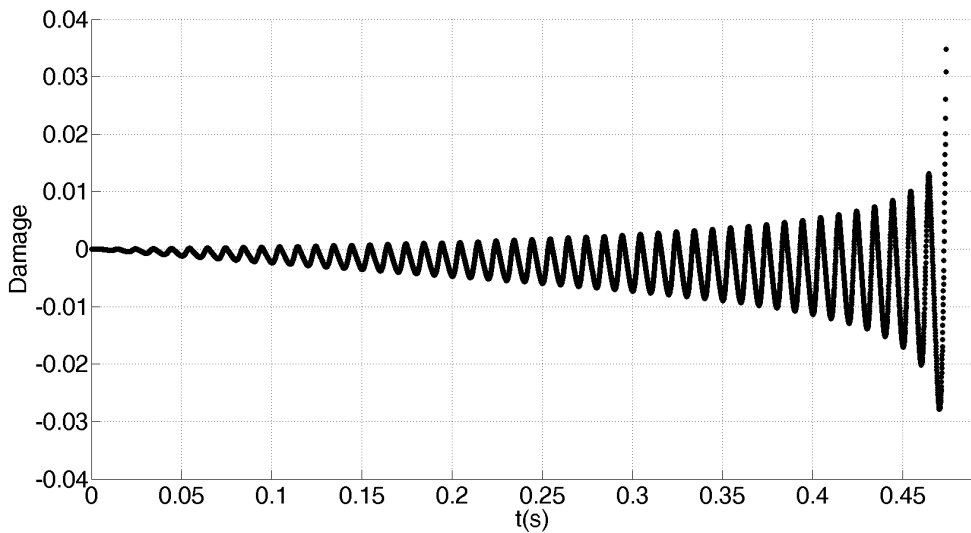


Fig. 35: Difference between cyclic load calculation and numerical method as function of time(time step=1/15000s)

and $\left(\frac{S}{2} - \frac{b}{2}\right)$ under 2 different scales ($s_1 = 21.21657929229650$ and $s_8 = 2.176132808422946$) are shown in Fig. 37. The damage evolves like Fig. 39.

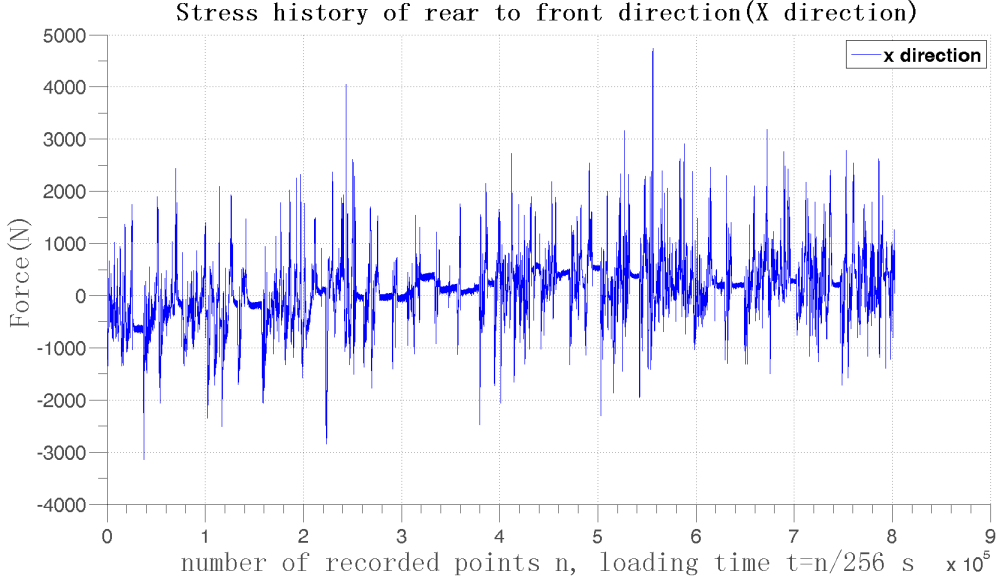
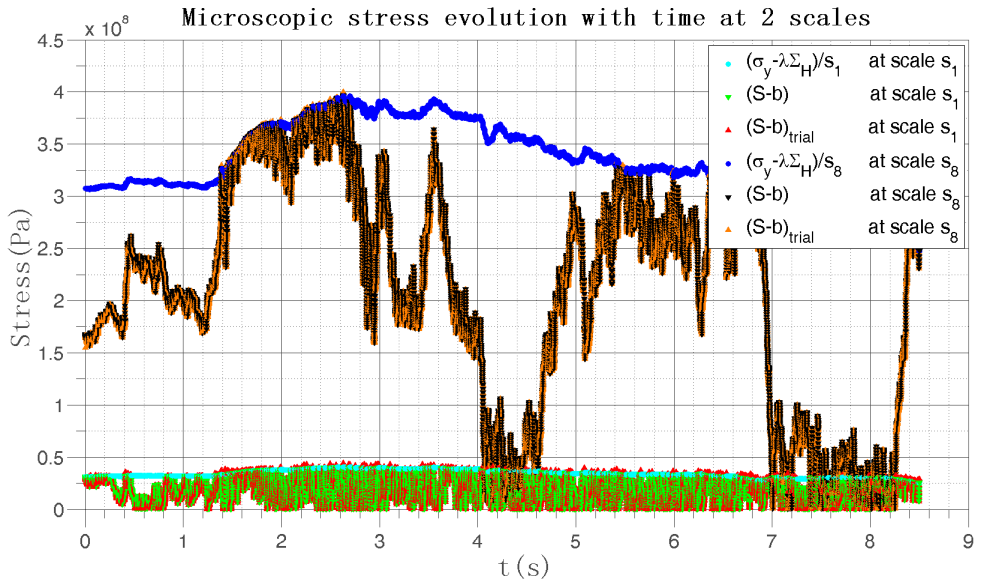


Fig. 36: Loading history of X direction, force vs the record index n, with 256 sample recorded per second

Fig. 37: $(\underline{\underline{S}} - \underline{\underline{b}})_{trial}$ and $(\underline{\underline{S}} - \underline{\underline{b}})$ evolution with time under different weakening scales in PSA load history

4.7.3. Multi-dimensional application to PSA data

We now consider a situation where we have force recorded measured in 3 different directions as shown in Fig. 40. In real case, the vertical force F_z is much larger than the axial and horizontal forces F_x and F_y , as shown in Fig. 40. However, in order to investigate large domains of interest, we first scale the axial and horizontal forces to reach comparable impact and transform them in principal stresses $c_x \frac{F_x}{A}$ applied along the stress principle vector \underline{e}_α (respectively \underline{e}_β) that we choose randomly (Fig. 41). We therefore consider the

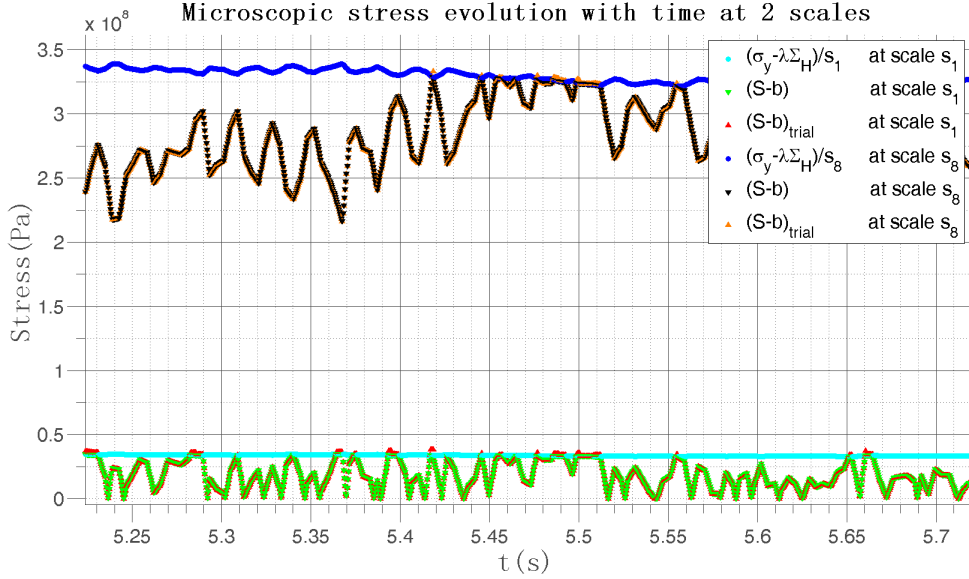


Fig. 38: Circled area magnification in Fig. 37 where there is more $\left(\underline{\underline{S}} - \underline{\underline{b}}\right)_{trial} > \sigma_y(\text{plasticity})$ at s_1 than at s_8

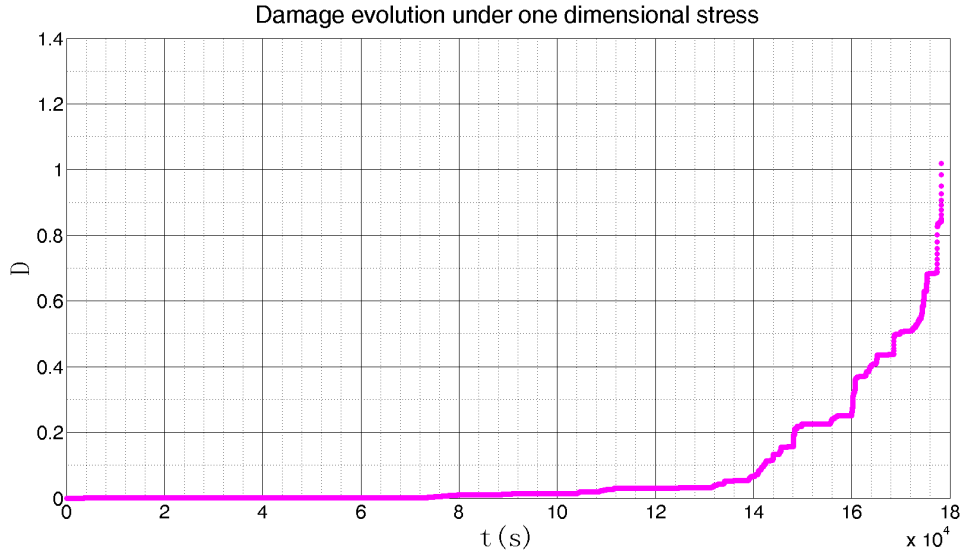


Fig. 39: Damage evolution with time at one dimension PSA load history

following macroscopic stress tensor:

$$\underline{\underline{\Sigma}} = \frac{F_z(t)}{A} \underline{\underline{e}}_1 \otimes \underline{\underline{e}}_1 + c_x \frac{F_x(t)}{A} \underline{\underline{e}}_\alpha \otimes \underline{\underline{e}}_\alpha + c_y \frac{F_y(t)}{A} \underline{\underline{e}}_\beta \otimes \underline{\underline{e}}_\beta \quad (136)$$

where $\underline{\underline{e}}_\alpha$ and $\underline{\underline{e}}_\beta$ are principal vectors whose spherical coordinate are $\theta_x, \varphi_x, \theta_y$ and φ_y respectively:

$$\underline{\underline{e}}_\alpha = \cos\theta_x \underline{\underline{e}}_1 + \sin\theta_x \cos\varphi_x \underline{\underline{e}}_2 + \sin\theta_x \sin\varphi_x \underline{\underline{e}}_3,$$

$$\underline{\underline{e}}_\beta = \cos\theta_y \underline{\underline{e}}_1 + \sin\theta_y \cos\varphi_y \underline{\underline{e}}_2 + \sin\theta_y \sin\varphi_y \underline{\underline{e}}_3.$$

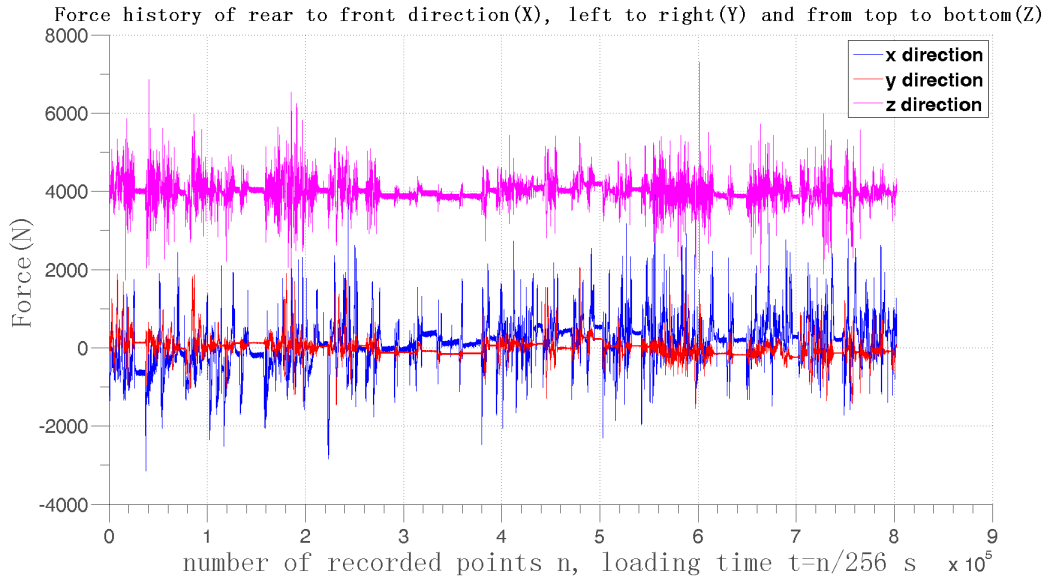


Fig. 40: Loading history of 3 different directions

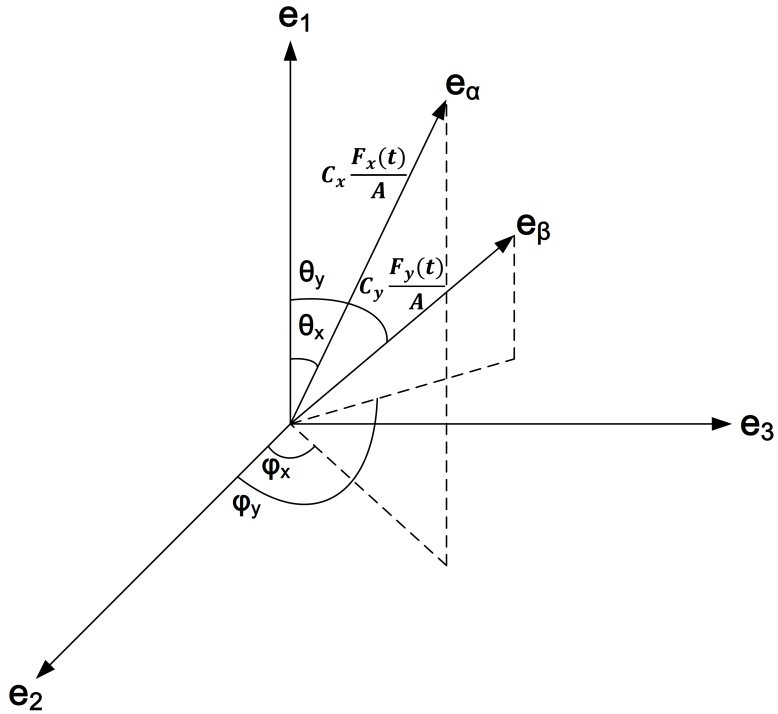


Fig. 41: Loading in 3 different directions

Here $F_x(t)$, $F_y(t)$, $F_z(t)$ are from test data, and θ_x , φ_x , θ_y , φ_y are structural parameters to be chosen randomly. The physical data are the same with parameters in Table 5. The structural data we choose is shown in Table 6.

The underlying assumption is that a unit load on wheel in direction e_x creates a stress tensor at point M

Parameter	$A(m^2)$	c_x	c_y	θ_x	φ_x	θ_y	φ_y
Value	1/6e4	10	60	0.5	0.3	0.6	0.4

Table 6: The structural data in 3D analysis

given by:

$$c_x \frac{F_x(t)}{A} \underline{e}_\alpha \otimes \underline{e}_\alpha,$$

where $\underline{e}_\alpha \otimes \underline{e}_\alpha$ defines the local structural response of the vehicle.

Replacing \underline{e}_α and \underline{e}_β in Eq.(136) we get the stress tensor in Eq.(137).

$$\begin{aligned}
\underline{\underline{\Sigma}} &= \frac{F_z}{A} \underline{e}_1 \otimes \underline{e}_1 + c_x \frac{F_x}{A} \underline{e}_\alpha \otimes \underline{e}_\alpha + c_y \frac{F_y}{A} \underline{e}_\beta \otimes \underline{e}_\beta \\
&= \frac{F_z}{A} \underline{e}_1 \otimes \underline{e}_1 + c_x \frac{F_x}{A} (\cos\theta_x \underline{e}_1 + \sin\theta_x \cos\varphi_x \underline{e}_2 + \sin\theta_x \sin\varphi_x \underline{e}_3) \otimes (\cos\theta_x \underline{e}_1 + \sin\theta_x \cos\varphi_x \underline{e}_2 + \sin\theta_x \sin\varphi_x \underline{e}_3) \\
&\quad + c_y \frac{F_y}{A} (\cos\theta_y \underline{e}_1 + \sin\theta_y \cos\varphi_y \underline{e}_2 + \sin\theta_y \sin\varphi_y \underline{e}_3) \otimes (\cos\theta_y \underline{e}_1 + \sin\theta_y \cos\varphi_y \underline{e}_2 + \sin\theta_y \sin\varphi_y \underline{e}_3) \\
&= \left(\frac{F_z}{A} + c_x \frac{F_x}{A} \cos^2 \theta_x + c_y \frac{F_y}{A} \cos^2 \theta_y \right) \underline{e}_1 \otimes \underline{e}_1 \\
&\quad + \left(c_x \frac{F_x}{A} \cos\theta_x \sin\theta_x \cos\varphi_x + c_y \frac{F_y}{A} \cos\theta_y \sin\theta_y \cos\varphi_y \right) (\underline{e}_1 \otimes \underline{e}_2 + \underline{e}_2 \otimes \underline{e}_1) \\
&\quad + \left(c_x \frac{F_x}{A} \cos\theta_x \sin\theta_x \sin\varphi_x + c_y \frac{F_y}{A} \cos\theta_y \sin\theta_y \sin\varphi_y \right) (\underline{e}_1 \otimes \underline{e}_3 + \underline{e}_3 \otimes \underline{e}_1) \\
&\quad + \left(c_x \frac{F_x}{A} \sin^2 \theta_x \cos^2 \varphi_x + c_y \frac{F_y}{A} \sin^2 \theta_y \cos^2 \varphi_y \right) \underline{e}_2 \otimes \underline{e}_2 \\
&\quad + \left(c_x \frac{F_x}{A} \sin^2 \theta_x \cos\varphi_x \sin\varphi_x + c_y \frac{F_y}{A} \sin^2 \theta_y \cos\varphi_y \sin\varphi_y \right) (\underline{e}_2 \otimes \underline{e}_3 + \underline{e}_3 \otimes \underline{e}_2) \\
&\quad + \left(c_x \frac{F_x}{A} \sin^2 \theta_x \sin^2 \varphi_x + c_y \frac{F_y}{A} \sin^2 \theta_y \sin^2 \varphi_y \right) \underline{e}_3 \otimes \underline{e}_3
\end{aligned} \tag{137}$$

The plot of $(\underline{\underline{S}} - \underline{\underline{b}})_{trial}$ and $(\underline{\underline{S}} - \underline{\underline{b}})$ under 2 different scales are shown in Fig. 42.

In the load history, when $(\underline{\underline{S}} - \underline{\underline{b}})_{trial} > \sigma_y$, the damage accumulates. However, under scale s_{10} , there are much less damage accumulation than under scale s_1 . In this way we do not neglect the small influences in load history and the big fluctuation in stress is magnified which reflects the real situation.

The damage evolves like in Fig. 43.

We can improve the result by inserting more arithmetic sequence points between every 2 recorded points. As is shown in Table.7 :

Table 7: Arithmetic sequence points density effect

Arithmetic sequence points between every two points	Total time to failure(s)
10	78.63711
20	72.24630
30	70.25793
50	68.69148
100	67.49223

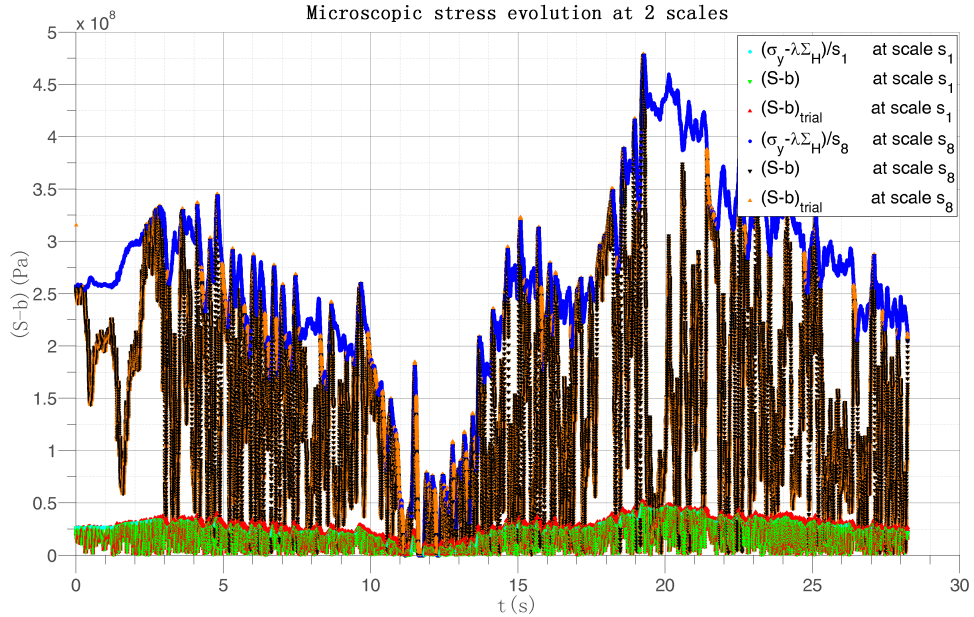


Fig. 42: $(\underline{S} - \underline{b})_{trial}$ and $(\underline{\underline{S}} - \underline{\underline{b}})$ evolution with time under different weakening scales in PSA load history

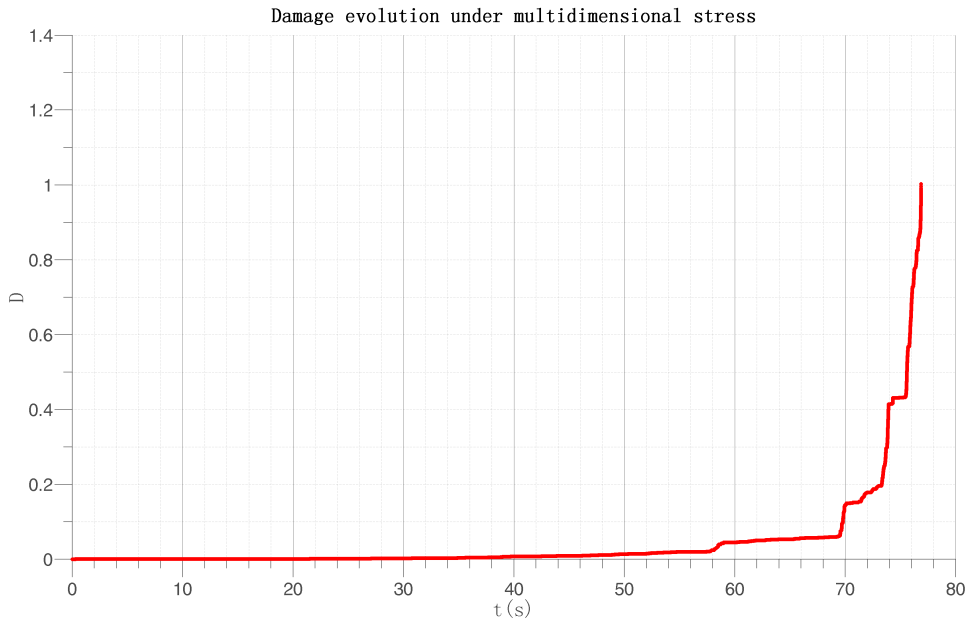


Fig. 43: Damage evolution under multidimensional stress

4.8. Discussion

The strategy can be made more complex by introducing a local space averaging process in the calculation of the local damage, and by taking more general plastic flows. The energy based fatigue approach takes into account impurities and hardness in the material which affect the fatigue life. The load sequence effects for complex multiaxial loading history are included in damage accumulation process. The small step-by-step

Loading direction	max(N)	mean(N)	min(N)
FX_RAVG	4739	113	-3145
FY_RAVG	2050	0	-1558
FZ_RAVG	7301	4012	1219
FZ_RARG	5858	3272	647

Table 8: Summary of the signals in the center of LFW

Table 9: My caption

Signal	nb of cycles	Max of Range	Min of Mean	Max of Mean
FX_RAVG	206636	7884	-3106	4704
FY_RAVG	205359	3608	-1489	2032
FZ_RAVG	237703	6082	2225	6224
FZ_RARG	340967	5211	1482	5122

Table 10: Rainflow counting results of the force data

strategy does not ignore small fluctuations in the load history. In addition, it can take into account any type of micro plasticity law and multiaxial load geometry.

Further research of energy based failure criteria should be focused on the following aspects:

1. The accommodation law might be more elaborate than kinematic hardening.
2. The differentiation of shear stress and normal stress effect on fatigue life should be clarified.
3. The non-linearity parameter α contains the stress σ , so it can evolve with time. But for complex loading history, should it change at every time step?

5 Application to real data

5.1. Time filtering of load signal

We have a 52 minutes recording of an average customer which have driven 18.3 kilometers. A complete set of forces were recorded at the center of the left front wheel (LFW in English but RAVG in French for Roue AVant Gauche). This wheel is driving and sustains the engine mass (half of it).

FX: Force in the axial direction (from rear to front), a positive (resp. negative) force corresponds to an acceleration (resp. deceleration) of the vehicle.

FY: Force in the horizontal direction (from driver to shotgun), a positive (resp. negative) force corresponds to an right (resp. left) turn.

FZ: Force in the vertical direction (from top to bottom), a more (resp. less) than average force corresponds to a bump (resp. pot hole) in the road, the average is the vehicle mass to the wheel.

The summary of the signals are :

From a comparison point of view, the rainflow counting in the Range/Mean diagram of these signals gives:

So all the signals present a significant amounts of fatigue cycles (above 2e5) but the rear wheel is richer (by 50%), hence it is presented here.

The starting point is the data of a loading history on different macroscopic directions $(F_i)_i = 1, N$. Typically, in the data sent recently by PSA, the elementary loads are the three components of the force applied at the rear center wheel $(q_i(t))_i = 1, N$. The objective is to construct from this data a multi-scale stochastic mesoscopic plastic damage accumulation at the different materials points M inside the structure, and identify the time to failure as the time when the cumulated energy dissipated by this mesoscopic plastic accumulation reaches a given material threshold.

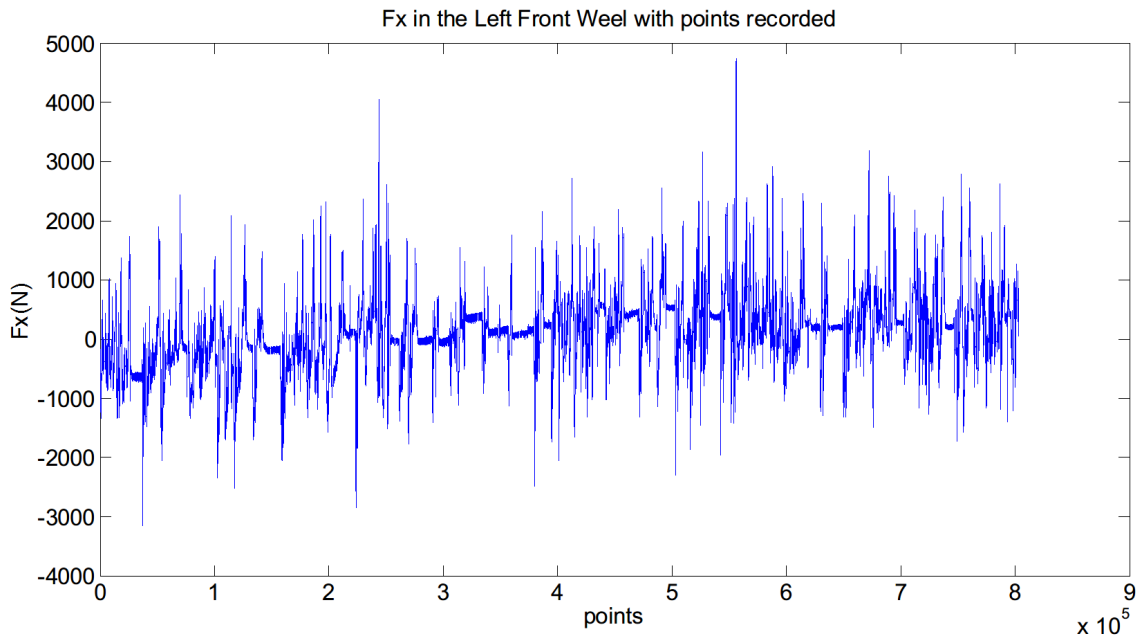


Fig. 44: Fx in the Left Front Weel with points recorded

The material under high cycle fatigue does not undergo local strain concentration. But physically the internal residual stress causes slip of grains in the weaker parts in the material. The grain slip system is determined by the orientation of the stress and the size of grain. To predict failure we have to consider both shear and hydrostatic stress of the loading.

The whole process of loading history has no macroscopic plastic deformation. But instead of thinking mesoscopic stress concentration, we assume there are local weak points where the stress yield limit is smaller than the macroscopic one. To put this thought into formula we assume the mesoscopic strain is the same as macroscopic strain:

$$\hat{\epsilon} = E$$

And the mesoscopic shear stress is the difference between macroscopic stress and the local residual stress.

$$\hat{\sigma} = \Sigma - \sigma_R$$

To get the residual stress evolution with time we need to find a filter to get rid of the signals with small variation which have negligible influence on residual stress, see Fig. 45. The filtered rainflow signal 'shortened' the actual time that the material endured but this does not influent our damage prediction because we consider the trivial signals has no impact on fatigue life.

From the filtered loading history we use Dang Van or Habbibou's law to get the residual stress evolution history at given slip(orientation) or scale. By making the difference between the actual stress and residual stress we get $\hat{\sigma}$.

When the accumulated energy reached a certain limit then fatigue occurs. Locally we have the expression of dissipated energy:

$$\Delta W \doteq \int \hat{\sigma} : \hat{\epsilon} dt$$

To start with simple case we assume our signal is sinusoidal. Now we want the distribution of orientation of the slips in the metal. Statistics method gives us the yield limit distribution.

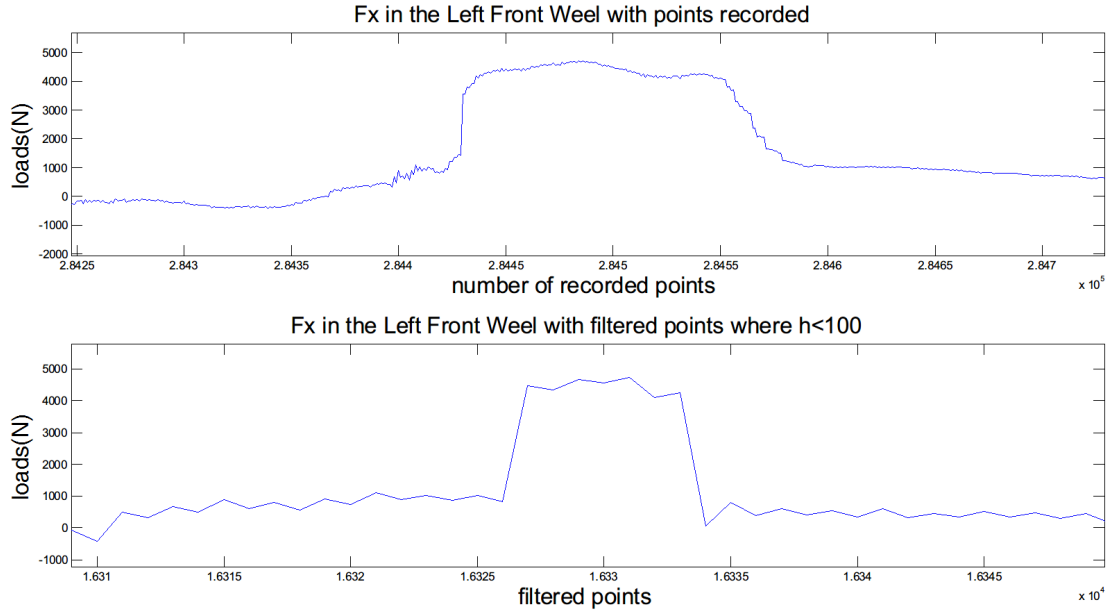


Fig. 45: Comparison between the recorded signal and filtered signal which removes the small variation points where the rainflow cycle amplitude $h \leq 100N$

5.2. Calculation of local stress histories (PSA)

5.3. Results from a standard Chaboche approach

5.4. Results from the new approach

6 Ideas to introduce chronology effects

Acknowledgments We are grateful for the financial and technical support of Chaire PSA.

References

- [1] Crossland B. Effect of large hydrostatic pressures on the torsional fatigue strength of an alloy steel. In: *Proceedings of the Inter-national Conference on Fatigue of Metals*, Institution of Mechan-ical Engineers, London, pages 138–149, 1956.
- [2] Ioannis V. Papadopoulos, Piermaria Davoli, Carlo Gorla, Mauro Filippini, and Andrea Bernasconi. A comparative study of multiaxial high-cycle fatigue criteria for metals. *International Journal of Fatigue*, 19(3):219 – 235, 1997.
- [3] P Ballard, K Dang Van, A Deperrois, and YV Papadopoulos. High cycle fatigue and a finite element analysis. *Fatigue & Fracture of Engineering Materials & Structures*, 18(3):397–411, 1995.
- [4] Ioannis V Papadopoulos. Long life fatigue under multiaxial loading. *International Journal of Fatigue*, 23(10):839–849, 2001.
- [5] Subra Suresh. *Fatigue of materials*. Cambridge university press, 1998.
- [6] DH Luu, MH Maitournam, and QS Nguyen. Formulation of gradient multiaxial fatigue criteria. *International Journal of Fatigue*, 2013.
- [7] Ioannis V. Papadopoulos and Vassilis P. Panoskaltsis. Invariant formulation of a gradient dependent multiaxial high-cycle fatigue criterion. *Engineering Fracture Mechanics*, 55(4):513 – 528, 1996.
- [8] R. Amargier, S. Fourny, L. Champon, C. Schwob, and C. Poupon. Stress gradient effect on crack initiation in fretting using a multiaxial fatigue framework. *International Journal of Fatigue*, 32(12):1904 – 1912, 2010.
- [9] Mahaman Habibou Maitournam, Ky Dang Van, and Jean-François Flavenot. Fatigue design of notched components with stress gradients and cyclic plasticity. *Advanced Engineering Materials*, 11(9):750–754, 2009.
- [10] David Taylor. *The theory of critical distances: a new perspective in fracture mechanics*. Elsevier, 2010.
- [11] J.A. Arajo, L. Susmel, D. Taylor, J.C.T. Ferro, and E.N. Mamiya. On the use of the theory of critical distances and the modified whler curve method to estimate fretting fatigue strength of cylindrical contacts. *International Journal of Fatigue*, 29(1):95 – 107, 2007.
- [12] JF Flavenot and N Skalli. Lépaisseur de couche critique ou une nouvelle approche du calcul en fatigue des structures soumisesa des sollicitations multiaxiales. *Mec. Mater. Electr.*, 397:15–25, 1983.
- [13] T Palin-Luc. Stress gradient and size effects in multiaxial fatigue. *Materials Week (Munich, Germany)*, 2000.
- [14] A. Banville, T. Palin-Luc, and S. Lasserre. A volumetric energy based high cycle multiaxial fatigue criterion. *International Journal of Fatigue*, 25(8):755 – 769, 2003.
- [15] Ioannis V Papadopoulos and Vassilis P Panoskaltsis. Invariant formulation of a gradient dependent multiaxial high-cycle fatigue criterion. *Engineering Fracture Mechanics*, 55(4):513–528, 1996.
- [16] William Nichols Findley, JJ Coleman, and BC Hanley. *Theory for Combined Bending and Torsion Fatigue with Data for SAE4340 Steel*. Division of Engineering, Brown University, 1956.
- [17] Jean Lemaitre and Jean-Louis Chaboche. *Mechanics of solid materials*. Cambridge university press, 1990.
- [18] J. L. Chaboche and P. M. Lesne. A non-linear continuous fatigue damage model. *Fatigue , Fracture of Engineering Materials , Structures*, 11(1):1–17, 1988.
- [19] Lu Xi and Zheng Songlin. Strengthening of transmission gear under low-amplitude loads. *Materials Science and Engineering: A*, 488(1):55–63, 2008.
- [20] Lu Xi and Zheng Songlin. Strengthening and damaging under low-amplitude loads below the fatigue limit. *International Journal of Fatigue*, 31(2):341–345, 2009.
- [21] Lu Xi and Zheng Songlin. Changes in mechanical properties of vehicle components after strengthening under low-amplitude loads below the fatigue limit. *Fatigue & Fracture of Engineering Materials & Structures*, 32(10):847–855, 2009.
- [22] GM Sinclair. An investigation of the coaxing effect in fatigue of metals. Technical report, DTIC Document, 1952.
- [23] Masaki Nakajima, Jae Woong Jung, Yoshihiko Uematsu, and Keiro Tokaji. Coaxing effect in stainless steels and high-strength steels. *Key Engineering Materials*, 345:235–238, 2007.
- [24] Li Yuan and Han Xu Liu Jie Jiang Chao. A prediction method on high-cycle fatigue parameters based on dissipated energy computation. *Chinese Journal of Theoretical and Applied Mechanics*, 3:008, 2013.
- [25] Thierry Palin-Luc and Serge Lasserre. An energy based criterion for high cycle multiaxial fatigue. *European Journal of Mechanics-A/Solids*, 17(2):237–251, 1998.
- [26] Tadeusz Łagoda, Ewald Macha, and Włodzimierz Bedkowski. A critical plane approach based on energy concepts: application to biaxial random tension-compression high-cycle fatigue regime. *International Journal of Fatigue*, 21(5):431–443, 1999.
- [27] Richard M Christensen. Yield functions, damage states, and intrinsic strength. *Mathematics and Mechanics of Solids*, 5(3):285–300, 2000.
- [28] M.H. Maitournam, C. Krebs, and A. Galtier. A multiscale fatigue life model for complex cyclic multiaxial loading. *International Journal of Fatigue*, 33(2):232 – 240, 2011.
- [29] Stefano Bosia and Andrei Constantinescu. Fast time-scale average for a mesoscopic high cycle fatigue criterion. *International Journal of Fatigue*, 45:39 – 47, 2012.
- [30] Ma Zepeng. Structures under multiaxial fatigue taking consideration of gradients of the constraints with time and space variation.
- [31] Legendre Gauss Quadrature weights and nodes. <https://www.mathworks.com/matlabcentral/fileexchange/4540-legendre-gauss-quadrature-weights-and-nodes>. Accessed: 2004-05-11.

Appendices

Appendix A MATLAB CODE LISTING

```

1 ****
2 *
3 * CODING OF DAMAGE AND STRESS EVOLUTION OF A SINUSOIDAL LOAD (3 METHODS)
4 *
5 ****
6 % Program to get the Gauss–Legendre Quadrature results (Vectorized)
7 clear;clc;
8 tic;
9 dbstop if error
10 format long e
11 [x]=[ -0.99555697 -0.976663921 -0.942974571 -0.894991998 -0.833442629
12 -0.759259263 -0.673566368...
13 -0.57766293 -0.473002731 -0.361172306 -0.243866884 -0.122864693 0 0.122864693
14 0.243866884 0.361172306...
15 0.473002731 0.57766293 0.673566368 0.759259263 0.833442629 0.894991998
16 0.942974571 0.976663921...
17 0.99555697];
18 [weight]=[0.011393799 0.026354987 0.040939157 0.054904696
19 0.068038334 0.0801407 0.091028262...
20 0.100535949 0.108519624 0.114858259 0.119455764 0.122242443
21 0.123176054 0.122242443 0.119455764...
22 0.114858259 0.108519624 0.100535949 0.091028262 0.0801407
23 0.068038334 0.054904696 0.040939157...
24 0.026354987 0.011393799];
25 % [x]=xlsread('Gauss–Legendre Quadrature ','Sheet1 ','b1:z1 ');
26 % [weight]=xlsread('Gauss–Legendre Quadrature ','Sheet1 ','b2:z2 ');
27
28 E=2e11; %Youngs modulus
29 k=6e8; %hardening parameter
30 b=3; %weakening scales distribution exponent
31 nu=0.3; %poisson's ratio
32 tt=2e8; %torsion fatigue limit
33 ff=2.5e8; %bending fatigue limit
34 ac=(tt-ff/sqrt(3))/(ff/3); %crossland criterial constant
35 bc=tt; %crossland criterial constant
36 sigu=8e8; %ultimite stress
37 gam=0.5; %material parameter from Chaboche law(Wohler curve
38 exponent)
39 y=6.38e8; %macroscopic yield stress
40 WF=3e6; %dissipated energy to failure per unit volume
41 load=5e8; %cyclic load
42 loadtensor=[load 0 0;0 0;0 0 0 0];
43 stepnumber=300; %devide one cycle in 200 parts
44 f=50; %frequency of load
45
46 %-----numerical method-----
47 alp=0.5;
48 D=0; %initial damage
49 n=1; %initial recording point
50 G=(1-(1-D).^(gam+1)).^(1-alp);
51 %-----to get the the first Sb-----
52 stress11=load*sin(2*pi/stepnumber);
53 m=1/3*sum(stress11+0+0);
54 dev1=[stress11 0 0 ;0 0 0 ;0 0 0 ]-m*diag([1,1,1]);
55 dev11=dev1(1,1); dev12=dev1(1,3); dev13=dev1(1,3);

```

```

49 | dev21=dev1(2,1); dev22=dev1(2,2); dev23=dev1(2,3);
50 | dev31=dev1(3,1); dev32=dev1(3,2); dev33=dev1(3,3);
51 | [s]= ([x]/2+1/2).^(1/(1-b)); %1*25
52 |
53 | trial11=dev11; trial12=dev12; trial13=dev13;
54 | trial21=dev21; trial22=dev22; trial23=dev23;
55 | trial31=dev31; trial32=dev32; trial33=dev33;
56 |
57 | normtrial(1)=norm([ trial11 , trial12 , trial13; trial21 , trial22 , trial23; trial31
58 | , trial32 , trial33 ],'fro');
59 | [ eta]=bsxfun(@minus,bsxfun(@times,normtrial(1)/y,s),1); %1*25
60 | eta(eta<0)=0;
61 |
62 | Sb11=bsxfun(@rdivide,trial11,bsxfun(@plus,[ eta ],1));Sb12=bsxfun(@rdivide,
63 | trial12,bsxfun(@plus,[ eta ],1));Sb13=bsxfun(@rdivide,trial13,bsxfun(@plus,[
64 | eta ],1));
65 | Sb21=bsxfun(@rdivide,trial21,bsxfun(@plus,[ eta ],1));Sb22=bsxfun(@rdivide,
66 | trial22,bsxfun(@plus,[ eta ],1));Sb23=bsxfun(@rdivide,trial23,bsxfun(@plus,[
67 | eta ],1));
68 | Sb31=bsxfun(@rdivide,trial31,bsxfun(@plus,[ eta ],1));Sb32=bsxfun(@rdivide,
69 | trial32,bsxfun(@plus,[ eta ],1));Sb33=bsxfun(@rdivide,trial33,bsxfun(@plus,[
70 | eta ],1));
71 | %1*25 for each Sb element
72 | Sbtensor=[Sb11; Sb12; Sb13; Sb21; Sb22; Sb23;Sb31; Sb32; Sb33];
73 | normSb=sqrt(sum(Sbtensor.^2));
74 |
75 | while G<1
76 | stress11=load*sin((n)*2*pi/stepnumber);
77 | m=1/3*sum(stress11+0+0);
78 | dev1=[ stress11 0 0 ;0 0 0 ;0 0 0 ]-m*diag([1,1,1]);
79 | dev11=dev1(1,1); dev12=dev1(1,3); dev13=dev1(1,3);
80 | dev21=dev1(2,1); dev22=dev1(2,2); dev23=dev1(2,3);
81 | dev31=dev1(3,1); dev32=dev1(3,2); dev33=dev1(3,3);
82 |
83 | stress11=load*sin((n+1)*2*pi/stepnumber);
84 | m=1/3*sum(stress11+0+0);
85 | devn=[ stress11 0 0;0 0 0;0 0 0 ]-m*diag([1,1,1]);
86 | dev11g=devn(1,1); dev12g=devn(1,3); dev13g=devn(1,3);
87 | dev21g=devn(2,1); dev22g=devn(2,2); dev23g=devn(2,3);
88 | dev31g=devn(3,1); dev32g=devn(3,2); dev33g=devn(3,3);
89 |
90 | trial11=bsxfun(@plus,Sb11,(dev11g-dev11)); trial12=bsxfun(@plus,Sb12,(dev12g-
91 | dev12));
92 | trial13=bsxfun(@plus,Sb13,(dev13g-dev13));
93 | trial21=bsxfun(@plus,Sb21,(dev21g-dev21)); trial22=bsxfun(@plus,Sb22,(dev22g-
94 | dev22));
95 | trial23=bsxfun(@plus,Sb23,(dev23g-dev23));
96 | trial31=bsxfun(@plus,Sb31,(dev31g-dev31)); trial32=bsxfun(@plus,Sb32,(dev32g-
97 | dev32));
98 | trial33=bsxfun(@plus,Sb33,(dev33g-dev33));
99 | trialtensor=[ trial11; trial12; trial13; trial21; trial22; trial23; trial31;
100 | trial32; trial33 ];
101 | normtrial=sqrt(sum(trialtensor.^2));
102 | [ eta]=bsxfun(@minus,bsxfun(@times,normtrial/y,s),1); %1*25
103 | eta(eta<0)=0;
104 |
105 | Sb11=bsxfun(@rdivide,trial11,bsxfun(@plus,[ eta ],1));Sb12=bsxfun(@rdivide,
106 | trial12,bsxfun(@plus,[ eta ],1));Sb13=bsxfun(@rdivide,trial13,bsxfun(@plus,[
107 | eta ],1));

```

```

92 Sb21=bsxfun(@rdivide, trial21, bsxfun(@plus, [eta], 1)); Sb22=bsxfun(@rdivide,
93 trial22, bsxfun(@plus, [eta], 1)); Sb23=bsxfun(@rdivide, trial23, bsxfun(@plus, [
94 eta], 1));
95 Sb31=bsxfun(@rdivide, trial31, bsxfun(@plus, [eta], 1)); Sb32=bsxfun(@rdivide,
96 trial32, bsxfun(@plus, [eta], 1)); Sb33=bsxfun(@rdivide, trial33, bsxfun(@plus, [
97 eta], 1));
98 %1*25 for each Sb element
99 Sbtensor=[Sb11; Sb12; Sb13; Sb21; Sb22; Sb23; Sb31; Sb32; Sb33];
100 normSb=sqrt(sum((Sbtensor.^2)));
101
102 Ws=(bsxfun(@minus, normtrial, bsxfun(@rdivide, y, [s]))<=0).*...
103 (0)+...
104 (bsxfun(@minus, normtrial, bsxfun(@rdivide, y, [s]))>0).*...
105 ((E-k)*(1+nu)/(2*E*(E+k*nu))*bsxfun(@times, [weight], bsxfun(@rdivide, bsxfun(
106 @times, bsxfun(@minus, normtrial, bsxfun(@rdivide, y, [s])), y), [s])));
107
108 W= sum(Ws);
109 G = G+WF;
110 D=1-(1-G.^((1/(1-alp))).^(1/(gam+1)));
111 % t=n/stepnumber*1/f;
112 hold on;
113 yield1=plot(n,y*s(1).^-1, 'LineStyle', 'none', 'LineWidth', 1, 'Marker', 'o', ...
114 'MarkerSize', 6, ...
115 'MarkerEdgeColor', 'none', 'MarkerFaceColor', 'c');
116 Trial1=plot(n, sign(trial11(1))*normtrial(1), 'LineStyle', 'none', 'LineWidth',
117 1, 'Marker', '^', 'MarkerSize', 6, ...
118 'MarkerEdgeColor', 'r', 'MarkerFaceColor', 'r');
119 Sb1=plot(n, sign(Sb11(1))*normSb(1), 'LineStyle', 'none', 'LineWidth', 1, 'Marker',
120 'v', 'MarkerSize', 6, ...
121 'MarkerEdgeColor', 'g', 'MarkerFaceColor', 'g');
122 yield8=plot(n,y*s(8).^-1,'LineStyle', 'none', 'LineWidth', 1,'Marker', 'o', ...
123 'MarkerSize', 6, ...
124 'MarkerEdgeColor', 'none', 'MarkerFaceColor', 'b');
125 Trial8=plot(n, sign(trial11(8))*normtrial(8), 'LineStyle', 'none', 'LineWidth',
126 1, 'Marker', '^', 'MarkerSize', 6, ...
127 'MarkerEdgeColor', [1 0.5 0], 'MarkerFaceColor',[1 0.5 0]);
128 Sb8=plot(n, sign(Sb11(8))*normSb(8), 'LineStyle', 'none', 'LineWidth', 1, 'Marker',
129 'v', 'MarkerSize', 6, ...
130 'MarkerEdgeColor', 'k', 'MarkerFaceColor', 'k');
131 % DamageN=plot(t,D,'LineStyle', 'none', 'LineWidth', 1, 'Marker', 'o', ...
132 % 'MarkerSize', 6, ...
133 % 'MarkerEdgeColor', 'none', 'MarkerFaceColor', 'm');
134 %-----Difference between cyclic load calculation and numerical
135 % method as function of time-----
136 % Gcyc = Gcyc+Wcyc/stepnumber/WF
137 % Dcyc=1-(1-Gcyc.^((1/(1-alp))).^(1/(gam+1)));
138 % hold on
139 % Damagecyc=plot(t,D-Dcyc,'LineStyle', 'none', 'LineWidth', 1, 'Marker', 'o', ...
140 % 'MarkerSize', 6, ...
141 % 'MarkerEdgeColor', 'k', 'MarkerFaceColor', 'k');
142 n=n+1;
143 end;
144 toc;
145 disp(['Number of points to failure is ' num2str(n) ' points.']);

```

```

134 % %-----chaboche method-----
135 % alp=0.5;
136 % D=0; %initial damage
137 % n=1; %initial recording point
138 % G = (1 - (1 - D).^(gam + 1)).^(1 - alp);
139 % m=1/3*sum(diag(loadtensor));
140 % S1=loadtensor-m*diag([1,1,1]);
141 % sqrj1=1/2*sqrt(1/2)*norm(S1, 'fro');
142 % M=ff^1.233*(1-3*m/sigu);
143 % while G<1
144 % NF=1/((gam+1)*(1-alp))*(sqrj1/M)^(-gam);
145 % G = G+1/stepnumber/NF
146 % D=1-(1-G.^((1/(1-alp))).^(1/(gam + 1)));
147 % t=n/stepnumber*1/f;
148 % hold on;
149 % DamageC=plot (t,D, 'LineStyle', 'none', 'LineWidth', 1, 'Marker', 'o', 'MarkerSize', 6, ...
150 % 'MarkerEdgeColor', 'none', 'MarkerFaceColor', 'g');
151 % n=n+1;
152 end
153 % %-----Cyclic load calculation-----
154 % Dcyc=0;
155 % n=1;
156 % Gcyc = (1 - (1 - Dcyc).^(gam + 1)).^(1 - alp);
157 % Wcyc=4*(E-k)*(1+nu)*(b-1)/(E*(E+k*nu)*b*(b+1))*norm(loadtensor -(1/3*sum(diag(
158 % loadtensor)))*diag([1,1,1]),'fro').^(b+1)*y.^((1-b));
159 % while Gcyc< 1
160 % Gcyc = Gcyc+Wcyc/stepnumber/WF
161 % Dcyc=1-(1-Gcyc.^((1/(1-alp))).^(1/(gam + 1)));
162 % t=n/stepnumber*1/f;
163 % hold on
164 % Damagecyc=plot (t,Dcyc, 'LineStyle', 'none', 'LineWidth', 1, 'Marker', 'o', 'MarkerSize', 6, ...
165 % 'MarkerEdgeColor', 'none', 'MarkerFaceColor', 'b');
166 % n=n+1;
167 end
168 %-----plot settings-----
169 grid on;
170 grid minor;
171 % axis([0 0.49 -0.04 0.04]);
172 set(gca , 'FontSize',30);
173 hXLabel = xlabel('Number of steps', 'Fontsize', 30);
174
175 hTitle = title('Microscopic stress evolution at 2 different scales ', 'Fontsize', 30);
176 hYLabel = ylabel('Stress(Pa)', 'Fontsize', 30);
177 hLegend=legend([yield1,Sb1,Trial1,yield8,Sb8,Trial8], '(\sigma_y-\lambda\sigma_H)/s_1 at scale s_1', '(S-b) at scale s_1', ...
178 '(S-b)_{trial} at scale s_1', '(\sigma_y-\lambda\sigma_H)/s_8 at scale s_8', ...
179 '(S-b)_{8} at scale s_8', '(S-b)_{trial} at scale s_8');
180
181 % hTitle = title('Damage evolution comparison of three methods ', 'Fontsize', 30);

```

```

182 % hYLabel = ylabel('Damage', 'FontSize', 30);
183 % hLegend=legend([DamageN,DamageC,Damagecyc],'Numerical method','Chaboche
184 % method',...
185 % 'Cyclic load calculation');
186 % hTitle = title('Difference between cyclic load calculation and numerical
187 % method as function of time(time step=1/15000)', 'FontSize', 30);
188 % Adjust font
189 set(gca, 'FontName', 'Helvetica')
190 set([hTitle, hXLabel, hYLabel], 'FontName', 'AvantGarde')
191
192 set([hXLabel, hYLabel], 'FontSize', 30)
193 set(hTitle, 'FontSize', 30, 'FontWeight', 'bold')
194 set([hLegend, gca], 'FontSize', 30)
195 % Adjust axes properties
196 set(gca, 'Box', 'off', 'TickDir', 'out', 'TickLength', [.02 .02], ...
197 'XMinorTick', 'on', 'YMinorTick', 'on', 'YGrid', 'on', ...
198 'XColor', [.3 .3 .3], 'YColor', [.3 .3 .3], ...
199 'LineWidth', 1)
200
201 set(gcf, 'color', 'w'); %set figure background transparent
202 set(gca, 'color', 'w'); %set axis transparent
203 % Maximize print figure
204 set(gcf, 'outerposition', get(0, 'screensize'));
205 set(gcf, 'PaperPositionMode', 'manual');
206 set(gcf, 'PaperUnits', 'points'); %[ {inches} | centimeters | normalized |
207 % points ]
208 set(gcf, 'PaperPosition', [0 0 1920 1080]); %set(gcf, 'PaperPosition',[left,
209 % bottom, width, height])
saveas(gcf, 'trialsin.png');
% saveas(gcf, 'damagesin.png');

```

```

1 ****
2 *
3 * CODING OF DAMAGE AND ENERGY EVOLUTION OF PSA LOAD (3 DIMENSIONAL)
4 *
5 ****
6 clear;clc;
7 dbstop if error
8 format long e
9
10 load('FX_RAVG.mat');
11 signal.data=double(signal.data);
12 forcex= transpose(signal.data);
13 load('FY_RAVG.mat');
14 signal.data=double(signal.data);
15 forcey= transpose(signal.data);
16 load('FZ_RAVG.mat');
17 signal.data=double(signal.data);
18 forcez= transpose(signal.data);
19 copy=3;
20 forcex=repmat(forcex, copy, 1);
21 forcey=repmat(forcey, copy, 1);
22 forcez=repmat(forcez, copy, 1);
23
24 %----- Arithmetic sequence between every recorded points
25 ari=10;
26 for i=2:(1*802805)
27 %force(1+ari*(i-1):1+ari*i)=linspace(forceorigin(i),forceorigin(i+1),ari+1);
28 forcelx(1+ari*(i-2):1+ari*(i-1))=linspace(forcex(i-1),forcex(i),ari+1);
29 forcely(1+ari*(i-2):1+ari*(i-1))=linspace(forcey(i-1),forcey(i),ari+1);
30 forcelz(1+ari*(i-2):1+ari*(i-1))=linspace(forcez(i-1),forcez(i),ari+1);
31 end;
32 % ari*(i-1)+1 ;%the number of points
33
34 %-----build the stress tensor-----
35 A=1/6e4;
36 cx=10;
37 cy=60;
38 thetax=0.5;
39 thetay=0.6;
40 phix=0.3;
41 phiy=0.4;
42 stress11=1/A*(forcelx+cx*forcey*cos(thetax)^2+cy*forcey*cos(thetay)^2);
43 stress12=1/A*(cx*forcelx*cos(thetax)*sin(thetax)*cos(phix)+cy*forcey*cos(thetay)*sin(thetay)*cos(phiy));
44 stress13=1/A*(cx*forcey*cos(thetax)*sin(thetax)*sin(phix)+cy*forcey*cos(thetay)*sin(thetay)*sin(phiy));
45 stress21=stress12;
46 stress22=1/A*(cx*forcelx*sin(thetax)^2*cos(phix)^2+cy*forcey*sin(thetay)^2*cos(phiy)^2);
47 stress23=1/A*(cx*forcelx*sin(thetax)^2*cos(phix)*sin(phix)+cy*forcey*sin(thetay)^2*cos(phiy)*sin(phiy));
48 stress31=stress13;
49 stress32=stress23;

```

```

50 | stress33=1/A*(cx*force1x*sin(thetax)^2*sin(phi1)^2+cy*force1y*sin(thetay)^2*sin(phi1)^2);
51 | % [max(stress11) max(stress12) max(stress13);
52 | % max(stress12) max(stress22) max(stress23);
53 | % max(stress23) max(stress13) max(stress33);]
54 | % [mean(stress11) mean(stress12) mean(stress13);
55 | % mean(stress12) mean(stress22) mean(stress23);
56 | % mean(stress23) mean(stress13) mean(stress33);]
57 |
58 | [x]= [-0.99555697 -0.976663921 -0.942974571 -0.894991998 -0.833442629
59 |      -0.759259263 -0.673566368...
60 |      -0.57766293 -0.473002731 -0.361172306 -0.243866884 -0.122864693 0 0.122864693
61 |      0.243866884 0.361172306...
62 |      0.473002731 0.57766293 0.673566368 0.759259263 0.833442629 0.894991998
63 |      0.942974571 0.976663921...
64 |      0.99555697];
65 | [weight]=[0.011393799 0.026354987 0.040939157 0.054904696
66 |      0.068038334 0.0801407 0.091028262...
67 |      0.100535949 0.108519624 0.114858259 0.119455764 0.122242443
68 |      0.123176054 0.122242443 0.119455764...
69 |      0.114858259 0.108519624 0.100535949 0.091028262 0.0801407
70 |      0.068038334 0.054904696 0.040939157...
71 |      0.026354987 0.011393799];
72 | % [x]=xlsread('Gauss-Legendre Quadrature ','Sheet1 ','b1:z1 ');
73 | % [weight]=xlsread('Gauss-Legendre Quadrature ','Sheet1 ','b2:z2 ');
74 | y=6.38e8; %macroscopic yield stress
75 | lam=0.5; %hydrostatic pressure sensitivity
76 | E=2e11; %Youngs modulus
77 | k=6e8; %hardening parameter
78 | b=3; %weakening scales distribution exponent
79 | nu=0.3; %poisson's ratio
80 | tt=2e8; %torsion fatigue limit
81 | ff=2.5e8; %bending fatigue limit
82 | ac=(tt-ff/sqrt(3))/(ff/3); %crossland criterial constant
83 | bc=tt; %crossland criterial constant
84 | sigu=8e8; %ultimite stress
85 | gam=0.5; %material parameter from Chaboche law(Wohler curve
86 |      exponent)
87 | samplerate=256; %recorded samples per second
88 |
89 | %-----Vectorization-----
90 | tic;
91 | WF=3e7; %dissipated energy to failure per unit volume
92 | alp=0.8;
93 | D=0; %initial damage
94 | n=1; %initial recording point
95 | step=1/samplerate/ari;
96 | t=n*step;
97 | G=(1-(1-D).^(gam+1)).^(1-alp);
98 | %-----to get the the first Sb-----
99 | m=1/3*sum(stress11(1)+stress22(1)+stress33(1));
100 | yield(1)=y-lam*m; %macro yield strength considering mean stress effect
101 | dev1=[stress11(1) stress12(1) stress13(1); stress21(1) stress22(1) stress23(1);
102 |      stress31(1) stress32(1) stress33(1)]-m*diag([1,1,1]);
103 | dev11=dev1(1,1); dev12=dev1(1,2); dev13=dev1(1,3);
104 | dev21=dev1(2,1); dev22=dev1(2,2); dev23=dev1(2,3);

```

```

97 dev31=dev1(3,1); dev32=dev1(3,2); dev33=dev1(3,3);
98
99 trial11=dev11; trial12=dev12; trial13=dev13;
100 trial21=dev21; trial22=dev22; trial23=dev23;
101 trial31=dev31; trial32=dev32; trial33=dev33;
102 trialtensor=[trial11; trial12; trial13; trial21; trial22; trial23; trial31;
103     trial32; trial33];
104 normtrial(1,1:length(x))=sqrt(sum(trialtensor.^2));
105 [s]= ([x]/2+1/2).^(1/(1-b)); %1*25
106 [eta]=bsxfun(@minus,bsxfun(@times,normtrial(1,1:length(x))/yield(1),s),1); %
107     1*25
108 eta(eta<0)=0;
109
110 Sb11=bsxfun(@rdivide,trial11,bsxfun(@plus,[eta],1));Sb12=bsxfun(@rdivide,
111     trial12,bsxfun(@plus,[eta],1));Sb13=bsxfun(@rdivide,trial13,bsxfun(@plus,[
112     eta],1));
113 Sb21=bsxfun(@rdivide,trial21,bsxfun(@plus,[eta],1));Sb22=bsxfun(@rdivide,
114     trial22,bsxfun(@plus,[eta],1));Sb23=bsxfun(@rdivide,trial23,bsxfun(@plus,[
115     eta],1));
116 Sb31=bsxfun(@rdivide,trial31,bsxfun(@plus,[eta],1));Sb32=bsxfun(@rdivide,
117     trial32,bsxfun(@plus,[eta],1));Sb33=bsxfun(@rdivide,trial33,bsxfun(@plus,[
118     eta],1));
119 %1*25 for each Sb element
120 Sbtensor=[Sb11; Sb12; Sb13; Sb21; Sb22; Sb23; Sb31; Sb32; Sb33];
121 normSb(1,:)=sqrt(sum(Sbtensor.^2));
122 Ws=(bsxfun(@minus,normtrial(1,1:length(x)),bsxfun(@rdivide, yield(1),[s]))<=0)
123     .*...
124 (0)+...
125 (bsxfun(@minus,normtrial(1,1:length(x)),bsxfun(@rdivide, yield(1),[s]))>0).*...
126 ((E-k)*(1+nu)/(2*E*(E+k*nu))*bsxfun(@times,[weight],bsxfun(@rdivide,bsxfun(
127     @times,bsxfun(@minus,normtrial(1,1:length(x)),bsxfun(@rdivide, yield(1),[s]
128     ))),yield(1)),[s])));
129 W= sum(Ws);
130 G = G+W/WF; %1.322163316411401e-03
131 D(1)=1-(1-G.^((1/(1-alp))).^(1/(gam+1)));
132 while G<1
133 m=1/3*sum(stress11(n)+stress22(n)+stress33(n));
134 dev1=[stress11(n) stress12(n) stress13(n); stress21(n) stress22(n) stress23(n);
135     stress31(n) stress32(n) stress33(n)]-m*diag([1,1,1]);
136 dev11=dev1(1,1); dev12=dev1(1,2); dev13=dev1(1,3);
137 dev21=dev1(2,1); dev22=dev1(2,2); dev23=dev1(2,3);
138 dev31=dev1(3,1); dev32=dev1(3,2); dev33=dev1(3,3);
139
140 m=1/3*sum(stress11(n+1)+stress22(n+1)+stress33(n+1));
141 yield(n+1)=y-lam*m; %macro yield strength considering mean stress effect
142 yield(yield<0)=0;
143 devn=[stress11(n+1) stress12(n+1) stress13(n+1); stress21(n+1) stress22(n+1)
144     stress23(n+1); stress31(n+1) stress32(n+1) stress33(n+1)]-m*diag([1,1,1]);
145 dev11g=devn(1,1); dev12g=devn(1,2); dev13g=devn(1,3);
146 dev21g=devn(2,1); dev22g=devn(2,2); dev23g=devn(2,3);
147 dev31g=devn(3,1); dev32g=devn(3,2); dev33g=devn(3,3);
148
149 trial11=bsxfun(@plus,Sb11,(dev11g-dev11)); trial12=bsxfun(@plus,Sb12,(dev12g-
150     dev12)); trial13=bsxfun(@plus,Sb13,(dev13g-dev13));
151 trial21=bsxfun(@plus,Sb21,(dev21g-dev21)); trial22=bsxfun(@plus,Sb22,(dev22g-
152     dev22)); trial23=bsxfun(@plus,Sb23,(dev23g-dev23));

```

```

138 trial31=bsxfun(@plus,Sb31,(dev31g-dev31)); trial32=bsxfun(@plus,Sb32,(dev32g-
139   dev32)); trial33=bsxfun(@plus,Sb33,(dev33g-dev33));
140 trialtensor=[trial11; trial12; trial13; trial21; trial22; trial23; trial31;
141   trial32; trial33];
142 normtrial(n+1,:)=sqrt(sum(trialtensor.^2));
143 [eta]=bsxfun(@minus,bsxfun(@times,normtrial(n+1,:)/yield(n+1),s),1); %1*25
144 eta(eta<0)=0;
145
146 Sb11=bsxfun(@rdivide,trial11,bsxfun(@plus,[eta],1));Sb12=bsxfun(@rdivide,
147   trial12,bsxfun(@plus,[eta],1));Sb13=bsxfun(@rdivide,trial13,bsxfun(@plus,[
148     eta],1));
149 Sb21=bsxfun(@rdivide,trial21,bsxfun(@plus,[eta],1));Sb22=bsxfun(@rdivide,
150   trial22,bsxfun(@plus,[eta],1));Sb23=bsxfun(@rdivide,trial23,bsxfun(@plus,[
151     eta],1));
152 Sb31=bsxfun(@rdivide,trial31,bsxfun(@plus,[eta],1));Sb32=bsxfun(@rdivide,
153   trial32,bsxfun(@plus,[eta],1));Sb33=bsxfun(@rdivide,trial33,bsxfun(@plus,[
154     eta],1));
155 %1*25 for each Sb element
156 Sbtensor=[Sb11; Sb12; Sb13; Sb21; Sb22; Sb23; Sb31; Sb32; Sb33];
157 normSb(n+1,:)=sqrt(sum((Sbtensor.^2)));
158
159 Ws=(bsxfun(@minus,normtrial(n+1,:),bsxfun(@rdivide, yield(n+1),[s]))<=0).*...
160 (0)+...
161 (bsxfun(@minus,normtrial(n+1,:),bsxfun(@rdivide, yield(n+1),[s]))>0).*...
162 ((E-k)*(1+nu)/(2*E*(E+k*nu))*bsxfun(@times,[weight],bsxfun(@rdivide,bsxfun(
163   @times,bsxfun(@minus,normtrial(n+1,:),bsxfun(@rdivide, yield(n+1),[s])),yield(n+1),[s]))));
164 W= sum(Ws);
165 G = G+W/WF;
166 D(n+1)=1-(1-G.^((1/(1 - alp))).^(1/(gam + 1)));
167 t=n*step;
168 % hold on;
169 % yield1=plot(t,yield(n)*s(1).^-1, 'LineStyle', 'none', 'LineWidth', 1, 'Marker',
170 %   'o', 'MarkerSize', 6, ...
171 %   'MarkerEdgeColor', 'none', 'MarkerFaceColor', 'c');
172 % Trial1=plot(t,normtrial(n,1), 'LineStyle', 'none', 'LineWidth', 1, 'Marker',
173 %   '^', 'MarkerSize', 6, ...
174 %   'MarkerEdgeColor', 'r', 'MarkerFaceColor', 'r');
175 % Sb1=plot(t,normSb(n,1), 'LineStyle', 'none', 'LineWidth', 1, 'Marker', 'v',
176 %   'MarkerSize', 6, ...
177 %   'MarkerEdgeColor', 'g', 'MarkerFaceColor', 'g');
178 % yield8=plot(t,yield(n)*s(8).^-1, 'LineStyle', 'none', 'LineWidth', 1, 'Marker',
179 %   'o', 'MarkerSize', 6, ...
180 %   'MarkerEdgeColor', 'none', 'MarkerFaceColor', 'b');
181 % Trial8=plot(t,normtrial(n,8), 'LineStyle', 'none', 'LineWidth', 1, 'Marker',
182 %   '^', 'MarkerSize', 6, ...
183 %   'MarkerEdgeColor', [1 0.5 0], 'MarkerFaceColor',[1 0.5 0]);
184 % Sb8=plot(t,normSb(n,8), 'LineStyle', 'none', 'LineWidth', 1, 'Marker', 'v',
185 %   'MarkerSize', 6, ...
186 %   'MarkerEdgeColor', 'k', 'MarkerFaceColor', 'k');
187 % DamageN=plot(t,D, 'LineStyle', 'none', 'LineWidth', 1, 'Marker', 'o', 'MarkerSize',
188 %   6, ...
189 %   'MarkerEdgeColor', 'none', 'MarkerFaceColor', 'r');
190 n=n+1;
191 end;
192 toc;

```

```

177 | time=num2str(toc)
178 | NF=num2str(n)
179 | testtime=num2str(t)
180 |
181 | % hold on;
182 | % yield1=plot ((1:n)*step ,yield(1:n)*s(1).^-1, 'LineStyle ', 'none ', 'LineWidth
183 | % , 1, 'Marker ', 'o', 'MarkerSize ', 6, ...
184 | % 'MarkerEdgeColor ', 'none ', 'MarkerFaceColor ', 'c');
185 | % Trial1=plot ((1:n)*step ,normtrial(1:n,1), 'LineStyle ', 'none ', 'LineWidth ',
186 | % 1, 'Marker ', '^', 'MarkerSize ', 6, ...
187 | % 'MarkerEdgeColor ', 'r', 'MarkerFaceColor ', 'r');
188 | % Sb1=plot ((1:n)*step ,normSb(1:n,1), 'LineStyle ', 'none ', 'LineWidth ', 1,
189 | % 'Marker ', 'v', 'MarkerSize ', 6, ...
190 | % 'MarkerEdgeColor ', 'g', 'MarkerFaceColor ', 'g');
191 | % yield8=plot ((1:n)*step ,yield(1:n)*s(8).^-1, 'LineStyle ', 'none ', 'LineWidth
192 | % , 1, 'Marker ', 'o', 'MarkerSize ', 6, ...
193 | % 'MarkerEdgeColor ', 'none ', 'MarkerFaceColor ', 'b');
194 | % Trial8=plot ((1:n)*step ,normtrial(1:n,8), 'LineStyle ', 'none ', 'LineWidth ',
195 | % 1, 'Marker ', '^', 'MarkerSize ', 6, ...
196 | % 'MarkerEdgeColor ', [1 0.5 0], 'MarkerFaceColor ', [1 0.5 0]);
197 | % Sb8=plot ((1:n)*step ,normSb(1:n,8), 'LineStyle ', 'none ', 'LineWidth ', 1,
198 | % 'Marker ', 'v', 'MarkerSize ', 6, ...
199 | % 'MarkerEdgeColor ', 'k', 'MarkerFaceColor ', 'k');
200 |
201 | % % -----
202 | % DamageN=plot ((1:n)*step ,D(1:n), 'LineStyle ', 'none ', 'LineWidth ', 1, 'Marker ',
203 | % 'o', 'MarkerSize ', 6, ...
204 | % 'MarkerEdgeColor ', 'none ', 'MarkerFaceColor ', 'r');
205 |
206 | %----- plot settings -----
207 | grid on;
208 | grid minor;
209 | set(gca , 'FontSize' ,30);
210 | hXLabel = xlabel('t(s)', 'Fontsize' ,30);
211 |
212 | hTitle = title('Damage evolution under multidimensional stress', 'Fontsize' ,25)
213 | ;
214 | hYLabel = ylabel('D', 'Fontsize' ,25);
215 |
216 | % hTitle = title('Microscopic stress evolution at 2 scales', 'Fontsize' ,30);
217 | % hYLabel = ylabel('(\sigma_y - \lambda \Sigma_H)/s_1', 'Fontsize' ,30);
218 | % hLegend=legend([yield1,Sb1,Trial1,yield8,Sb8,Trial8], '(\sigma_y - \lambda \Sigma_H)/s_1
219 | % at scale s_1', '(S-b) at scale s_1', ...
220 | % '(S-b)_{trial} at scale s_1', '(\sigma_y - \lambda \Sigma_H)/s_8
221 | % at scale s_8', '(S-b) at scale s_8');
222 | % set([hLegend, gca], 'FontSize', 30)
223 |
224 | % Adjust font
225 | set(gca , 'FontName' , 'Helvetica')
226 | set([hTitle , hXLabel , hYLabel], 'FontName' , 'AvantGarde')
227 | set([hXLabel , hYLabel], 'FontSize' , 30)
228 | set(hTitle , 'FontSize' , 30, 'FontWeight' , 'bold')
229 |
230 | % Adjust axes properties
231 | set(gca , 'Box' , 'off', 'TickDir' , 'out', 'TickLength' , [.02 .02], ...
232 | % 'XMinorTick' , 'on', 'YMinorTick' , 'on', 'YGrid' , 'on', ...

```

```
222 'XColor', [.3 .3 .3], 'YColor', [.3 .3 .3], ...
223 'LineWidth', 1)
224
225 set(gcf, 'color', 'w'); %set figure background transparent
226 set(gca, 'color', 'w'); %set axis transparent
227 % Maximize print figure
228 set(gcf, 'outerposition', get(0, 'screensize'));
229 set(gcf, 'PaperPositionMode', 'manual');
230 set(gcf, 'PaperUnits', 'points'); %[ {inches} | centimeters | normalized |
231 % points ]
232 set(gcf, 'PaperPosition', [0 0 1920 1080]); %set(gcf, 'PaperPosition',[left,
233 % bottom, width, height])
% saveas(gcf, 'damage3d.png');
saveas(gcf, 'trialreal3d.png');
```